A FUNCTIONAL CHARACTERIZATION OF CGI-58

By

Derek B. McMahon

A Dissertation submitted to the

Graduate School-New Brunswick

Rutgers, The State University of New Jersey

in partial fulfillment of the requirements

for the degree of

Doctor of Philosophy

Graduate Program in Nutritional Sciences

written under the direction of

Dr. Dawn L. Brasaemle

and approved by

_____

_____

_____

_____

_____

_____

New Brunswick, NJ

October, 2012

ABSTRACT OF THE DISSERTATION

A Functional Characterization of CGI-58

By Derek B. McMahon

Dissertation Director:

Dr. Dawn L. Brasaemle

Mutations in the gene CGI-58/ABHD5 cause Chanarin-Dorfman Syndrome, a Neutral Lipid Storage Disorder (NLSD) where many cells and tissues, including human skin fibroblasts, store excessive triacylglycerol (TAG). The protein, CGI-58, has been characterized *in vitro* as both a co-activator of adipose triglyceride lipase (ATGL) and a lysophosphatidic acid acyltransferase (LPAAT). We hypothesized that CGI-58 LPAAT activity is not necessary for co-activation of ATGL. This hypothesis was investigated through 3 specific aims: 1) to identify LPAAT active site residues, 2) to demonstrate that CGI-58 lacking LPAAT activity can co-activate ATGL, and 3) to analyze the lipid composition of cultured NLSD fibroblasts relative to normal human skin fibroblasts. A molecular model of CGI-58 was created to identify potential active site residues. In the model, the putative LPAAT active site residues H329 and D334 were not in close proximity, suggesting that they may not be active site residues. Recombinant H329A and D334A CGI-58 variants, when purified from BL21(DE3) *E. coli*, showed higher levels of LPAAT activity than purified wild-type CGI-58. LPAAT activity was linked to a protein contaminant, likely plsC, the endogenous *E. coli* LPAAT. The purification of recombinant CGI-58 was optimized to reduce contaminant proteins. These new preparations lacked LPAAT activity, yet retained the ability to co-activate ATGL. Additionally, extracts of Bl21(DE3) cells

expressing GST-tagged CGI-58 lacked LPAAT activity when plsC was removed by centrifugation. The previously observed LPAAT activity was due to a protein contaminant; thus, CGI-58 lacks LPAAT activity and LPAAT activity is not necessary for the co-activation of ATGL. Additionally, using a protein-lipid overlay, CGI-58 bound to phosphatidylinositol 3-phosphate [PI(3)P] and phosphatidylinositol 5-phosphate [PI(5)P] but not lysophosphatidic acid [LPA], the LPAAT substrate. CGI-58 binding of PI(3)P or PI(5)P does not alter co-activation of ATGL. Finally, CGI-58 variant H84R, found in humans with NLSDi, was expressed in cultured NLSD cells and studied *in vitro*. H84R CGI-58 failed to reduce accumulated TAG of NLSD fibroblasts, unlike unmodified CGI-58 or the H84A variant. Both H84 variants lacked the ability to co-activate ATGL *in vitro*. Thus, H84R CGI-58 contributes to the NLSD phenotype by failing to co-activate ATGL.

ACKNOWLEDGEMENTS

First and foremost I would like to thank Dr. Dawn Brasaemle for her patience, trust, guidance, and support throughout this project. Thank you for believing in me. I would also like to thank my committee members: Dr. George Carman and Dr. Gil-Soo Han, for their insight on various purification techniques and guidance of my project; Dr. Judith Storch, for her advice on protein purification, tryptophan quenching, and delipidation techniques; Dr. Joseph Dixon, for spending countless hours analyzing LC/MS data with me and for always being there on the weekends when I needed advice; and finally, Dr. Malcolm Watford, for always being available to talk whenever I needed his advice. I also would like to thank Rob Muldowney for his expertise and guidance in protein threading.

I've had the honor of working with very intelligent undergraduate students. I'd like to thank Dharika Shah for her work on the NLSDi projects, it was amazing to work alongside of a great friend; Dan Kurz for his work on optimizing the purification of CGI-58, we worked hard and had a lot of fun that summer; Nikhil Toraskar for his help when I was just starting in the lab; and Casey Fannell and Hilary Smith who described my life as a sitcom (and were correct). Thank you all for the laughs. I also would like to thank Sean Sullivan, Anna Dinh, Samantha Dori, Angela Gadja, and Amy Marcinkiewicz for their friendship, encouragement, and expertise.

A huge thanks goes out to some of the close friends I've made here. I'll never forget the days that I spent with my roommate and best friend Dan Hess, who I've spent countless hours at Taco Bell and Chipotle with talking about science, games,

cars, and life. A huge thanks to Miho Maeda, Gretchun Kim, Angelus Han, Roshni Patel, Ernesto Mendez, and Mayda Hernandez for all the time we've spent together and all of the laughs we've shared.

Finally, I'd like to thank my family for always being supportive. Thank you Mom, Dad, Jason, Olivia, and Ellie!

Table of Contents

List of Tables

List of Figures

List of Abbreviations

ABHD	α/β hydrolase domain
ABHD5	α/β hydrolase domain-5 (CGI-58)
AGPAT	acylglycerolphosphate acyltransferase
AMPK	AMP-activated protein kinase
ANOVA	Analysis of variance
ATGL	Adipose triglyceride lipase
ASO	Anti-sense oligo nucleotide
BAT	Brown adipose tissue
CE	Cholesterol ester
CGI-58	Comparative Gene Identification-58 (ABHD5)
COPI	Coat protein I
COPII	Coat protein II
CtBP/BARS	carboxy-terminal binding protein/brefeldin A-ribosylated substrate
DAG	Diacylglycerol
EDTA	Ethylenediaminetetraacetic acid
ELISA	Enzyme-linked immunosorbent assay
ER	Endoplasmic reticulum
FA	Fatty acid
FYVE	Fab1p, YOTB, Vac1p, EEA1
G0S2	G_0/G_1 switch gene 2
GST	Glutathione S-transferase

HFD	High fat diet
HSL	Hormone-sensitive lipase
hVps	Human vacuolar protein sorting homologue
IPTG	Isopropyl β-D-1 thiogalactopyranoside
LB	Luria broth
LPAAT	Lysophosphatidic acid acyltransferase
LPA	Lysophosphatidic acid
LSB	Laemmli sample buffer
M6PRBP	Mannose 6-phosphate receptor binding protein
MAG	Monoacylglycerol
1-MAG	1-Monoacylglycerol
2-MAG	2- Monoacylglycerol
MGL	Monoacylglycerol lipase
mTOR	Mammalian target of rapamycin
NLSD	Neutral lipid storage disorder
NLSDi	Neutral lipid storage disorder with ichthyosis
NLSDm	Neutral lipid storage disorder with myopathy
PA	Phosphatidic acid
PBS	Phosphate buffered saline
PC	Phosphatidylcholine
PCR	Polymerase chain reaction
PE	Phosphatidylethanolamine
PG	Phosphatidylglycerol

PH	Pleckstrin homology
PI	Phosphatidylinositol
PI3K	Phosphatidylinositol 3-kinase
PIP	Phosphatidylinositol phosphate
PI(3)P	Phosphatidylinositol 3-phosphate
PI(4)P	Phosphatidylinositol 4-phosphate
PI(5)P	Phosphatidylinositol 5-phosphate
$PI(3,5)P_2$	Phosphatidylinositol 3,5-bisphosphate
$PI(4,5)P_2$	Phosphatidylinositol 4,5-bisphosphate
PKA	Protein kinase A
PLIN1	Perilipin 1
PLIN2	Perilipin 2
PLIN3	Perilipin 3
PLIN4	Perilipin 4
PLIN5	Perilipin 5
PNPLA1	Patatin-like phospholipase domain containing 1
PX	Phox, phagocyte oxidase
RE	Retinol ester
TAG	Triacylglycerol
TLC	Thin layer chromatography
WAT	White adipose tissue
WT	Wild-type

I. Introduction

Obesity is a widespread problem in the United States and a growing problem in most countries of the world. According to the 2012 National Center for Health Statistics (NCHS) data brief, in 2009-2010, 35.7% of adults and 16.9% of children and adolescents were considered obese [1]. In this study, obesity was defined as having a body mass index (weight in kg divided by height in meters squared) greater than or equal to 30. Obesity is caused by an increase in percent body fat mass (adipose tissue) due to excessive caloric intake, sedentary life-style, and, in some cases, genetics.

Specialized cells located within adipose tissue called adipocytes store excess calories in the form of TAG. Each molecule of TAG is composed of three fatty acids (FA) esterified to a molecule of glycerol. Due to this structure, TAG is highly hydrophobic and is stored in specialized compartments within cells called lipid droplets. Lipid droplets contain a neutral lipid core of mainly TAG and cholesterol esters (CE); although in some cells, the core may contain retinol esters or monoalk(en)yldiacylglycerol [2]. The hydrophobic core is surrounded by a phospholipid monolayer composed of mainly phosphatidylcholine (PC), phosphatidylethanolamine (PE), phosphatidylinositol (PI), and ether-linked phosphatidylcholine; of these lipids, PC is the most abundant [2,3]. This phospholipid monolayer provides a surface for proteins to interact with or embed into [4]. Proteins, such as lipases, access the hydrophobic core of the lipid droplet to hydrolyze stored lipids. Neutral lipid lipases cleave TAG into three molecules of FA and one molecule of glycerol. In adipocytes, FA is either 1) exported into the

bloodstream bound to albumin and subsequently available for uptake by the heart, skeletal muscle, or liver, or 2) re-esterified into TAG (reviewed in [5]). The heart and skeletal muscle use fatty acids for ATP production via β-oxidation but esterify some of the fatty acids into TAG for storage. Adipocytes also release the glycerol produced from complete TAG hydrolysis into the bloodstream for uptake by the liver. The liver enzyme, glycerol kinase, is not expressed in adipocytes, but is a necessary enzyme for the re-utilization of glycerol in TAG formation.

In obesity, lipolysis in adipocytes is altered. Adipose tissues in obese patients have a decreased lipolytic response to catecholamines relative to lean patients [6,7]. This may be due to a decrease in hormone-sensitive lipase (HSL), a major lipase in adipocytes, in obese [8-10] and insulin-resistant subjects [11,12]. However, obese patients also contain lower levels of perilipin1 (PLIN1), a protein that coordinates lipase interaction with the surfaces of lipid droplets, in omental and subcutaneous adipose tissue [13]. These studies suggest that obese subjects have impaired FA release from adipocytes during fasting or exercise, but increased release of FA during basal lipolysis. Excessive circulating FA and ectopic fat deposition in liver and muscle has been correlated to increase insulin resistance [14].

In the past 20 years, significant progress has been made in identifying lipid droplet associated proteins and understanding the role that they play in regulating intracellular lipid homeostasis. Through studying the proteins involved in lipolysis and how their activities are regulated, a greater understanding of the causes and treatment of obesity can be achieved.

Overview of Lipolysis in Adipocytes

Lipolysis of TAG stores in adipocytes is studied in two states: basal and stimulated (Figure 1). The basal state approximates the fed state, when insulin is present; in the absence of catecholamines, adipose triglyceride lipase (ATGL), the major TAG lipase, is localized both in the cytosol and on the surfaces of lipid droplets. ATGL associated with lipid droplets during the basal state is thought to be responsible for a low level of TAG hydrolysis. Recent findings suggest that ATGL forms a complex with an inhibitor protein, G0S2 (G_0/G_1 switch gene 2), in the cytosol, which reduces ATGL lipase activity [15,16]. Moreover, CGI-58 (comparative gene identification-58), the co-activator protein for ATGL, is bound to PLIN1 at the surfaces of lipid droplets [17], where it is thought to be sequestered from interacting with ATGL, thus repressing maximal lipase activity. Hormone-sensitive lipase (HSL), another major adipose lipase, is localized in the cytosol, away from its substrate lipids [18,19]. As a result of these conditions, there is low lipolytic activity; TAG is hydrolyzed to diacylglycerol (DAG) and most of the released fatty acid (FA) is re-esterified to DAG to form TAG [5]. Due to this continuous recycling, TAG levels remain relatively constant.

Lipolysis is stimulated during times of energy deprivation, such as fasting, starvation, or exercise. The classically defined pathway starts when catecholamines bind to β-adrenergic receptors on the plasma membranes of adipocytes. This interaction initiates a G-protein-mediated signaling cascade leading to activation of adenylyl cyclase and elevation of intracellular cAMP levels [20,21]. The increased cAMP levels activate protein kinase A (PKA), which can then phosphorylate both

Figure 1

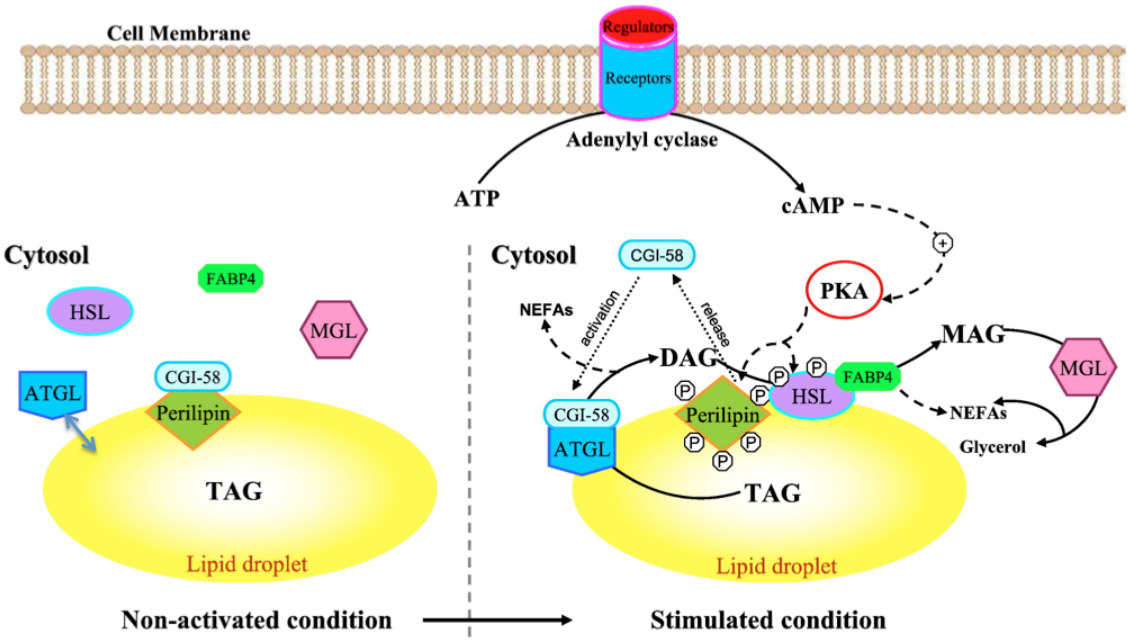

Figure 1. Basal (non-activated) lipolysis and stimulated lipolysis in adipocytes. During basal lipolysis, CGI-58 is bound to PLIN1 (perilipin) on the surfaces of lipid droplets, sequestered from interaction with ATGL. ATGL localizes to both the cytosol and lipid droplets. HSL remains cytosolic, unable to access stored lipids. During stimulated lipolysis, increased levels of cAMP activate PKA, leading to the phosphorylation of PLIN1 and HSL. CGI-58 is subsequently released from PLIN1, and interacts with ATGL on the surfaces of lipid droplets, increasing rates of TAG hydrolysis. Cytosolic HSL translocates and docks through a protein-protein interaction with PLIN1, gaining access to the lipid droplet, where it cleaves DAG. The resulting MAG is cleaved by MGL. Figure reprinted with permission and adapted from Lampidonis *et al*. [22].

PLIN1 [23] and HSL [24]. HSL, once phosphorylated by PKA, translocates from the cytosol and binds to PLIN1 at the surfaces of lipid droplets, gaining access to substrate lipids within the droplet [18,19,25]. Phosphorylation of PLIN1 causes CGI-58 to disperse from PLIN1 on lipid droplets [17]. CGI-58 is then available to interact with ATGL to activate TAG hydrolase activity on the surfaces of lipid droplets [26]. ATGL translocates from the cytosol, increasing binding to lipid droplets through a PLIN1-independent mechanism [15,27]. It is unclear if ATGL binds to lipid droplets through interactions with CGI-58 or G0S2, or directly binds to lipids. With ATGL and HSL now on the surfaces of the lipid droplets, TAG is hydrolyzed to DAG via ATGL working in partnership with CGI-58. DAG is hydrolyzed by HSL to monoacylglycerol (MAG). The remaining MAG is cleaved by monoglyceride lipase (MGL) to release the final FA [28]. In total, one molecule of TAG is hydrolyzed to three molecules of fatty acid and one molecule of glycerol. Fatty acids and glycerol are exported from adipocytes for use by other tissues. The components of these pathways will now be discussed in greater depth.

Hormone-Sensitive Lipase

For 40 years, hormone-sensitive lipase (HSL) was thought to be the major lipase in adipocytes responsible for breaking down TAG, DAG, and MAG. HSL is highly expressed in white adipose tissue (WAT) and brown adipose tissue (BAT), and at lower levels in steroidogenic cells, macrophages, skeletal and smooth muscle [29,30]. *In vitro*, HSL can hydrolyze TAG, DAG, MAG, CE, RE, short chain esters and p-nitrophenyl butyrate [31-35]. Of these substrates, HSL cleaves DAG at a 10-fold

higher rate of hydrolysis than either TAG or MAG. HSL enzymatic activity is regulated through phosphorylation by PKA [24] and AMP-activated Protein Kinase (AMPK) [31]. Under basal, unstimulated, conditions AMPK phosphorylates HSL on serine 565, preventing subsequent phosphorylation by PKA and thus inhibiting HSL lipase activity [32] and translocation to lipid droplets. HSL has three PKA phosphorylation sites: serine 563, serine 659, and serine 660 [24]. *In vitro* phosphorylation of amino acid residues serine 659 and serine 660 causes a 2-fold increase in TAG lipase activity. During β-adrenergic receptor activation of adipocytes, cAMP levels increase to activate PKA [20,21]. PKA phosphorylates both PLIN1 and HSL, allowing HSL to translocate from the cytosol and bind to PLIN1 on lipid droplets [18,25]. Mutagenesis studies suggest that phosphorylation of all three PKA site serine residues of HSL is required for HSL translocation to lipid droplets [33]. HSL, once bound to PLIN1, gains access to substrates within the lipid droplet.

To understand HSL activity, several groups have studied whole-body HSL knockout mouse models [34-36]. Interestingly, these mice were not obese, revealing that HSL is not the sole lipase necessary for TAG hydrolysis in adipose tissue. Instead, these mice showed DAG accumulation in WAT, BAT, testis, skeletal and cardiac muscle, suggesting that HSL functions as a major DAG lipase [36]. Explants of WAT tissue of *HSL*$^{-/-}$ mice were tested for lipase activity in the presence of the β-adrenergic agonist isoproterenol. When compared to WAT from WT mice, WAT from *HSL*$^{-/-}$ mice showed significantly lower release of FA and glycerol over a time course of 3 hours, yet significant lipolysis was still observed [36]. In addition, *HSL*$^{-/-}$ mice are resistant to diet-induced obesity [37], revealing that lipolysis of TAG can

still occur in the absence of HSL. Together, these data reveal that, in the absence of HSL, other enzymes are able to compensate; thus, HSL is not the sole lipase responsible for TAG hydrolysis.

Taken has a whole, the *in vitro* and *in vivo* data suggest that HSL acts as the major DAG lipase in adipocytes. Though *HSL*$^{-/-}$ mice accumulated DAG, they retained the ability to hydrolyze TAG. These observations led researchers to search for additional TAG lipases, which lead to the discovery of ATGL.

Adipose Triglyceride Lipase (ATGL)

In the search for additional adipose TAG lipases, three independent research groups identified transport-secretion protein 2.2 as a TAG hydrolase within a few months of each other. Thus, transport-secretion protein 2.2 gained three different names: adipose triglyceride lipase (ATGL) [38], desnutrin [39], and calcium-independent phospholipase $A_2\zeta$ [40]. ATGL, as it is more predominantly known, cleaves a fatty acyl chain from TAG both in *in vitro* assays [38,40] and when overexpressed in cells [39] but has no further reactivity towards DAG [41]. ATGL has also been shown to have transacylase activity, forming TAG, using DAG and MAG as substrates [40,42]; this activity has only been observed *in vitro* and has yet to be observed *in vivo*. Therefore, ATGL is currently regarded as primarily a TAG lipase.

Detectable levels of ATGL mRNA have been found in various tissues in humans and mice. Although ATGL appears to be ubiquitously expressed, expression is highest in white and brown adipose tissue, with moderate levels in cardiac muscle, skeletal muscle, and testis [38,39,42]. In mice, ATGL mRNA expression

increases in WAT during starvation [39]. These data suggest that ATGL plays a role in mobilizing fatty acids from TAG in adipocytes.

Recent research has provided insight into the regulation of ATGL localization and activity. Bonifacino and colleagues localized ATGL to both endoplasmic reticulum (ER) and lipid droplets and showed that ATGL transport from the ER to the lipid droplet is dependent upon the coat proteins I and II (COPI and COPII) and their regulatory proteins [27]. Previously, these proteins were thought to function in protein transport only between ER and Golgi compartments. This research raises the question as to whether other proteins such as HSL or CGI-58, which also translocate to lipid droplets under specific metabolic conditions, are controlled by these mechanisms. Additionally, during lipolytic stimulation in cultured adipocytes, ATGL translocation to the surfaces of lipid droplets is increased [15,27]. This suggests that ATGL is not a constitutive component of lipid droplets, but is recruited upon hormonal stimulation of lipolysis. It was observed that the protein encoded by G0S2 also translocates to the surfaces of lipid droplets with ATGL [15]. G0S2 mRNA is highly expressed in adipose tissue and increases during differentiation of preadipocytes to adipocytes [43]. G0S2 binds to ATGL and decreases ATGL-mediated TAG hydrolysis both *in vitro* and in cells, even in the presence of the ATGL-activating protein CGI-58 [15,16]. Following β-adrenergic receptor stimulation of adipocytes, lipolysis increases dramatically due to the combined lipase activity of ATGL and HSL. Therefore it is unclear why G0S2, a negative regulator of ATGL activity, translocates to the lipid droplet with ATGL under conditions in which lipase activity is elevated.

As found for HSL, post-translational modifications of lipases are important components of the control of enzyme activity. ATGL is phosphorylated on serine 406 by AMPK both *in vitro* and in cultured cells leading to a small increase in lipase activity [44]. However, the mechanism by which phosphorylation increases ATGL lipase activity is unclear. In adipocytes, AMPK-mediated phosphorylation of HSL prevents subsequent activation of HSL by PKA [32]. Thus, the activation of ATGL-mediated lipolysis by AMPK is counterintuitive; ATGL activity would be increased when HSL (the major DAG lipase) is inactivated. Interestingly, in cultured C_2C_{12} myotubes, a skeletal muscle cell model, neither PKA nor AMPK increase ATGL TAG hydrolase activity [45]. Thus, ATGL phosphorylation has different consequences in different types of cells.

To clarify these data, ATGL phosphorylation was studied *in vivo*, revealing that ATGL is most likely phosphorylated by PKA and not AMPK [46]. These results are complimentary to our current understanding of PKA regulation of HSL lipase activity; PKA mediated phosphorylation activates HSL, thus driving lipolysis. Therefore, it might be expected that ATGL would be modulated by the same, or similar, mechanism. However, phosphorylation of ATGL does not dramatically increase lipase activity in cultured cells [46] and is not necessary for interaction with G0S2 [15]. Therefore, further work is necessary to unambiguously identify the relevant kinase and to determine if phosphorylation of ATGL is required to modulate its interaction with its coactivator, CGI-58, or for ATGL's translocation and interaction with the lipid droplet.

To study ATGL's function, in 2006, Dr. Zechner's group developed a whole-body ATGL knockout mouse. *ATGL*$^{-/-}$ mice maintained on a chow diet (4.5% w/w fat) showed modest weight gain when compared to WT mice on the same diet. Their increased weight was attributed to a doubling of whole body fat mass (both BAT and WAT) rather than a change in lean body mass. Histological sections of both WAT and BAT of the *ATGL*$^{-/-}$ mouse WAT and BAT revealed enlarged lipid droplets, suggesting an impairment of TAG lipolysis. To identify the mechanisms for the increased fat mass, WAT explants from either *ATGL*$^{-/-}$ or WT mice were incubated in the presence of isoproterenol to activate lipolysis. Under these conditions, the WAT explants from *ATGL*$^{-/-}$ mice released 74% less FAs and 78% less glycerol than those of WT mice, revealing reduced stimulated lipolysis and an impairment of complete TAG hydrolysis. These results paralleled *in vivo* findings, since *ATGL*$^{-/-}$ mice displayed lower circulating FA's during fasting conditions than WT mice [47]. These results define ATGL as a major TAG lipase, however they also suggest that there are other unknown lipases that are able to partially compensate for loss of ATGL.

Although ATGL is not expressed as highly in cardiac muscle as it is in adipose tissue, study of *ATGL*$^{-/-}$ mice revealed an important function for ATGL in cardiac energy metabolism. *ATGL*$^{-/-}$ mice, when compared to WT mice, display 1.4 times greater heart weight due to an accumulation of TAG; excessive accumulation of TAG is responsible for premature death from congestive heart failure [47]. Overall, these findings show that ATGL is an important TAG lipase in multiple tissues and plays a key role in TAG hydrolysis in the heart that cannot be compensated for by other

lipases. However, the *ATGL*$^{-/-}$ mice were not extremely obese; these data suggest that adipocytes have other mechanisms that can compensate for TAG hydrolysis.

Comparative Gene Identification 58 (CGI-58)

In 2000, Lin *et al*. aligned the *Caenorhabditis elegans* genome sequence with the protein sequences predicted by the human genome project in a search for orthologs [48]. Through use of bioinformatics, 150 Comparative Genes were Identified and thus each was termed a CGI followed by an identification number. A year later, mutations in the CGI-58 gene were associated with a condition known as Neutral Lipid Storage Disorder (NLSD) [49]. CGI-58 is the fifth member of the α/β hydrolase (ABHD) protein family and is therefore also referred to as α/β hydrolase domain 5 (ABHD5). To date, 19 different mutations (either single base substitutions or truncations) in the gene for CGI-58/ABHD5 have been identified that cause NLSD [50].

In 1974, NLSD was identified as a rare autosomal disorder characterized by excess accumulation of TAG in various tissues and cell types including: skin fibroblasts, liver, striated muscle, intestinal mucosa, and neutrophils [51-53]. These findings suggest that CGI-58 functions in normal turnover of TAG in multiple tissues. Some patients also suffer from hearing loss, stunted growth and mental retardation. Interestingly, these patients have not been reported to be obese. In 1997, researchers studying NLSD were able to categorize patients as having either NLSD with ichthyosis (NLSDi) or NLSD with myopathy (NLSDm) [54]. NLSDm patients suffer from skeletal muscle myopathy and cardiomyopathy. Interestingly, these

patients did not have ichthyosis, which is observed in the NLSDi patients [55,56]. More recently, NLSDi has been linked to mutations in the gene encoding CGI-58 [49], whereas NLSDm has been linked to mutations in the gene encoding ATGL [56]. These two studies confirmed that NLSDi and NLSDm are distinct variations of NLSD caused by various mutations in two different genes.

Based on its amino acid sequence, CGI-58 has been predicted to belong to a class of enzymes called α/β hydrolases [49]. Members of this family are predominantly lipases, esterases, and thioesterases. α/β hydrolases have a defined conserved catalytic triad containing an acidic residue (normally an aspartate), a basic residue (normally a histidine), and a nucleophilic serine residue in the consensus sequence GXSXG. However, in CGI-58, an asparagine residue replaces this serine residue [49]. Although CGI-58 does not function as a TAG lipase [41], the NLSD phenotype suggests that CGI-58 has an important role in maintaining TAG homeostasis.

CGI-58 increases TAG hydrolysis catalyzed by ATGL

In 2006, Zechner's group reported that ATGL binds to CGI-58 in a one-to-one molar ratio, causing a 20-fold increase in TAG hydrolytic activity *in vitro* [41]. These experiments were initially done by mixing post-nuclear COS-7 cell lysates containing ectopic CGI-58 with cell lysates containing ectopic ATGL. To date, experiments showing this synergy effect while using both purified CGI-58 and purified ATGL have not been published, although multiple groups have now reported purifications of both proteins. Thus, there may be an additional component

contributed by the cell lysates that enhances synergy. However, if an additional component contributes to the observed synergy, then it can be supplied by cell lysates of both bacterial and mammalian cells [57]. Further work is necessary to determine if synergy can be observed with purified ATGL and purified CGI-58 or if an additional factor is required, and whether this factor is another protein or a small molecule.

ATGL belongs to the patatin-like phospholipase domain containing (PNPLA) family of proteins [58], whereas CGI-58 is a member of the ABHD family of proteins [49]. Although the crystal structure of neither protein has been solved, the patatin (α/β/α) fold is predicted to be close to ATGL's N-terminus, while a hydrophobic domain is predicted near the C-terminus [59]. In contrast, CGI-58 contains a predicted α/β hydrolase fold close to its C-terminus. Humans with truncations in ATGL removing sections of the C-terminus have NLSDm [56]. Although these truncated forms of ATGL contain the lipase consensus sequence, ATGL function in TAG homeostasis is impaired. Hence, the C-terminal domain must play an as yet undefined role in localization or regulation of activity. Further, little is known about the functional role of either the N-terminal region or the α/β hydrolase domain of CGI-58.

Recently, Oberer's group has studied partially purified recombinant truncated forms of ATGL to determine the role of the various domains in ATGL function [60]. ATGL is 486 amino acids long with amino acids 1-254 critical for lipase activity. Interestingly, truncation of the C-terminus yields a form of ATGL with greatly increased TAG lipase activity *in vitro* when compared to full length ATGL.

However, this truncated protein was unable to localize to lipid droplets when expressed in cultured cells. These results revealed that the C-terminus of ATGL is inhibitory to TAG lipase activity, yet necessary for the translocation of ATGL from the cytosol to the surfaces of lipid droplets, where ATGL gains access to TAG. It is possible that CGI-58, when bound to ATGL, causes a conformational change in ATGL, moving the inhibitory C-terminus into a position that does not interfere with ATGL TAG hydrolase activity.

To investigate how ATGL and CGI-58 interact, Oberer and colleagues examined the binding of truncated forms of CGI-58 and ATGL to each other and to lipid droplets, and the consequent effects on ATGL's TAG lipase activity [57]. By expressing YFP-tagged truncated forms of CGI-58 in cultured COS-7 cells, Oberer's group determined that truncation of the first 32 amino acids completely abolished targeting of CGI-58 to lipid droplets. This truncated form of CGI-58 was also unable to activate ATGL TAG lipase activity *in vitro* and showed a 30% reduced ability to bind to ATGL in an enzyme-linked immunosorbent assay (ELISA). The first 32 amino acids of CGI-58 contain three tryptophan residues that these researchers hypothesized to be important for activation of ATGL. When the tryptophan residues at positions 21, 25, and 29 were mutated to alanine residues, CGI-58 was able to bind to ATGL in an ELISA, but unable to increase ATGL TAG lipase activity. Moreover, CGI-58 with the tryptophan to alanine mutations failed to localize to lipid droplets. Collectively, these results suggest that the N-terminal region of CGI-58 is important for CGI-58's interaction with lipid droplets; however, this region is not critical for binding to ATGL.

It has been hypothesized that ATGL has an inhibitory domain in its C-terminus that requires interaction with CGI-58 to produce optimal lipase activity [57,60]. However, to date, the mechanism of how CGI-58 increases ATGL activity has not been clearly defined. Further studies are needed to determine whether binding of CGI-58 to ATGL changes the conformation of ATGL, or activates TAG hydrolase activity through a different mechanism such as presentation of substrate to ATGL, or removal of end products to reduce inhibition of activity.

Study of CGI-58 function using mouse models

To study CGI-58 function, Zechner and colleagues created a *CGI-58*$^{-/-}$ mouse [61]. These mice died within 16 hours after birth and were smaller in both size and weight relative to newborn WT mice. An analysis of the *CGI-58*$^{-/-}$ mouse carcass revealed 1.8-fold increased TAG content when compared to WT littermates. The knockout mice had glossy, dry skin that prevented movement and caused complete dehydration; thus the mice were unable to suckle. Even by increasing chamber humidity and applying Vaseline® to the mice, the researchers were not able to prolong their lifespan. Since *ATGL*$^{-/-}$ mice did not display a skin barrier defect comparable to *CGI-58*$^{-/-}$ mice, these data suggest an important role for CGI-58 that is independent of ATGL. In addition, the phenotypes of both humans with CGI-58 mutations and *CGI-58*$^{-/-}$ mice suggest an important function of CGI-58 in the formation of a proper skin barrier to prevent dehydration.

To explore this hypothesis, Zechner and colleagues utilized ultra performance liquid chromatography-tandem mass spectrometry to observe changes

in lipid composition of the epidermis of WT, *ATGL*$^{-/-}$, and *CGI-58*$^{-/-}$ mice [61]. When compared to WT or *ATGL*$^{-/-}$ mice, *CGI-58*$^{-/-}$ mice showed significantly reduced levels of protein-bound ω-OH-ceramides and elevated levels of free ω-OH-ceramides. Moreover, acylceramides (free ω-OH-ceramides esterified to oleic or linoleic acid) were undetectable only in the skin of *CGI-58*$^{-/-}$ mice. Although CGI-58's role in the epidermis is not currently understood, this study strongly suggests an ATGL-independent function of CGI-58. Moreover, humans with NLSDi do not characteristically have heart function defects, and survive longer than humans with ATGL mutations, many of whom have heart disease [55,56,62].

To overcome the lethality of CGI-58 ablation, Dr. Mark Brown and colleagues utilized CGI-58 antisense oligonucleotides (ASOs) to reduce CGI-58 levels and thereby study the function of CGI-58 in tissues [63]. In these experiments, ASO treatment caused an 80-95% knockdown of CGI-58 mRNA and protein expression in WAT and liver and a 50% or greater knockdown in BAT, heart, skin, and spleen. When fed a high fat diet (HFD) (45% energy from fat) over 8 weeks, the CGI-58 ASO treated mice were resistant to diet-induced obesity relative to control ASO treated mice. Although they were not obese, CGI-58 ASO treated mice showed hepatic steatosis when fed either a HFD or chow, but the steatosis was more severe with the HFD. Following a HFD feeding, hepatic DAG and ceramides were elevated, while FA and long chain fatty acyl-CoAs were reduced in ASO-treated mice relative to control mice. In mice on a chow diet, CGI-58 knockdown did not affect body weight, but caused a 50% decrease in epididymal fat pad weight relative to control mice; this observation contrasts with the expectation that WAT mass should be elevated when

reducing expression of a factor (CGI-58) needed for ATGL-mediated TAG turnover. Once again, these results contrast with findings in *ATGL*$^{-/-}$ mice, suggesting that CGI-58 serves additional functions that are unrelated to ATGL in WAT. Moreover, the phenotype of the CGI-58 ASO treated mice resembles the phenotype of NLSDi patients; TAG accumulates in various tissues in the absence of obesity.

CGI-58 is highly expressed in cultured adipocytes, making these cells a great model to study endogenous CGI-58 localization. In 3T3-L1 adipocytes, CGI-58 localizes to lipid droplets by binding to the carboxyl-terminus of PLIN1 during basal conditions (mimicking fed conditions) and is released into the cytosol following PLIN1 phosphorylation during lipolytic stimulation [17,26,64]. Upon release from PLIN1, CGI-58 binds to ATGL at the surfaces of lipid droplets, promoting ATGL hydrolysis of TAG [26]. At this time, it is unclear whether CGI-58, ATGL, or both proteins interact with the phospholipid monolayer of adipocyte lipid droplets. In fibroblasts and most other cells, lipid droplets are coated with perilipin 2 (PLIN2); CGI-58 is less abundant, and dispersed throughout the cytosol [17], where ATGL is located. To catalyze TAG hydrolysis, both ATGL and CGI-58 need to translocate to the surfaces of lipid droplets. Recent data from Sztalryd and colleagues suggests that CGI-58 recruits ATGL to lipid droplets in cells where PLIN2 is the major lipid droplet protein [65], although it is still unclear how CGI-58 and ATGL interact with the surfaces of lipid droplets.

Monoglyceride Lipase (MGL)

In 1976, Belfrage and colleagues purified monoglyceride lipase (MGL) from rat adipose tissue [28]. *In vitro*, MGL was observed to cleave 1-MAG and 2-MAG at equal rates, but not TAG or DAG. For many years MGL has been considered the major lipase necessary for cleavage of MAG in adipocytes. MGL belongs to the α/β hydrolase fold family of lipases and esterases and is ubiquitously expressed, with high mRNA levels in adipose tissue, kidney and testis [66]. *MGL*$^{-/-}$ mice have increased levels of MAG in adipose tissue, brain and liver [67], demonstrating that MGL is necessary for cleaving MAG in these tissue and organs. These knockout mice also exhibited increased levels of 2-arachidonoyl glycerol [67], which has been previously identified as a potent signaling molecule regulating food intake [68]. However, whole body *MGL*$^{-/-}$ mice did not display differences in energy intake compared to WT mice [67]. Tissue specific knockout models may further define the role that MGL plays in 2-arachidonoyl glycerol generation.

PLIN1 (Perilipin 1)

PLIN1 is the most well studied member of the perilipin family. In 1991, Greenberg *et al*. identified a new protein enriched in the fat cake of rat epididymal adipocyte lysates subjected to centrifugation [23]. This protein is highly abundant in cultured 3T3-L1 adipocytes and less abundant in steroidogenic cells [69]. In both types of cells, PLIN1 is located around the perimeter of lipid droplets; thus it was named perilipin, which is Greek for “surrounding lipid.” There are three protein isoforms that arise from splice variants of PLIN1: PLIN1A, 1B, and 1C [70,71].

PLIN1A and 1B are expressed in adipocytes, while PLIN1A and 1C are expressed in steroidogenic cells. Ectopic PLIN1A expression in 3T3-L1 pre-adipocytes (cells that do not normally express PLIN1) causes a 6-30 fold increase in TAG content relative to controls cells [72]. This work suggests that PLIN1 functions to limit the access of lipases to lipid droplets, thus protecting the TAG content of adipocytes from lipases.

The access of lipases to the lipid droplet depends on PLIN1's phosphorylation state. PLIN1 is phosphorylated on multiple sites by PKA [23] and dephosphorylated by protein phosphatase 1 [73] (Figure 2). In order for HSL to interact with PLIN1, both proteins must be phosphorylated by PKA [18,25,33]. In 2003, Greenberg and colleagues defined the phosphorylation sites of PLIN1 in relation to HSL activity [74]. They used C-terminal FLAG epitope-tagged PLIN1 constructs in which PKA site serine residues were mutated to alanine, to show that binding of HSL to lipid droplets during PKA stimulated lipolysis was regulated by phosphorylation of one or more of the first three PKA site serine residues (S81, S222, and S276). It was later confirmed that all three serine residues (S81, S222, and S276) must be phosphorylated for HSL to bind to PLIN 1A [25]. This binding interaction is required for HSL catalyzed lipolysis, presumably by bringing HSL into contact with lipid substrates. Phosphorylation of these PKA sites, as well as three others (S433, S492, and S517) was implicated in facilitation of PKA stimulated lipolysis by non-HSL lipases [74]. Greenberg and colleagues later confirmed these findings, revealing serine residue 517 as the "master regulator" of PKA stimulated lipolysis [75]. Overexpression of PLIN1 harboring an alanine substitution of serine 517 eliminated 95 percent of PKA-stimulated release of fatty acids and glycerol

Figure 2

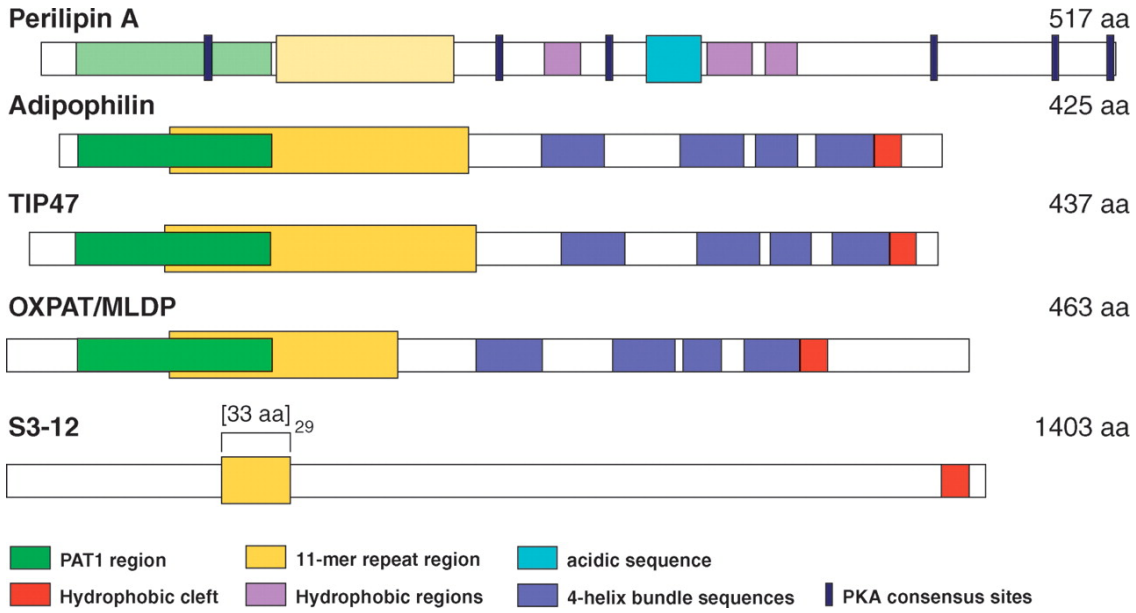

Figure 2. Structural features of the perilipin family of proteins. This image depicts the sequence similarity of perilipin family members PLIN1 (Perilipin A), PLIN2 (Adipophilin), PLIN3 (TIP47), PLIN4 (S3-12), and PLIN5 (OXPAT/MLDP). In this image, lighter colors represent areas of low sequence homology and darker colors represent areas of high sequence homology. The highly conserved amino terminal PAT1 regions of PLIN1-3, and 5, yet lacking in PLIN4, are important for interaction with HSL. PLIN2, 3, and 5 have a 4-helix amphipathic bundle sequence. In PLIN3, this sequence is predicted to collapse when cytosolic and open while interacting with the surfaces of lipid droplets [76]. The 4-helix bundle sequence is not found in PLIN1, instead, a hydrophobic and acidic region is present. PLIN2-5 contains a hydrophobic cleft near the C-terminal region. In PLIN3, this region is predicted to interact with a small molecule or lipid [76]. Figure reprinted with permission from Brasaemle [77].

relative to cells overexpressing WT PLIN1. When ATGL was present, phosphorylation of this site contributes to the control of lipolysis catalyzed by ATGL with CGI-58.

In cultured adipocytes, the carboxyl-terminus of PLIN1 is able to bind CGI-58 under basal (unstimulated) conditions [17,26,64]. Following PKA activation, CGI-58 is released from PLIN1 and disperses throughout the cytosol [17]. CGI-58 binds to the TAG lipase ATGL and increases its lipase activity *in vitro* [41]. Imaging work in live cultured fibroblasts expressing fluorescent fusion proteins of these three proteins suggests that CGI-58 needs to be released from PLIN1 before it can interact with ATGL [26]. These results suggest that during PKA stimulation, CGI-58 is released from PLIN1 to the cytosol to recruit ATGL to the lipid droplet, thus initiating TAG lipolysis.

To study PLIN1 function, PLIN1 knockout mice (*PLIN1*$^{-/-}$) were generated, and revealed an interesting phenotype [78]. Though *PLIN1*$^{-/-}$ mice consumed equal amounts of food relative to WT mice, they had 30% less fat mass, increased lean body mass, and an increased metabolic rate [78,79]. Adipocytes isolated from *PLIN1*$^{-/-}$ mice showed elevated basal lipolysis and reduced stimulated lipolysis. This is most likely attributable to the compensatory increase in protein levels of PLIN2 on lipid droplets of adipocytes of *PLIN1*$^{-/-}$ mice [79]. PLIN2, unlike PLIN1, is not phosphorylated by PKA and does not coordinate major recruitment of HSL or ATGL/CGI-58 to lipid droplets. Therefore, these lipases are able to gain access to the lipid droplet under basal conditions, thus increasing rates of lipolysis. These observations support previous findings that PLIN1 regulates lipolysis; *PLIN1*$^{-/-}$ mice

are unable to regulate access of lipases to lipid droplets so basal lipolysis is higher, and stimulated lipolysis is also reduced, likely due to two factors: 1) total TAG is reduced and 2) PLIN1 is not available to recruit HSL to lipid droplets.

In humans, two frame-shift mutations in PLIN1 have been described that cause lipodystrophy, hypertriglyceridemia, insulin resistance, and type 2 diabetes [80]. PLIN1 harboring these mutations (Leu-404fs and Val-398fs) were overexpressed in 3T3-L1 preadipocytes, and caused an increase in basal lipolysis [81]. These variants lack the C-terminal region of PLIN1, which interacts with CGI-58 [17]; thus CGI-58 is not sequestered under basal conditions and can interact with ATGL to increase TAG hydrolysis. Use of siRNA to knock down protein expression of either CGI-58 or ATGL in cell lines stably expressing these PLIN1 variants reduced basal lipolysis [81], suggesting that one of the mechanisms by which PLIN1 regulates basal lipolysis is through preventing CGI-58 from interacting with ATGL.

Overall, these efforts have described PLIN1 as a scaffolding protein on the surface of lipid droplets that binds various proteins. It interacts with the DAG lipase HSL and the ATGL co-activator CGI-58, thus providing an essential role in regulating lipolysis in adipocytes under both stimulated and basal conditions.

PLIN2 (ADRP, ADFP, Adipophilin)

PLIN2 was first discovered in 1992 by Serrano *et al.* as a mRNA that increases in quantity during adipocyte differentiation; therefore, it was named adipose differentiation related protein (ADRP) [82]. Brasaemle, *et al*. scanned various cultured cell lines for mRNA expression of PLIN2 in mouse tissues and

found that it is ubiquitously expressed [83]. Interestingly, they observed PLIN2 on the surfaces of lipid droplets only in pre-adipocytes and during early stages of adipose differentiation; during later stages of differentiation it is replaced by PLIN1, which coats the larger, mature lipid droplets of fully differentiated adipocytes. Wolins and colleagues later observed that the addition of fatty acids to cultures of fully differentiated adipocytes drives cytosolic PLIN2 onto the surfaces of both small and large lipid droplets [84]. These results suggest that PLIN2 has a role during the development of lipid droplets and under high fat conditions.

Overexpression of a GFP-PLIN2 fusion construct in 3T3 fibroblasts (which endogenously express PLIN2) revealed a 2-fold increase in cellular TAG content when cells were incubated in growth medium with or without serum relative to control cells under similar conditions [85,86]. These results demonstrate the ability of PLIN2 to have a protective effect on cellular TAG levels in a fibroblast line, which contain low levels of ATGL and CGI-58. Relative to PLIN1, PLIN2 is not altered under stimulated (PKA-activated) conditions. PLIN2 binds HSL [25], but does not facilitate major recruitment of HSL to lipid droplets, and PLIN2 does not interact with ATGL or CGI-58 [26,65]. Therefore, PLIN2 is not protective against ATGL-mediated TAG hydrolysis because it is unable to sequester CGI-58 from interacting with ATGL.

To study PLIN2 function in a mouse model, Chan and colleagues created a PLIN2 knockout mouse (*PLIN2*$^{-/-}$) [87]. *PLIN2*$^{-/-}$ mice were resistant to HFD-induced fatty liver and displayed normal adipogenesis and fat mass *in vivo*, revealing that PLIN2 is not essential for the development or function of adipose tissue. Although

these mice showed similar hepatic FA uptake, hepatic β-oxidation, VLDL secretion, and plasma TAG levels relative to WT mice, *PLIN2*$^{-/-}$ knockout mice had 60% less hepatic TAG content. The results of this study suggest that PLIN3 [88] and PLIN5 [89,90], which are also expressed in the liver, are unable to fully compensate for the role that PLIN2 may have in the formation of new lipid droplets in hepatocytes [84]. The investigators did not report skeletal muscle TAG content; it is possible that PLIN2 also plays an important role in muscle. Overall, PLIN2 is a ubiquitously expressed protein that plays a role in the formation of new lipid droplets. PLIN2 is relatively permissive to lipolysis and lacks the ability to regulate lipolysis via post-translational mechanisms such as phosphorylation.

PLIN3 (TIP47, M6PRBP)

Tail interacting protein of 47 kDa (TIP47, PLIN3) was first identified in a yeast two-hybrid screen for proteins that interact with the mannose 6-phosphate receptor binding protein (M6PRBP) in the endosomal/*trans*-Golgi transport pathways [91]. In 2001, Brasaemle and colleagues observed that the amino acid sequence of PLIN3 is 43% similar to PLIN1 and PLIN2 (Figure 2), and thus hypothesized that PLIN3 localizes to lipid droplets [88]. They used immunofluorescence microscopy to show that endogenous PLIN3 and M6PR do not co-localize in HeLa cells; PLIN3 localizes diffusely throughout the cytosol, whereas M6PR localizes to specific structures adjacent to the nucleus. Under fatty acid supplemented conditions, both PLIN3 and PLIN2 localize to lipid droplets in HeLa cells and co-localized to the same lipid droplets. Thus, PLIN3 is a lipid droplet

protein that can reversibly translocate between the cytosol and the surfaces of lipid droplets.

The crystal structure of PLIN3's C-terminal region (~60%) has been solved [76]. This region, which is conserved in PLIN2 and PLIN5, folds into a four-helix bundle of amphipathic alpha helices, with a separate sequence forming a hydrophobic cleft hypothesized to interact with a small hydrophobic molecule or lipid (Figure 2). This structure is highly similar to the four-helix bindle of the amino terminus of apolipoprotein E [92], an exchangeable apolipoprotein. Apolipoprotein E can be both soluble in the blood stream and bound to lipoproteins, the key to this behavior is the collapsible four-helix bundle [93]. Thus, it is possible that the four α-helices of PLIN3 also open to bind to lipid droplets via the hydrophobic surfaces of the helices and retract when the protein is cytosolic [77]. This structure supports the previous findings that PLIN3 is both a cytosolic and a lipid-droplet bound protein, unlike PLIN1, which is constitutively bound to lipid droplets and rapidly degraded in the absence of stored lipids [94,95].

Recent work has shown that PLIN3 is ubiquitously expressed [88,91,96] and functions in the formation new lipid droplets [97,98]. Interestingly, these studies reveal that when silencing PLIN3 mRNA expression in cultured cells, PLIN2 mRNA expression increases as a compensatory mechanism. Wolins and colleagues have found that PLIN3 localization to lipid droplets increases around tiny nascent lipid droplets when fatty acids are added to cultured differentiated 3T3-L1 adipocytes [84]. Thus, PLIN3 may support the rapid formation of new lipid droplets. Together,

these findings define PLIN3 as playing an important role in the formation of new lipid droplets PLIN3 is not thought to control TAG lipolysis.

PLIN4 (S3-12)

PLIN4 (originally named S3-12) was identified in a screen for adipocyte-specific secreted or plasma membrane proteins [99]. PLIN4 is expressed at low levels in heart, and skeletal muscle, and higher levels in adipocytes of WAT [99,100]. In 2003, Wolins *et al.* used immunofluorescence microscopy to show PLIN4 localization to tiny lipid droplets in cultured 3T3-L1 adipocytes [84,100]. When adipocytes were incubated with oleate over a time-course of four hours, PLIN3 and PLIN4 localized to the smallest, newly formed lipid droplets, PLIN2 coated intermediate-sized lipid droplets, and PLIN1 coated only the largest, most mature droplets [84]. These results suggest a role for PLIN4 in the formation of new lipid droplets in adipocytes; like PLIN3, PLIN4 has not been defined as having a role in coordinating lipase interaction with lipid droplets. Interestingly, PLIN1 and PLIN4 were not observed on the same lipid droplets, therefore there is likely an undefined mechanism that removes or degrades PLIN4 from the growing lipid droplet when it is replaced by PLIN1 during droplet maturation.

PLIN5 (MLDP, OXPAT, LSDP5, PAT1)

In 2006, Yamaguchi *et al.* and Wolins *et al.* discovered a fifth member of the perilipin family in highly oxidative tissues, such as smooth and skeletal muscle, thus naming it MLDP (myocardial lipid droplet protein) [89] or OXPAT [90], respectively.

PLIN5 is highly expressed in brown adipose tissue, heart, and skeletal muscle and at lower levels in liver. PLIN5 and PLIN2 coat the same lipid droplets within these tissues. Ectopic expression of PLIN5 in cultured COS-7 fibroblasts increased TAG accumulation relative to control cells ectopically expressing β-galactosidase [90], suggesting that PLIN5 plays a role in controlling lipase access to lipid droplets. PLIN5 was found to be both cytosolic and on the surfaces of lipid droplets under fasting, low insulin conditions, when lipase activity is increased [89,90,101].

PLIN5 controls ATGL and HSL activity unlike the other members of the perilipin family. PLIN5 binds HSL under basal unstimulated conditions through a conserved amino terminal sequence found in PLIN1, 2, 3, and 5 (Figure 2) [25]. However, this interaction does not increase the rate of lipolysis; lipolysis increases only following activation of PKA, presumably through phosphorylation and activation of HSL. The carboxyl terminal region of PLIN5 is able to bind either ATGL or CGI-58 [65,102], but not both simultaneously [102]. PLIN5, when HSL or ATGL is bound, reduces TAG hydrolysis in the absence of PKA stimulation [65]. However, under PKA-stimulated conditions, PLIN5 is phosphorylated, by either PKA or an unidentified kinase downstream of PKA, leading to an increase in lipolysis through an as yet undefined mechanism. It is possible that phosphorylation of PLIN5 releases CGI-58 and ATGL, allowing the two proteins to interact at the surfaces of lipid droplets, thus increasing hydrolysis of TAG. Subsequent studies identifying the phosphorylation sites and relevant kinase and investigating the consequences of alanine substitutions of these sites would help to identify the mechanism by which phosphorylation of PLIN5 affects lipolysis.

Given that PLIN5 is expressed in highly oxidative tissues, PLIN5 has been hypothesized to play a role in channeling fatty acids towards mitochondria for β-oxidation [90,103,104]. Recently, PLIN5 has been shown to either 1) localize to mitochondria in smooth and skeletal muscle cells [104], or 2) link lipid droplets to mitochondria by binding to lipid droplets, but interacting with an as yet unidentified component of mitochondria through a carboxyl terminal sequence of PLIN5 [103]. Together, these results suggest that PLIN5 has a functional role in mediating ATGL-dependent lipolysis, releasing fatty acids in close proximity to the mitochondria for β-oxidation.

CGI-58 has LPAAT activity

Recently, CGI-58 has been identified as a LPAAT. Rajasekharan's group was the first to publish this finding [105]. In these studies, recombinant 6-His tagged CGI-58 was expressed in the *E. coli* strain Bl21(DE3) and purified using a nickel affinity resin. To assay for LPAAT activity *in vitro*, partially purified CGI-58 was mixed with a lysophospholipid acceptor and a radiolabeled fatty acyl-CoA donor and the production of radiolabeled phospholipids was evaluated. After testing various combinations of acceptor and donor lipids, LPA was identified as the only significant acceptor molecule. Oleoyl-CoA, palmitoyl-CoA, and stearoyl-CoA were all useful acyl group donor molecules, however oleoyl-CoA was the preferred substrate. The product of the enzyme reaction was phosphatidic acid (PA).

In support of these findings, our group has published additional findings on CGI-58 LPAAT activity, as well as more detailed kinetic analysis [106]. We reported

that CGI-58 is also able to utilize arachidonoyl-CoA as a fatty acyl donor and that oleoyl-CoA and arachidonoyl-CoA were preferred substrates. To further understand lipid-binding activity of CGI-58, the intrinsic fluorescence of CGI-58's tryptophan residues was measured in the presence of increasing substrate concentrations. Addition of lipid substrates quenched tryptophan fluorescence; the apparent dissociation constants were determined for LPA (K_d = 0.063 μM), arachidonoyl-CoA (K_d = 0.16 μM), oleoyl-CoA (K_d = 1.08 μM), and palmitoyl-CoA (K_d = 0.62 μM) [106]. These results support the previous findings that oleoyl-CoA is a preferred substrate. Moreover, by saturating CGI-58 with oleoyl-CoA and then sequentially adding increasing concentrations of LPA, additional quenching of CGI-58's tryptophan fluorescence was reported. These results suggest that oleoyl-CoA and LPA bind two different sites on CGI-58.

These findings raise a very important question; what is the fate of PA produced by CGI-58? PA can serve as either a signaling molecule or an intermediate in TAG or phospholipid synthesis. It is also unclear if CGI-58 LPAAT activity is necessary to activate TAG hydrolase activity of ATGL.

Lysophosphatidic Acid Acyltransferases

There are ten related putative acylglycerolphosphate acyltransferase (AGPAT) enzymes found in humans, all sharing four conserved sequence motifs; these enzymes are also referred to as LPAATs (Figure 3). Most of these enzymes have been characterized as having LPAAT activity: AGPAT1 (LPAAT-α) [107-110], AGPAT2 (LPAAT-β) [109-111], AGPAT 7 [112], and AGPAT9 [113]. AGPAT3, 4, and 5

Figure 3

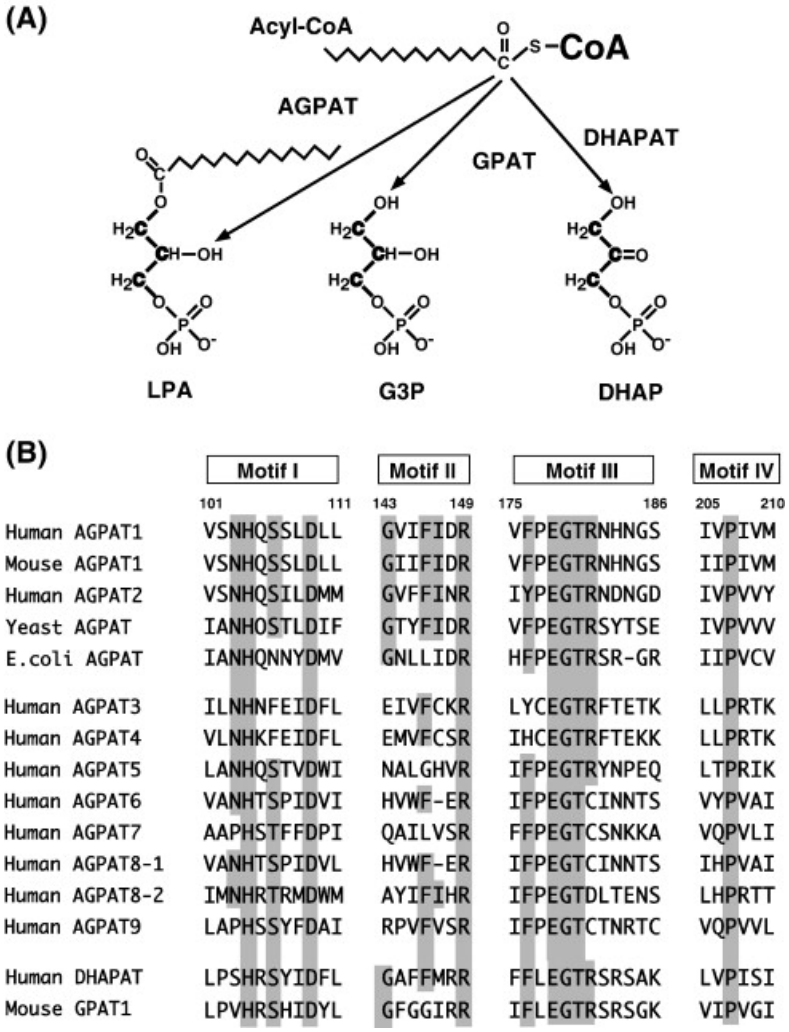

Figure 3. Conserved sequence motifs found in all acyltransferases. Motif I contains histidine and aspartate residues that are necessary for catalysis of the reaction [114]. Motif I and the conserved proline of motif III are predicted play a role in acyl-CoA binding. Motif II and III are responsible for lysophospholipid, glycerol 3-phosphate, or dihydroxyacetone binding. Of the four conserved motifs, CGI-58 was reported to contain motif I, the acyltransferase active site residues [105,106]. Figure was reprinted with permission from Yamashita *et al* [114].

display LPAAT activity, but are much less active than AGPAT2 [115], suggesting that there may be other possible substrates in addition to LPA and oleoyl-CoA. Not all putative AGPATs display LPAAT activity (reviewed in [116]); AGPAT7 and 9 preferentially use lysoPC as a substrate [117-119]. For this chapter I will focus on AGPAT1 and AGPAT2 since they are well defined as LPAATs both *in vitro* and *in vivo* and their activity is similar to CGI-58's recently described LPAAT activity.

AGPAT1 and AGPAT2 mRNA are ubiquitously expressed [111,120,121]. AGPAT1 expression is highest in skeletal muscle, kidney, and testis, while AGPAT2 expression is highest in visceral adipose tissue, liver, and heart. The enzymes vary slightly in their acyl-CoA substrate preferences; AGPAT1 prefers 14:0, 16:0, and 18:2 acyl-CoA, but can also use 18:0, 18:1 and 20:4 acyl-CoA [110]. In contrast, AGPAT2 prefers 18:1 acyl-CoA and has moderate activity towards 14:0, 16:0 and 18:2 acyl-CoA. In cultured COS-7 or CHO fibroblasts, AGPAT1 and AGPAT2 are localized to the ER [120,122,123]. In contrast, CGI-58, is localized either diffusely in the cytoplasm or on the surfaces of lipid droplets, bound to PLIN1 in cultured adipocytes [17]. Interestingly, none of the previously described AGPATs belong to the α/β hydrolase-fold family of proteins, making CGI-58 the only member of that protein family to show LPAAT activity. However, the enzyme activity of many members of the ABHD family is as yet uncharacterized.

AGPATs, as well as glycerol phosphate acyltransferases and dihydroxyacetone-phosphate acyltransferases, have four conserved sequence motifs characteristic of acyltransferases (Figure 3) [116]. Motif I consists of histidine and aspartate residues separated by four amino acid residues, that, along with a

conserved proline residue in motif IV, are hypothesized to be important for acyl-CoA binding [114]. Studies of AGPAT1 reveal that a substitution of either residue in motif I with alanine causes a dramatic in acyltransferase activity [114], suggesting that these are active site residues. Motif II has conserved phenylalanine and arginine residues, while motif III has conserved glutamate, glycine, and threonine residues. Together, motif II and motif III are hypothesized to be responsible for LPA binding. Interestingly, CGI-58 has been reported to contain only motif I of the four motifs characteristic of known acyltransferases [105,106]. Further studies on CGI-58 structure/function relationships are required to determine how CGI-58 binds LPA or an acyl-CoA without the other conserved motifs.

In humans, mutations in AGPAT2 cause congenital generalized lipodystrophy type 1 [124]. Patients suffer from hyperinsulinemia, dyslipidemia, insulin resistant diabetes, hyperphagia, and an inability to store TAG in adipose tissue [125]. Interestingly, patients lacked metabolically active fat pads including both subcutaneous and visceral fat depots, although they retain mechanical, non-metabolically active fat pads in the palms of hands and soles of feet [126,127]. In contrast, NLSDi patients (humans lacking functional CGI-58) display an accumulation of TAG in various tissues, suggesting that PA produced by CGI-58 is not used as an intermediate for TAG synthesis.

To better understand the role of AGPAT2 in congenital generalized lipodystrophy type 1, an AGPAT2 knockout (*AGPAT2*$^{-/-}$) mouse was generated [128]. About 80% of *AGPAT2*$^{-/-}$ mice did not survive to weaning due to hyperglycemia or hypothermia. Those that survived past weaning completely lacked brown and white

adipose tissue; they had 2% body fat relative to the 24-29% body fat of WT mice. These data support previous findings that AGPAT2 is necessary for adipocyte differentiation in cultured cells [123]. Interestingly, reducing AGPAT2 protein levels in cultured adipocytes leads to decreased TAG storage but no change in overall levels of PA or other phospholipids. These data suggest that, in adipocytes, PA produced from AGPAT2 is converted to TAG.

Due to the absence of adipose tissue, *AGPAT2*$^{-/-}$ mice have very low circulating leptin, leading to hyperphagia. *AGPAT2*$^{-/-}$ mice also display enlarged kidneys, small intestine, spleen, and liver [128]. Compared to WT mice, *AGPAT2*$^{-/-}$ mice have up to 6.4-fold increased liver TAG, suggesting that an alternate AGPAT is required for TAG synthesis in liver. Excessive hepatic TAG accumulation was attributed to dietary fat intake and *de novo* fatty acid synthesis from dietary carbohydrates; there were no impairments in hepatic fatty acid β-oxidation or VLDL secretion. Adenoviral-driven overexpression of human AGPAT1 or AGPAT2 in *AGPAT2*$^{-/-}$ mice did not reduce hepatic TAG levels, suggesting that hepatic TAG accumulation is due to the lack of adipose tissue in *AGPAT2*$^{-/-}$ mice [129]. Overall, the phenotype of *AGPAT2*$^{-/-}$ mice is drastically different than that of *CGI-58*$^{-/-}$ mice. As described in the CGI-58 section of this chapter, *CGI-58*$^{-/-}$ mice unable to wean due to a skin barrier defect impairing their ability to move, and die shortly after birth [61]. TAG levels were elevated in the carcasses of *CGI-58*$^{-/-}$ mice and livers of *AGPAT2*$^{-/-}$ mice, however *AGPAT2*$^{-/-}$ mice do not display a lethal skin barrier defect, suggesting that these two enzymes function in different pathways.

Although CGI-58 has been described as a LPAAT *in vitro*, a comparison of *AGPAT2*$^{-/-}$ and *CGI-58*$^{-/-}$ mice show two distinct phenotypes. Likewise, the phenotypes of congenital generalized lipodystrophy type 1 and NLSDi patients are very different; the latter patients suffer from a lack of TAG synthesis, where as NLSDi patients accumulate TAG in various tissues. It is possible that the PA produced by CGI-58 is directed towards a signaling pathway or phospholipid synthesis rather than towards TAG synthesis. Overall, these data describe CGI-58 as an LPAAT with unique cellular localization, structure, and physiological relevance.

Specific Aims

Given the phenotype of excessive TAG in many cells and tissues of NLSDi patients, CGI-58 must play a critical role in lipid homeostasis. To date, CGI-58 has been described as a LPAAT [105,106] and a co-activator of ATGL [41]. The major question we sought to address in this dissertation project is whether CGI-58 LPAAT activity is necessary for activation of ATGL TAG hydrolase activity. The first step of this project was to identify the active site residues responsible for LPAAT catalytic activity, most likely a conserved acidic residue and a conserved histidine. To address this question, we used sequence alignments for CGI-58 from diverse species and molecular modeling programs to determine potential LPAAT active site residues. We then mutated basic and acidic amino acid residues in mouse CGI-58, including point mutations responsible for NLSDi in humans and the putative LPAAT active site residues H329 and D334. We determined whether these mutated variants retained LPAAT activity and the ability to activate ATGL TAG hydrolase activity *in vitro*. We also expressed these variants in cultured human NLSDi fibroblasts to determine their effect on turnover of accumulated TAG. Through these experiments, we addressed our **original hypothesis** that CGI-58 is a LPAAT involved in channeling fatty acids from TAG to phospholipids and that CGI-58-mediated activation of ATGL lipase activity is a separate function. The hypothesis was tested in the following aims:

Aim 1: <u>To determine the amino acid residues necessary for CGI-58 LPAAT activity</u>. CGI-58's amino acid residues H329 and D334 constitute a putative LPAAT active site motif. Partially purified recombinant CGI-58 containing point mutations to either of

these two residues was tested for LPAAT activity *in vitro*. We planned to use tryptophan quenching to compare the ability of these variants to bind LPAAT substrates relative to WT CGI-58.

Aim 2: To show that CGI-58's LPAAT activity is not related to co-activation of ATGL. We hypothesized that partially purified CGI-58 containing H329A and D334A mutations would increase ATGL's TAG lipase activity similarly to WT CGI-58. To test this, post-nuclear Sf9 cell extracts containing ectopic ATGL were mixed with partially purified recombinant CGI-58 and emulsified TAG to measure TAG hydrolase activity.

Aim 3: To demonstrate that CGI-58 is an acyltransferase involved in channeling lipids from TAG to PL. We hypothesized that cultured NLSDi fibroblasts would contain altered phospholipid species and more TAG than WT human fibroblasts. We planned to use LC/MS to analyze the lipid content and composition of NLSDi cell lines (NLSD1, 74/76, 120/83) and WT cell lines (WS1, BJ, AG01518).

During the execution of these experiments, we unexpectedly discovered that CGI-58 is not an LPAAT; LPAAT activity observed in partially purified preparations of CGI-58 was due to the presence of a contaminant protein from *E. coli*. Our aims have changed to reflect this finding. We have instead focused on demonstrating that partially purified CGI-58 is not an acyltransferase. Further, we revisited lipid-binding activity of CGI-58. Finally, we investigated the activity of mutated variants of CGI-58, H84A and H84R, in activation of ATGL. The H84R variant is an uncharacterized mutation of CGI-58 found in individuals with NLSDi.

Experimental Procedures

Materials

Dr. Vidya Subramanian kindly provided the mouse cDNA for CGI-58 and β-galactosidase contained within the pShuttle-CMV vector (Agilent Technologies). Dr. Gabriela Montero-Moran kindly provided the mouse cDNA of CGI-58 contained within the pET-28a vector (Novagen). Dr. Gil-Soo Han generously donated the pGEX-4T-1 vector. The cDNA for murine ATGL (IMAGE: 30024535) was purchased from American Type Cell Culture (Manassas, Virginia). Oligonucleotides were purchased from Operon (Fisher Scientific). pFastBac 1 and pCR-Blunt were purchased from Invitrogen. QIAprep Spin Miniprep Kit, QIAquick Gel Extraction Kit, and QIAquick PCR Purification Kit were obtained from Qiagen. Wizard Plus Midipreps DNA Purification System was purchased from Promega. Restriction digestion enzymes and corresponding buffers were obtained from New England BioLabs, Inc. SM2-1 *E. coli* were obtained from Jack Wertz at the Coli Genetic Stock Center at Yale University. TOP10 *E. coli* were purchased from Invitrogen. DH10Bac *E. coli* strain was purchased from Invitrogen. BJ5183 and XL 10-Gold *E. coli* strains were purchased from Agilent Technologies. Bl21(DE3) cells were obtained from Novagen. Nickel and Cobalt affinity resins were obtained from Qiagen and Clontech Laboratories, Inc., respectively. Glutathione Sepharose 4B was purchased from GE Healthcare Life Sciences. NLSD cells were generously donated by Dr. R. A. Coleman (University of North Carolina, Chapel Hill, NC) [130,131]. WS1 human skin fibroblasts and Sf9 cells were purchased from American Type Culture Collection.

Delbecco's Modified Eagle's Medium (DMEM) and Minimum Essential Medium (MEM) were purchased from Mediatech. Bovine serum albumin, fatty acid-free bovine serum albumin, and fetal bovine serum were purchased from Sigma. Lipofectamine, Plus Reagent, and Cellfectin, and Grace's Medium were purchased from Invitrogen. Coomassie Plus "The Better Bradford Assay Reagent" and GelCode Blue Stain Reagent were purchased from Pierce. Rabbit polyclonal antiserum raised against full length CGI-58 was previously described [17]. Anti-6-His antibody was purchased from Clontech Laboratories, Inc. Anti-GST antibody was purchased from GE Healthcare. Anti-β-galactosidase, anti-calnexin, and peroxidase-conjugated anti-mouse, anti-rabbit, and anti-goat antibodies were purchased from Sigma. Enhanced chemiluminescence reagent was purchased from Pierce. PIP Strips, PIP Arrays, Membrane Lipid Strips, Sphingo Strips, phosphatidylinositol diC8, phosphatidylinositol 3-phosphate [PI(3)P] diC8, phosphatidylinositol 5-phosphate diC8 [PI(5)P], and phosphatidylinositol 4,5-bisphosphate [PI(4,5)P_2] diC8 were purchased from Echelon, Inc (Salt Lake City, UT). Phosphatidic acid and lysophosphatidic acid were purchased from Sigma. Phosphatidylcholine (egg) and phosphatidylinositol (soy) were purchased from Avanti Polar Lipids. Radiolabeled [^{3}H]triolein and [^{14}C]oleoyl-CoA were purchased from PerkinElmer Life Sciences (Boston, MA). Hydrofluor was purchased from National Diagnostics and ScintiVerse BD Cocktail was purchased from Fischer Scientific. Silica gel hard layer fluorescent TLC plates were obtained from Analtech (Newark, DE). Additional chemicals and organic solvents were purchased from Fisher Scientific or Sigma.

Methods

Generation of 3D protein model of CGI-58 – The primary amino acid sequence for mouse CGI-58 (NP_080455.1) was submitted to the online Protein Homology/analogy Recognition Engine (PHYRE) version 0.1 [132]. Resulting models were submitted to the Structural Analysis and Verification Server (SAVES) (http://nihserver.mbi.ucla.edu/SAVES/). The SAVES program includes five programs, PROCHECK [133], WHAT_CHECK [134], ERRAT [135], VERIFY 3D [136], and PROVE [137], which assess the structural stability of the computer generated models. The highest ranked model was based on a putative hydrolase (2632844) from *Bacillus subtilis* (Protein Data Bank ID: 2R11). Images of the model were captured by PyMOL software (The PyMOL Molecular Graphics System, Version 1.5.0.1 Schrödinger, LLC.).

Generation of CGI-58 variants – Variants of CGI-58 were produced through mutagenesis of mouse CGI-58 cDNA contained within the pShuttle-CMV or pET-28a vector using the QuikChange Site-Directed Mutagenesis kit (Agilent Technologies) [138]. Polymerase chain reaction (PCR) reactions contained 15 ng of CGI-58 cDNA template, 125 ng of each primer (forward and reverse), 1x reaction buffer, 0.2 mM dNTPs, 3 μL of Quiksolution and 2.5 units of *Pfu* Ultra DNA Polymerase. After an initial denaturation of 1 minute at 95°C, PCR was performed using 18 cycles of denaturation at 95°C for 50 seconds, annealing at 60°C for 50 seconds, and extension at 68°C for 7 minutes and 30 seconds. The amplified vector was treated with DpnI at 37°C for 2 hours to digest the original methylated template DNA. The

undigested product was then transformed into XL10-Gold *E. coli* and grown on agar plates. DNA plasmids were isolated from single clones and mutations were confirmed by sequence analysis. Mutations to mouse CGI-58 cDNA harbored in the pShuttle-CMV vector created the variants E262A/K, D303A/N, D334A/N, N155A/S, H84A/R, and H329A/R (Table 1). Mutations to mouse CGI-58 cDNA contained in the pET-28a vector produced variants D110A, E179A, H84A/R, H154A, and H329A/R (Table 1). Using cDNA with these mutations as a template, further variants were created producing CGI-58 with alanine substitutions to multiple sites (Table 2).

Generation of the SM2-1(DE3) line – The SM2-1(DE3) line was created from the SM2-1 *E. coli* strain using a λDE3 lysogenization kit (Novagen) to allow for IPTG-induced expression of T7 RNA polymerase; this permits for translation of 12-His tagged CGI-58 within the pET-28a vector. Bacteria clones were analyzed for protein levels of T7 RNA polymerase pre- and post-induction by western blot analysis. The presence of T7 RNA polymerase was detected using anti-T7 RNA Polymerase antibody (1:10,000) (Novagen) and peroxidase conjugated anti-mouse IgG (1:5,000) (Sigma). The best clone was selected using the criteria of minimal T7 RNA polymerase expression before isopropyl β-D-1 thiogalactopyranoside (IPTG) induction and maximal expression after IPTG induction, relative to other clones.

Growth and purification of recombinant glutathione S-transferase (GST) tagged CGI-58 from E. coli – Bl21(DE3) *E. coli* containing the cDNA for WT murine CGI-58 subcloned into the pGEX-4T-1 expression plasmid were grown in Luria Broth (LB)

Table 1. Oligonucleotide sequences used to generate various mutations in CGI-58 cDNA

Primer Name	Sequence
D110A-Forward	5'-CCTGTCTATGCCTTTGCCCTATTGGGCTTCGG-3'
D110A-Reverse	5'-CCGAAGCCCAATAGGGCAAAGGCATAGACAGG-3'
E179A-Forward	5'-GTCACCTCATTTTAGTAGCGCCATGGGGTTTTCCT-3'
E179A-Reverse	5'-AGGAAAACCCCATGGCGCTACTAAAATGAGGTGAC-3'
E262A-Forward	5'-GTACAAACCCCAAGTGGTGCGACAGCTTTCAAAAACATG-3'
E262A-Reverse	5'-CATGTTTTTGAAAGCTGTCGCACCACTTGGGGTTTGTAC-3'
E262K-Forward	5'-TAATGTACAAACCCCAAGTGGTAAGACAGCTTTCAAAAACATG-3'
E262K-Reverse	5'-CATGTTTTTGAAAGCTGTCTTACCACTTGGGGTTTGTACATTA-3'
D303A-Forward	5'-GCCCGATCCTGCATAGCTGGCAACTCTGGAAC-3'
D303A-Reverse	5'-GTTCCAGAGTTGCCAGCTATGCAGGATCGGGC-3'
D303N-Forward	5'-TGGAGCCCGATCCTGCATAAATGGCAACTCTG-3'
D303N-Reverse	5'-CAGAGTTGCCATTTATGCAGGATCGGGCTCCA-3'
D334A-Forward	5’-GGGCATTATGTGTATGCAGCTCAGCCAGAAGAATTCAAC-3’
D334A-Reverse	5’-GTTGAATTCTTCTGGCTGAGCTGCATACACATAATGCCC-3’
D334N-Forward	5’-GGGGCATTATGTGTATGCAAATCAGCCAGAAGAATTCAAC-3’
D334N-Reverse	5’-GTTGAATTCTTCTGGCTGATTTGCATACACATAATGCCCC-3’
N155A-Forward	5'-TGATCTTGCTTGGACACGCCCTGGGAGGGTTCTTGG-3'
N155A-Reverse	5'-CCAAGAACCCTCCCAGGGCGTGTCCAAGCAAGATCA-3'
N155S-Forward	5'-CAAAATGATCTTGCTTGGACACAGCCTGGGAGGGTT-3'
N155S-Reverse	5'-AACCCTCCCAGGCTGTGTCCAAGCAAGATCATTTTG-3'
H84A-Forward	5'-AGACGCCACTTGTCCTCCTTGCTGGTTTTGGAGGAG-3'
H84A-Reverse	5'-CTCCTCCAAAACCAGCAAGGAGGACAAGTGGCGTCT-3'
H84R-Forward	5'-CCACTTGTCCTCCTTCGTGGTTTTGGAGGAGGT-3'
H84R-Reverse	5'-ACCTCCTCCAAAACCACGAAGGAGGACAAGTGG-3'
H154A-Forward	5'-CAAAATGATCTTGCTTGGAGCCAACCTGGGAGGGTTCTTG'-3
H154A-Reverse	5'-CAAGAACCCTCCCAGGTTGGCTCCAAGCAAGATCATTTTG-3'
H329A-Forward	5'-CATCCTCGGGGCGGGGGCTTATGTGTATGCAGATC-3'
H329A-Reverse	5'-GATCTGCATACACATAAGCCCCCGCCCCGAGGATG-3'
H329R-Forward	5'-CTCGGGGCGGGGCGTTATGTGTATGCAG-3'
H329R-Reverse	5'-CTGCATACACATAACGCCCCGCCCCGAG-3'

with shaking at 225 rpm at 37°C. Cultures were grown to an $O.D._{600}$ of 0.6-0.8, and then incubated further with 1 mM IPTG for 1 hour. Cultures were centrifuged for 10 min at 4,000 x *g* and pellets were stored at -20°C until further use.

Frozen pellets were resuspended in 1x extraction buffer (10 mM sodium phosphate, 1.8 mM potassium phosphate, 0.14 mM sodium chloride, 1 mM dithiothreitol, 1 mg/mL lysozyme, and 1 EDTA-free protease inhibitor cocktail tablet) and incubated on ice for 30 minutes. The cell resuspension was loaded with glass beads into a Bead-Beater® (Biospec Products, Inc. Bartlesville, OK) chamber surrounded by ice water. Cells were disrupted with 10 cycles of 15 seconds of blending and 2 minutes of cooling. The lysed cells were centrifuged at 21,000 x *g* for 20 minutes at 4°C. The clarified supernatant was incubated with 2 mL of glutathione sepharose 4B (GE Healthcare) for 1.5 hours. The resin-lysate mixture was centrifuged at 800 x *g* and the pelleted resin was loaded into a column and washed with 20 mL of 1x extraction buffer. The GST-CGI-58 was eluted from the resin in 7 1 mL with elution buffer (50 mM Tris, 400 mM sodium chloride, 10 mM reduced glutathione, and 40% glycerol (v/v)). The resulting partially purified enzyme was stored at either 4°C or -20°C until further use.

Growth and purification of recombinant 12-Histidine-tagged CGI-58 from E. coli – Bl21(DE3) or SM2-1(DE3) *E. coli* strains containing the cDNA for WT CGI-58 within the pET-28a expression plasmid were grown in LB while shaking at 225 rpm at 37°C. After an $O.D._{600}$ of 0.6-0.8 was reached, cells were treated with 1 mM IPTG for

5 or 3 hours, Bl21 or SM2-1 cells, respectively. The cells were collected by centrifugation at 4,000 x *g* for 10 minutes and frozen at -20°C until use.

Frozen pellets were resuspended in lysis buffer (50 mM sodium phosphate, 100 mM potassium chloride, 30 mM imidazole, 1 mM dithiothreitol, 1 mg/mL lysozyme, and 1 EDTA-free protease inhibitor cocktail tablet) and incubated on ice for 30 minutes. The cell resuspension was loaded with glass beads into a Bead-Beater® (Biospec Products, Inc.) chamber surrounded by ice water. Cells were disrupted with 10 cycles of 15 seconds of blending and 2 minutes of cooling. The lysed cells were centrifuged at 21,000 x *g* for 20 minutes at 4°C. The clarified supernatant was incubated with 0.5 mL of TALON His-Tag Purification Resin for 1.5 hours. The resin-lysate mixture was centrifuged at 800 x *g* and the pelleted resin was loaded into a column and washed with 100 mL of wash buffer (lysis buffer with 100 mM imidazole). The 12-His-tagged CGI-58 was eluted from the resin in 7 1 mL using elution buffer (lysis buffer with 250 mM imidazole and 40% glycerol (v/v)). The resulting partially purified enzyme was stored at -20°C until further use.

Subcloning of ATGL into bacmid and expression in Sf9 insect cells – The cDNA for ATGL was amplified by PCR using the Forward (5'-GCCACCATGTTCCCGAGGG-3') and Reverse (5'-TTAGTGATGGTGATGGTGATGTCCGCAAGGCGGGAG-3') primers to add DNA encoding a Kozak sequence before the start of the ATGL cDNA and a glycine-linked 6-His tag to the 3' end. The blunt-ended PCR product was ligated into pCR-blunt (Invitrogen) and transferred into the pFastBac 1 vector (Invitrogen) using the restriction sites SpeI and XhoI.

Using the Bac-to-Bac Baculovirus Expression System (Invitrogen), the ATGL-6-His fusion construct from pFastBac1 was recombined into the bacmid within DH10Bac *E. coli*. Successfully recombined bacmids containing the ATGL cDNA were identified through blue/white screening, as well as PCR using M13 Forward (-40) and M13 Reverse primers (Invitrogen). The recombined plasmids were purified from TOP10 *E. coli* using the Wizard Plus Midiprep kit (Promega) and then complexed with Cellfectin Reagent (Invitrogen) for transfection of Sf9 insect cells for generation and propagation of baculovirus. Sf9 insect cells were grown in Sf-900II SFM media (Invitrogen) at 28°C without supplemental CO_2. Seventy-two hours post-transfection, media were collected and centrifuged at 800 x *g* to remove cell debris; the supernatant containing baculovirus was stored at 4°C.

Growth of Sf9 insect cells and expression of ATGL – For expression of recombinant 6-His tagged ATGL, Sf9 cells were grown to approximately 70% confluence in 150 mm dishes and were incubated in growth medium containing 200 µL of baculovirus for 72 hours to induce protein expression of recombinant 6-His-tagged ATGL. Media were removed and cell monolayers were washed with PBS. Infected cells were detached from the culture dish by scraping into PBS, followed by centrifugation at 800 x *g* for 10 minutes at 4°C. The supernatant was removed by aspiration and -pellets were stored at -70°C until further use.

Production of adenovirus – Adenovirus was produced following the protocol supplied in the AdEasy Adenoviral Vector Systems (Agilent Technologies) [139]. The

pShuttle vector with inserted CGI-58 cDNA was linearized with PmeI and transformed into BJ5183 *E. coli* for recombination with adenoviral elements contained within the cells. Individual clones were screened using PacI digestion for confirmation of recombination. Plasmids for two positive clones of each variant were amplified in XL10-Gold or TOP10 *E. coli* strains and isolated using an endotoxin-free midiprep kit (Promega Corporation). These plasmids were transfected into AD-293 human embryonic kidney cells for assembly of adenovirus following the AdEasy protocol [139]. After 50% of cells detached from the surface of the culture dishes (4-5 days post-transfection), cells were collected by scraping the cells into PBS followed by centrifugation at 800 x *g* for 10 minutes at 4°C and subjected to 4 cycles of freezing and thawing in a minimal volume of PBS. The lysates were then centrifuged at 12,000 x *g* for 10 minutes at 4°C to remove insoluble debris. The supernatants containing crude adenoviral preparations were divided into aliquots and stored at -70°C until further use. Passage 1 virus was used to infect AD293 cells to amplify the titer, producing passage 2 virus. In these experiments, passage 3 virus was used to express each CGI-58 variant in cultured human fibroblasts. Adenoviruses used to drive the overexpression of WT CGI-58 and β-galactosidase were obtained from Vidya Subramanian, a former graduate student, and were amplified to passage 5.

Growth and transduction of NLSDi fibroblasts – NLSDi and WS1 normal human skin fibroblasts were cultured in MEM supplemented with 10% fetal bovine serum, 1% non-essential amino acids, 10 mM sodium pyruvate, 10 units/mL penicillin, and 100

μg/mL streptomycin at 37°C in 5.5% CO_2. WT CGI-58, mutated variants of CGI-58, and β-galactosidase were overexpressed in NLSDi fibroblasts using expression vectors. Mixtures of crude virus preparations, Plus reagent (Invitrogen), and Lipofectamine reagent (Invitrogen) were mixed with DMEM. NLSDi cells were incubated in this virus-containing medium at 37°C in 5.5% CO2. After 3 hours, the virus-containing medium was removed and cells were supplemented with MEM containing 10% fetal bovine serum, 1% non-essential amino acids, 10 mM sodium pyruvate, 10 units/mL penicillin and 100 μg/mL streptomycin.

Harvest of cultured fibroblasts – Forty-eight hours post-infection, cells were washed in PBS and collected through trypsinization. After centrifugation at 800 x *g* for 10 minutes at 4°C, the resulting cell pellets were resuspended in 300 μL hypotonic lysis buffer containing 20 mM Tris pH 7.4, 1 mM EDTA, 10 mM sodium fluoride, and 1x protease inhibitor cocktail (Sigma P8340). Samples were incubated on ice for 10 minutes and subjected to probe sonication using a Branson Sorvall Sonicator for 3 rounds of 10-second pulses, each followed by a 1 minute incubation on ice. Protein content of samples was determined with a Bradford assay (Pierce) for immunoblot or TAG analysis. Expression of CGI-58 was normalized between samples using densitometry of immunoblot analysis of CGI-58 signals relative to signals of the loading control calnexin.

Immunoblot analysis – Following protein quantification, equal amounts of total cell lysate were boiled in a 1X solution of Laemmli sample buffer (LSB) [140] to

solubilize and denature proteins. Samples were eluted on a 10% SDS-polyacrylamide gel, then transferred to nitrocellulose for immunoblot analysis. Membranes were incubated with either 1) antiserum raised against mouse CGI-58 (1:25,000), 2) anti β-galactosidase antibody (1:25,000) (Sigma), or 3) anti-calnexin antibody (1:5,000) (Sigma) in 5% bovine serum albumin in a Tris-Saline-Tween-20 solution. To detect the presence of the primary antibody, membranes were incubated in peroxidase-conjugated anti-rabbit IgG (1:5,000) diluted in 5% milk in Tris-Saline-Tween-20. Membranes were treated with enhanced chemiluminescence reagents (Pierce) and exposed to X-ray film for detection of proteins.

TAG analysis of NLSDi cells – TAG content of NLSDi cell lysates was measured using a previously published protocol [141]. Solvent extracts of lipids were dried in glass tubes under vacuum using a Speed Vac Concentrator equipped with a cold trap (ThermoSavant, Farmingdale, NY). The dried lipids were incubated with 300 µL of Infinity Triglyceride Stable Reagent (Thermo Scientific) with shaking at 37°C for 1 hour. Samples were transferred to a 96-well plate and measured at a 540 nm wavelength. Data were compared to a standard curve produced from known concentrations of corn oil in ethanol that were extracted and assayed using the same procedures.

Protein-lipid overlay assay – PIP Strips, PIP Arrays, Membrane Lipid Strips, or Sphingo Strips (Echelon, Inc) were incubated in 5% nonfat dry milk in PBS with 0.1% Tween-20 for 1 hour at room temperature to block nonspecific protein

binding during subsequent antibody treatments. Membranes were then incubated with 12.8 nM (0.5 μg/mL) of partially purified recombinant 12-His-tagged CGI-58 in 5% milk in PBS for 1 hour at room temperature. Following each incubation step, membranes were briefly washed three times in 10 mL of PBS with 0.1% Tween-20. Next, membranes were incubated with either rabbit polyclonal anti-CGI-58 antiserum or mouse anti-6-His antibody for 1 hour at room temperature followed by peroxidase-conjugated anti-rabbit or anti-mouse IgG for 1 hour and then enhanced chemiluminescence reagent (Pierce). Finally, membranes were exposed to x-ray film for detection of CGI-58.

Assay for LPAAT activity – LPAAT activity of purified recombinant CGI-58 was assessed by mixing protein solutions with 50 μM LPA and 10 μM [1-^{14}C-oleoyl] oleoyl-CoA in 50 mM Tris-HCL buffer, pH 7.5, at a final volume of 100 μl [105]. Reactions were incubated for 10 minutes at 37°C, then terminated by sequential addition of 0.5 mL 0.1 N HCL in methanol, 1 mL chloroform, and 1.5 mL $MgCl_2$. Samples were centrifuged at 800 x *g* for 10 minutes. After phase separation, the top aqueous phase was discarded and the bottom organic phase was dried via speed vacuum centrifugation. The dried organic phase was dissolved in chloroform and spotted onto a silica gel hard layer fluorescent TLC plate. Lipids were separated using chloroform:methanol:acetone:acetic acid:water (50:10:20:15:5 v/v/v/v/v) as the solvent system. Radiolabeled lipids were visualized using a Storm System Phosphorimager (Molecular Dynamics). Bands corresponding to PA corresponded

to a cold PA standard, and were scraped from the TLC plate and measured by liquid scintillation counting for quantification.

Assay for TAG lipase activity – To determine TAG lipase activity of ATGL in the presence or absence of CGI-58, 40 μg of Sf9 cell extract containing ATGL was mixed with up to 1 μg of purified recombinant CGI-58 in a final volume of 100 μl of 0.1 M potassium phosphate buffer. Proteins were then mixed with 100 μl substrate containing 330 μM [9,10-^{3}H] triolein emulsified with 145 μM PC:PI 3:1 [142]. Reactions were incubated at 37°C for 1 hour and terminated with the addition of 3.25 mL of chloroform:heptane:methanol (10:9:7) and 0.1 mL of 0.1 M potassium carbonate, 0.1 M boric acid. Reactions were centrifuged at 800 x *g* for 20 minutes at room temperature, after which 1 mL of each top phase was removed and radioactivity was quantified using a scintillation counter (PerkinElmer Life Sciences).

Statistical analysis – Data were analyzed using GraphPad Prism 6 software. Data represent the means of duplicate or triplicate reactions ± standard deviation. Variance was measured using either one-way or two-way analysis of variance (ANOVA) as described in the legend of each figure. One-way ANOVAs were followed with Tukey's multiple comparisons post-hoc test while two-way ANOVAs used Bonferroni's multiple comparisons post-hoc test.

Results

To address the overall question, "Is LPAAT activity necessary for co-activation of ATGL TAG hydrolase activity?" the active site residues required for LPAAT catalytic activity first needed to be identified. All characterized LPAATs contain the proposed active site motif HX_4D [143]. Murine CGI-58 contains H329 and D334 residues that form this motif; therefore, it was hypothesized that they are LPAAT active site residues [105,106]. These residues are highly conserved in CGI-58/ABHD5, from multiple species, including *C. elegans*, as well as in the closely related protein, ABHD4 (Figure 4). In addition, CGI-58 contains more than 20 highly conserved acidic residues and four highly conserved basic residues, pairs of which may serve as active site residues. Since the crystal structure of CGI-58 has not yet been solved, a hypothetical 3D model of CGI-58 protein structure was developed to gain a better understanding of the spatial positioning of these proposed active site residues.

Development of the 3D computer model of CGI-58 by protein threading – Various on-line programs are available to provide users with hypothetical models of their protein of interest. Six servers were chosen based on their public availability and their performance at CASP (Critical Assessment of Protein Structure Prediction) competitions (http://predictioncenter.org/casp8/groups_analysis.cgi). The predicted primary amino acid sequence of the mouse gene encoding CGI-58 was submitted to the programs LOOPP [144-148], I-TASSER [149-151], WURST [152],

Figure 4

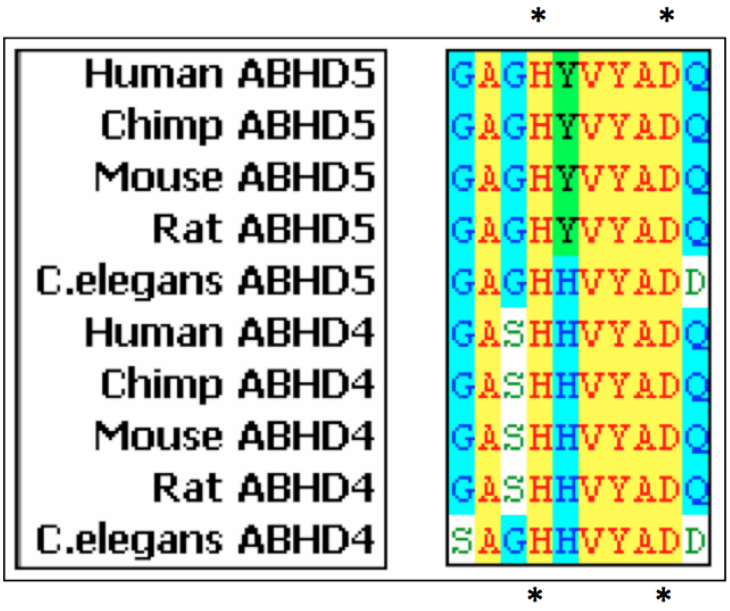

Figure 4. Putative acyltransferase active site residues H329 and D334 are highly conserved amongst species of CGI-58. Primary amino acid sequences of CGI-58 and close-relative ABHD4 were aligned from human, chimpanzee, mouse, rat, and *C. elegans*. Asterisks denote conserved residues H329 and D334 in mouse CGI-58.

SAM-T08 [153-158], ROBETTA [159-161], and PHYRE [132]. In total, over 300 models were generated and ranked according to structural integrity as defined by the SAVES (Structural Analysis and Verification Server) program (http://nihserver.mbi.ucla.edu/SAVES/). The SAVES program is a compilation of five other programs: PROCHECK [133], WHAT_CHECK [134], ERRAT [135], VERIFY 3D [136], and PROVE [137]; these programs function to determine structural stability of the computer-generated model. SAVES produces 1) a Ramachandran plot, which evaluates the position of amino acid side-chains and ranks them as favorable, additionally allowed, generously allowed, or disallowed, 2) an assessment of bond lengths to determine if the model stretches or compresses the backbone of CGI-58's amino acids, and 3) an overall verification of how well the amino acid sequence fits into the three dimensional structure, based on polarity, alpha/beta structures, etc. The highest ranked model was acquired using the Protein Homology/analogY Recognition Engine (PHYRE) version 0.2 [132]. The server calculated a model using the primary amino acid sequence of CGI-58 threaded through the crystal structure of putative hydrolase (2632844) from *Bacillus subtilis* (Protein Data Bank ID: 2R11).

Since CGI-58 is a member of the ABHD family of proteins, it was reasoned that the conserved GXSXG sequence (GXNXG in CGI-58) should be found in an active site cleft or pocket. Potential catalytic residues should be positioned near the asparagine residue A155. In this computer-generated model, CGI-58 has a globular shape (Figure 5), forming a hydrophobic pocket, which contains the motif GXNXG. The asparagine in the center of this motif, N155, is in close proximity to two

Figure 5

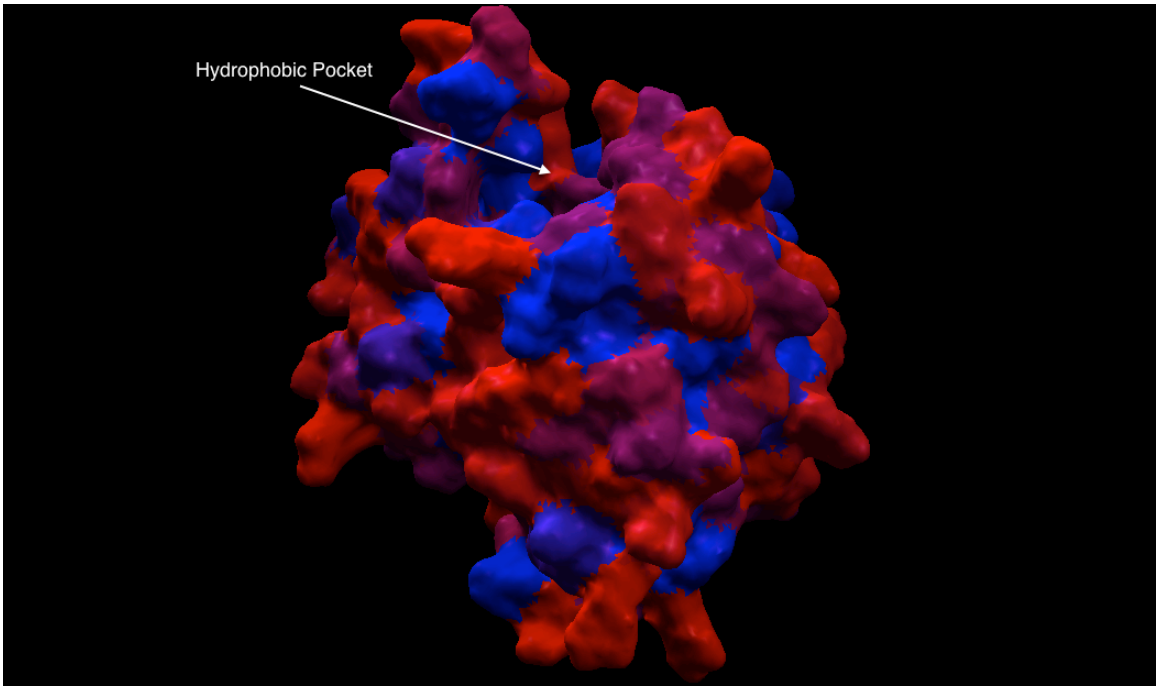

Figure 5. A computer-generated model of CGI-58. This image was produced by threading the primary amino acid sequence of CGI-58 through the 3D crystal structure of putative hydrolase (2632844) from *Bacillus subtilis* (Protein Data Bank ID: 2R11). The structure is globular, with an opening to a small pocket containing N155, H154, H329, and E179 residues within close proximity. Hydrophilic residues are colored red and hydrophobic residues are colored blue.

histidine residues, H154 and H329, and one glutamate residue, E179 (Figure 6). Further, H154, H329, and E179 are all conserved basic and acidic residues in a wide range of species. Therefore, these residues may play a role in catalytic activity. In the computer-generated model of CGI-58, the reactive oxygen of the side chain of E179 is 3 and 6 angstroms from the reactive nitrogen of H154 and H329, respectively. Due to their close proximity, these amino acids were suspected to be active site residues and were chosen for mutagenesis studies.

Using this model, the positions of the putative LPAAT active site residues H329 and D334 were assessed. H329 appears to be internal (Figure 7), within a hydrophobic pocket near the center of the protein. In previously described acyltransferases, active site residues are located within 2.5 – 4 angstroms of each other to mediate transfer of electrons between residues and substrate [162]. D334 is located on the protein surface, 12.5 angstroms from H329. Due to the location and distances between these two residues, it is unlikely that H329 or D334 are acyltransferase active site residues. Nonetheless, given the conservation of these residues across species (Figure 4), and their inclusion in a HX_4D acyltransferase signature sequence, these residues were mutated to test for loss of acyltransferase activity.

Figure 6

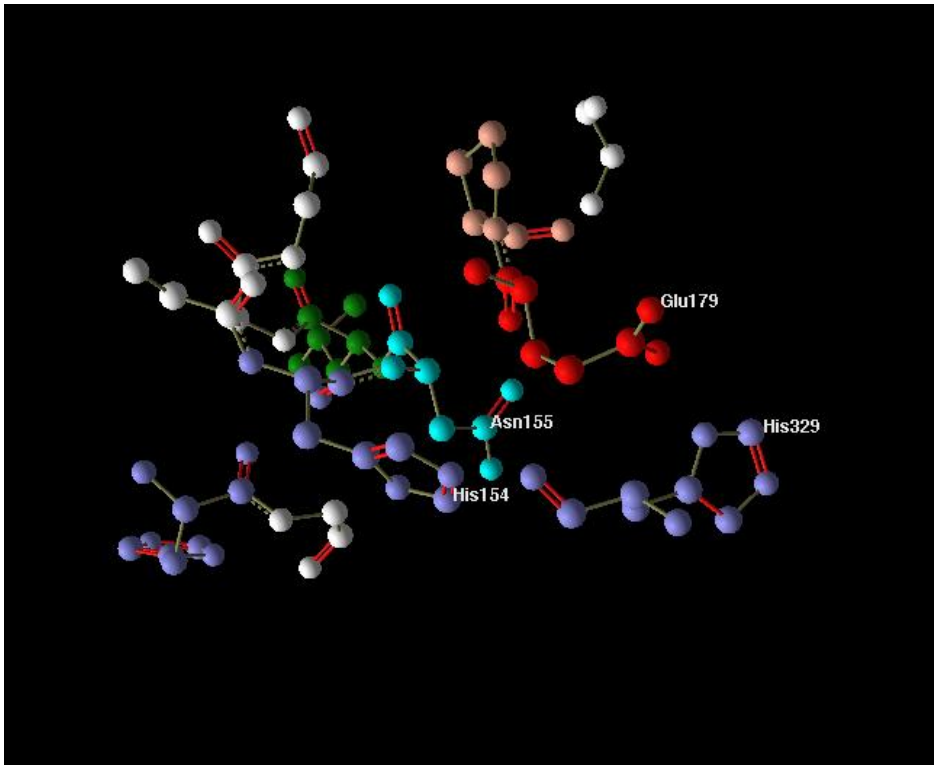

Figure 6. Acidic and basic residues near the lipase motif GXNXG of CGI-58. H154, H329, and E179 are in close proximity (≤ 6 angstroms) from each other. These residues surround N155, which, is in the lipase active site consensus sequence GXNXG of CGI-58.

Figure 7

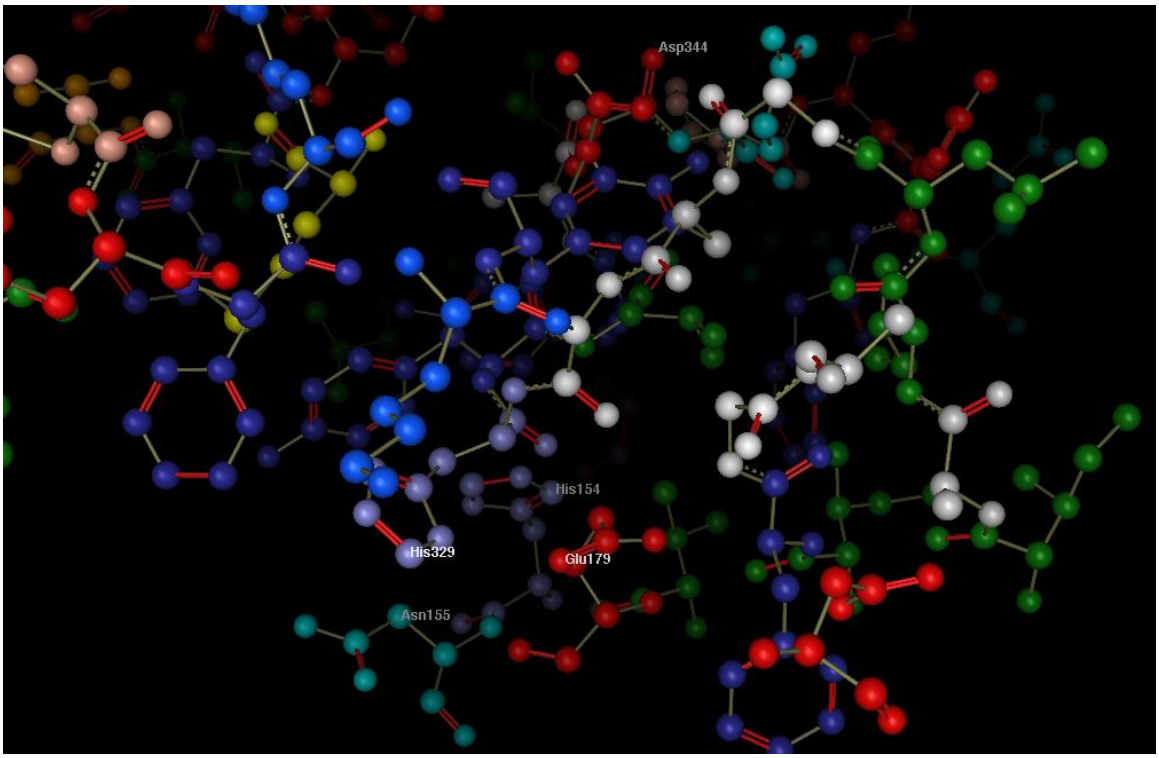

Figure 7. The putative acyltransferase active site residues HX_4D. Residues H329 and D334 are the putative acyltransferase active site residues. H329 is located in an internal pocket near the lipase consensus motif, while D334 is located 12.5 angstroms away, on the exterior surface of the protein.

Mutation of H329 and D334 to alanine residues fails to reduce LPAAT activity - Recombinant 12-His tagged WT, H329A, or D334A variants of murine CGI-58 were partially purified from BL21(DE3) *E. coli* using cobalt affinity chromatography and tested for LPAAT activity. Each partially purified protein (tested at 0.5, 1.5, or 3 μg) showed a dose-dependent response of increasing LPAAT activity (Figure 8). At 3 μg of protein, CGI-58 harboring the mutation D334A showed the highest level of activity at 8.0 pmol of PA formed/min; H329A displayed activity of 4.9 pmol of PA formed/min; WT CGI-58 showed the lowest activity at 3.6 pmol of PA formed/min. The relative purity of each preparation was determined using a Coomassie-stained SDS-PAGE gel (Figure 9). The D334A preparation had the highest level of contaminants; both H329A and WT CGI-58 showed lower levels of contaminant proteins.

Due to these findings, it was important to determine if contaminant proteins that bind and elute from cobalt or nickel affinity resins have LPAAT activity. Each resin was incubated with the supernatant of a 16,000 x *g* centrifugation of Bl21(DE3) cell extracts harboring empty pET-28a vector. The extract was eluted using the same conditions and buffers as the previous preparations. Eluants from nickel and cobalt resins were tested for LPAAT activity and showed a dose-dependent increase in LPAAT activity in the absence of CGI-58 (Figure 10). When visualized on a Coomassie-stained SDS-PAGE gel, the preparations contained many contaminant proteins, including a prominent band at approximately 27 kDa protein (Figure 11). A search of the literature revealed that plsC, the sole bacterial

Figure 8

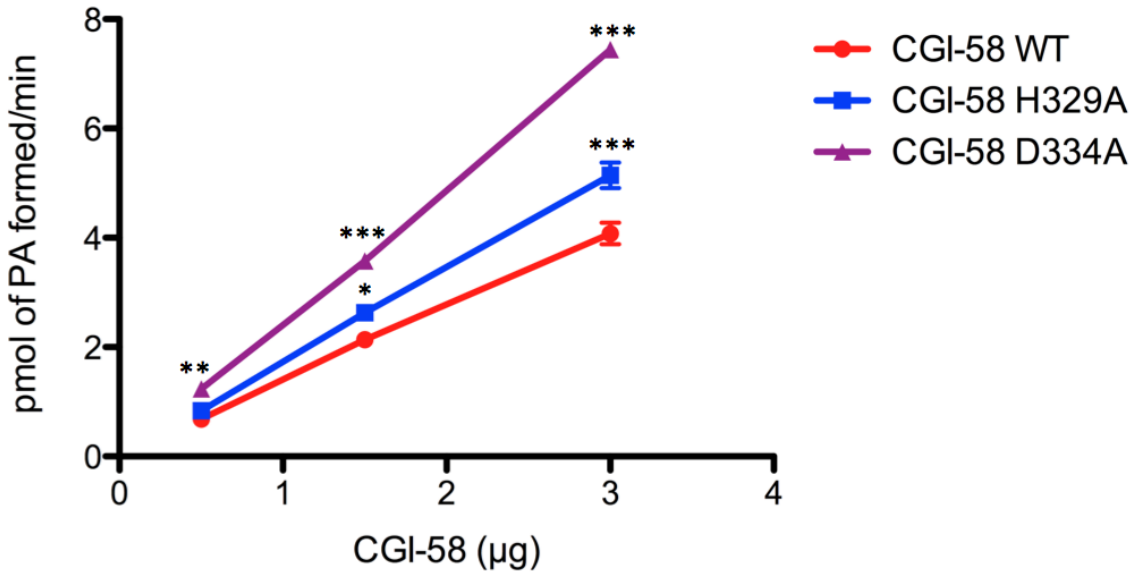

Figure 8. Partially purified 12-His tagged CGI-58 harboring either H329A or D334A mutations exhibits LPAAT activity. [1-^{14}C-oleoyl] oleoyl-CoA (10 µM) and LPA (50 µM) were incubated in duplicate reactions with 0.5, 1.5, or 3 µg of partially purified CGI-58 for 10 minutes at 37°C. Lipids were extracted from the reaction mixture and spotted onto a TLC plate for separation of PA from unreacted substrate. The location of radiolabeled PA corresponded to a cold PA standard, spotted on the same plate. Bands corresponding to PA were scraped and radioactivity was quantified by scintillation counting. Data are the mean ± standard deviation of duplicate reactions. Data for H329A and D334A were compared to WT values using two-way ANOVA (*, $p < 0.05$; **, $p < 0.001$, ***, $p < 0.001$). Where error bars are not visible, they are contained within the symbol. This figure is from one representative experiment of five.

Figure 9

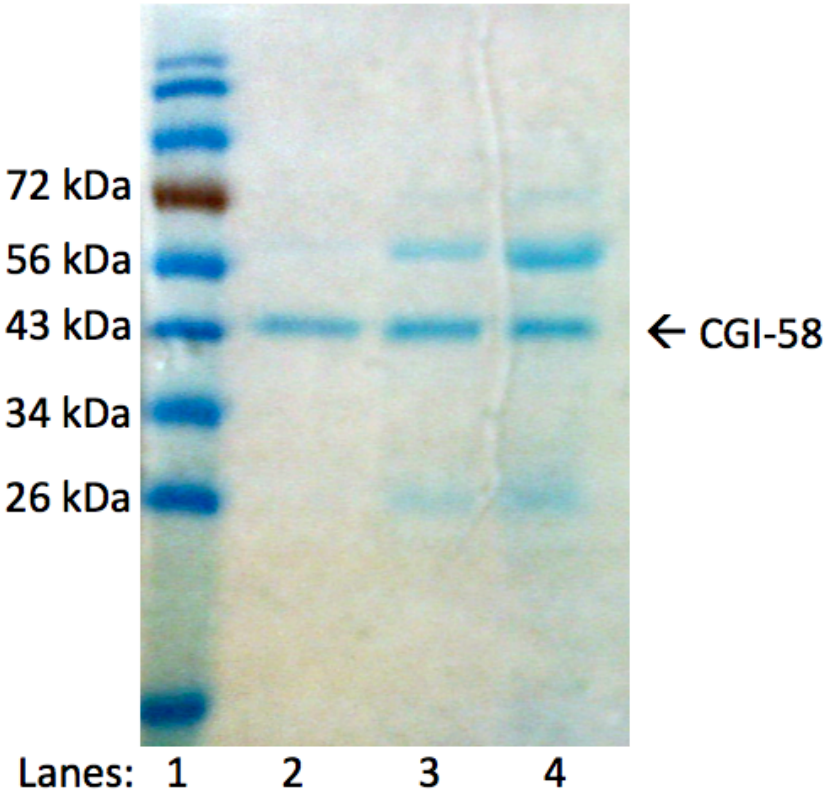

Figure 9. Relative purity of WT, H329, and D334 preparations. 1 µg of 12-His CGI-58 purified over cobalt resin was eluted on a 12% SDS-PAGE gel and proteins were visualized with Coomassie stain. Lanes contain: EZ Run Molecular Weight Marker (lane 1), WT CGI-58 (lane 2), H329A CGI-58 (lane 3), and D334A CGI-58 (lane 4).

Figure 10

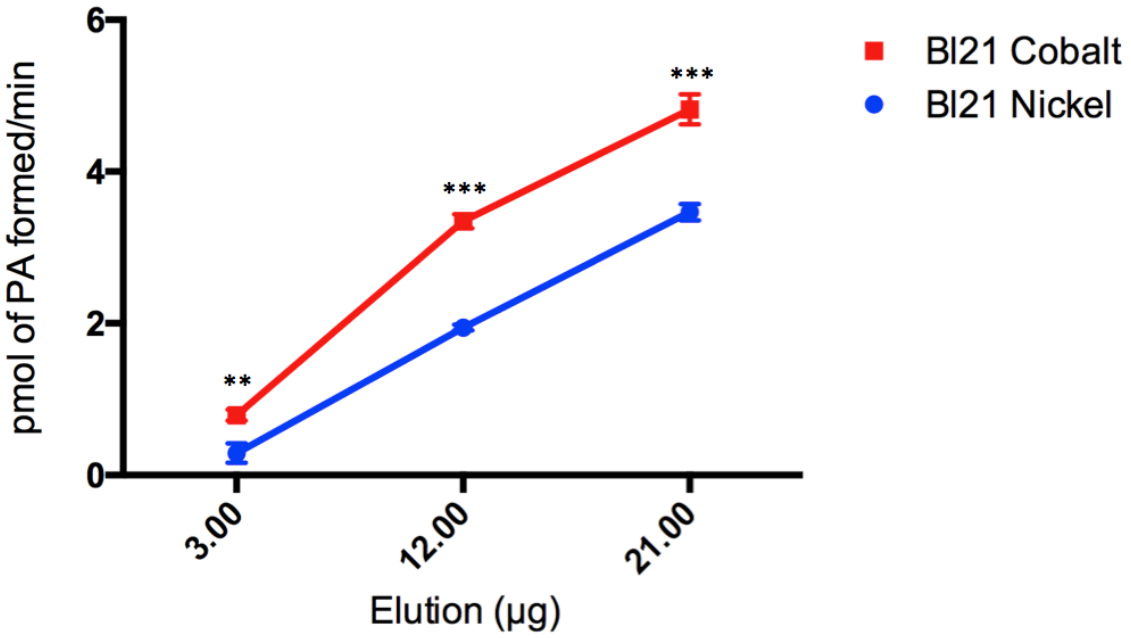

Figure 10. *E coli* contain a contaminant LPAAT that binds to cobalt and nickel affinity resins. [1-^{14}C-oleoyl] oleoyl-CoA (10 µM) and LPA (50 µM) were incubated in duplicate reactions with 3, 12, or 21 µl of partially purified cell lysate for 10 minutes at 37°C. Lipids were extracted from the reaction mixture and spotted onto a TLC plate for separation of PA from unreacted substrate. The location of radiolabeled PA corresponded to a cold PA standard, spotted on the same plate. Bands corresponding to PA were scraped and radioactivity was quantified by scintillation counting. Data are the mean ± standard deviation of duplicate reactions. Data for Bl21 Cobalt were compared to BL21 Nickel using a two-way ANOVA (**, $p < 0.001$, ***, $p < 0.001$). Where error bars are not visible, they are contained within the symbol.

Figure 11

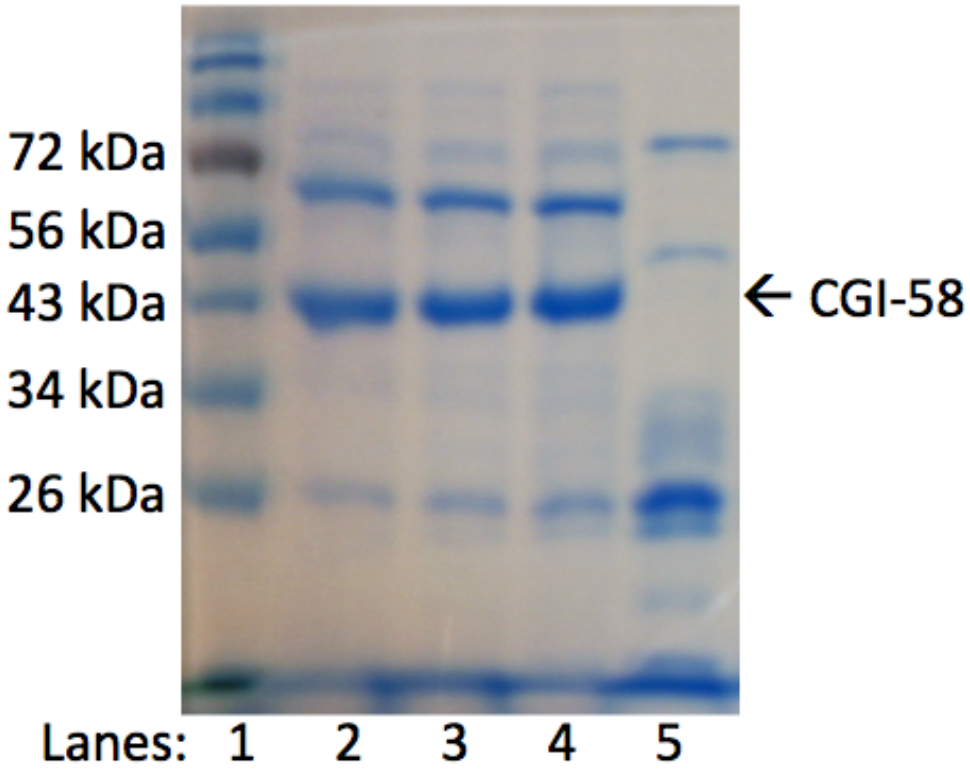

Figure 11. *E coli* contain contaminant proteins that bind to cobalt and nickel affinity resins. BL21(DE3) extracts containing or lacking 12-His-tagged CGI-58 were purified over cobalt resin and eluted on a 12% SDS-PAGE gel. Resolved proteins were visualized with Coomassie stain. A 27 kDa band, which may be plsC, is present in all lanes. Lanes contain: EZ Run Molecular Weight Marker (lane 1), three separate preparations of WT CGI-58 (lane 2-4), and BL21(DE3) extracts lacking CGI-58 (lane 5).

LPAAT, is approximately 27 kDa [163]. These results led us to suspect that plsC contamination is the source of LPAAT activity in preparations of CGI-58, since increased LPAAT activity correlated with increased levels of the 27 kDa protein.

CGI-58 activity in SM2-1(DE3) plsC knockout cell lysates – The SM2-1(DE3) *E. coli* strain [164] was used to express CGI-58. The SM2-1(DE3) line was created from the SM2-1 *E. coli* strain, which lack functional plsC [164], using a λDE3 lysogenization kit (Novagen) to allow for IPTG-induced expression of T7 RNA polymerase for subsequent translation of 12-His tagged CGI-58. After induction with IPTG and cell lysis, SM2-1(DE3) cells lysates expressing either WT CGI-58 or CGI-58 with various mutations (Table 2) were screened for LPAAT activity. All lysates, including those containing WT CGI-58, were observed to lack LPAAT activity (data not shown). This preliminary result suggested that all variants tested, including WT CGI-58, are not LPAATs.

To evaluate if WT CGI-58 is capable of LPAAT activity, SM2-1(DE3) cells were transformed with empty pET-28a vector, or pET-28a vector with cDNA for 12-His CGI-58 or 6-His plsC. Incubation of cells with IPTG induced the expression of 12-His CGI-58 or 6-His plsC. Since plsC targets to membranes in *E. coli*, whole cell lysates (duplicate samples of 5, 10, or 20 μg) were tested for LPAAT activity. Samples containing 12-His tagged WT CGI-58 lacked LPAAT activity (Figure 12). Lysates containing the empty pET-28a vector did not display LPAAT activity, as they lack the endogenous LPAAT plsC. Lysates expressing low amounts of plsC (Figure 13) produced radiolabeled PA (Figure 12). However, these samples did not show a

Table 2

CGI-58 mutations	LPAAT activity *in vitro*	Reduction of TAG content in NLSDi cells
H84A	-	+
H84R	-	-
D110A	-	not tested
H154A	-	not tested
N155A	not tested	+
N155S	not tested	+
E179A	-	not tested
E260A	not tested	+
E260K	not tested	+
D301A	not tested	+
D301N	not tested	+
H329A	-	+
H329R	not tested	+
D334A	-	+
D334N	not tested	+
E179A/H329A	-	not tested
D110A/H84A	-	not tested
E179A/H154A/H329A	-	not tested

Table 2. Summary of results from experiments using CGI-58 variants.

Mutations in these acidic and basic residues of CGI-58 were made based on known human NLSDi mutations or highly conserved acidic and basic residues. Site directed mutagenesis was performed on CGI-58 cDNA in the pET-28a vector for expression in *E. coli* or in the pShuttle-CMV vector for generation of adenovirus to drive overexpression in NLSDi fibroblasts. Some of these variants of CGI-58 were tested for LPAAT activity *in vitro* ("-" represents a lack of LPAAT activity). Variants of CGI-58 overexpressed in NLSDi cells were assessed for their function to reduce accumulated TAG ("+" represents reduction of TAG similar to cells expressing WT CGI-58, "-" represents retention of accumulated TAG)

Figure 12

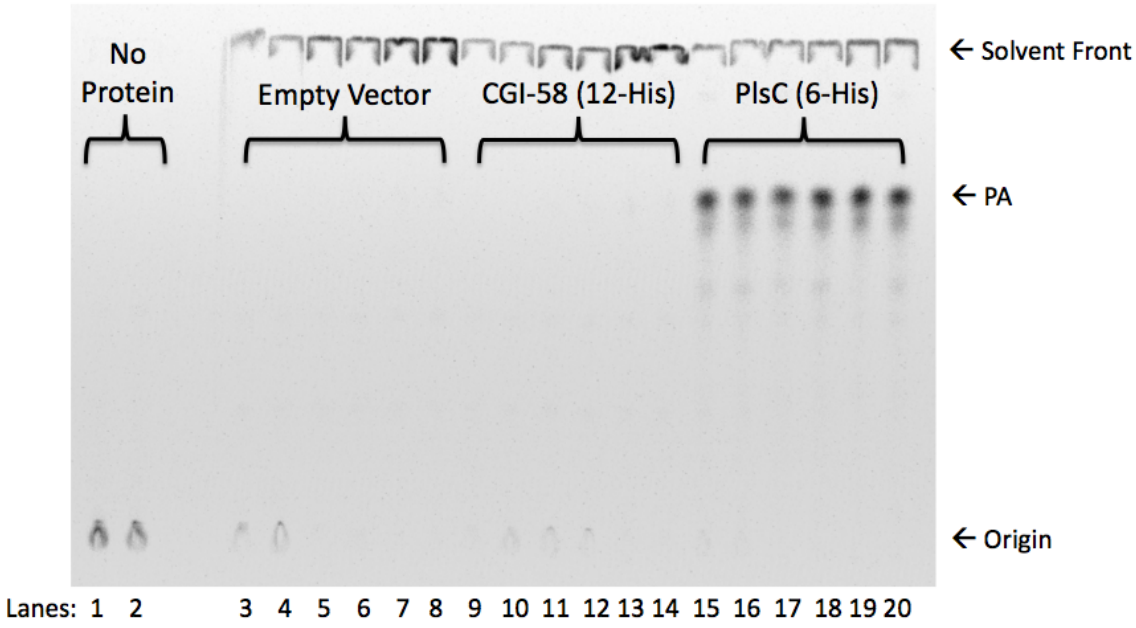

Figure 12. SM2-1(DE3) cell lysates containing 12-His tagged CGI-58 lack LPAAT activity. Whole cell lysates of SM2-1(DE3) cells containing empty pET-28a vector or over-expressing 12-His tagged CGI-58 or 6 His-tagged plsC were subjected to a LPAAT activity assay. [1-^{14}C-oleoyl] oleoyl-CoA (10 µM) and LPA (50 µM) were incubated in duplicate reactions with 5, 10, or 20 µg of whole cell lysate protein for 10 minutes at 37°C. Lipids were extracted from the reactions and spotted on a TLC plate for separation of products from unreacted substrate. The position of radiolabeled PA corresponded to a cold PA standard eluted on the same plate. The lanes were spotted as follows: No protein blank (lanes 1,2), 5-20 µg of empty vector lysate (lanes 3-8), 5-20 µg of CGI-58 extract (lanes 9-14), 5-20 µg of plsC lysate (lanes 15-20).

Figure 13

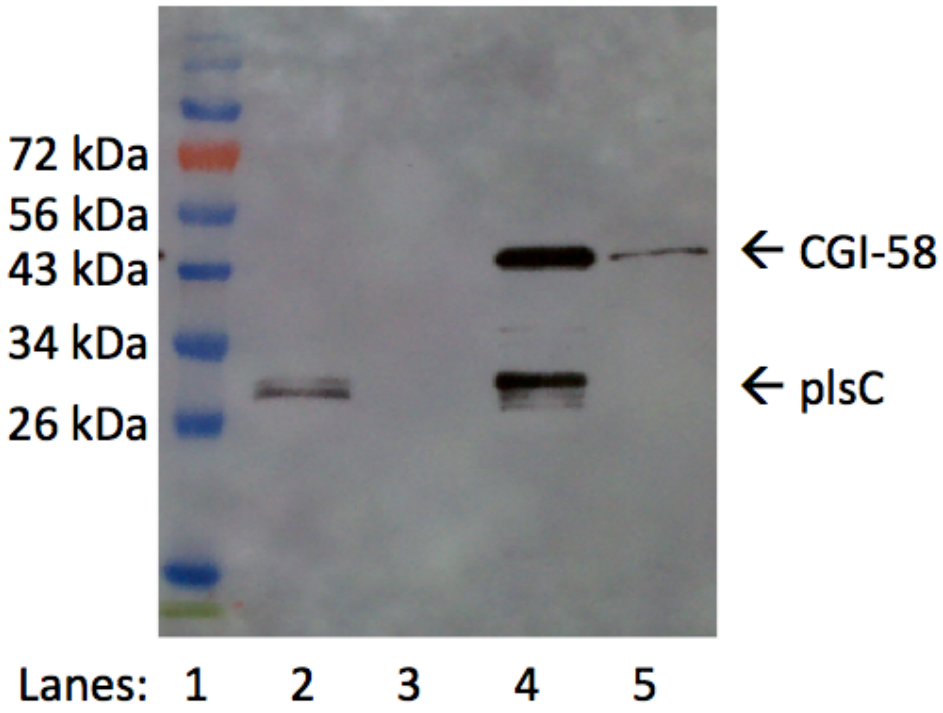

Figure 13. Immunoblot of SM2-1(DE3) lysates containing 12-His tagged CGI-58 or 6-His tagged plsC. A 12% SDS-PAGE gel was loaded with 20 µg of cell lysate protein. After electrophoresis, samples were then transferred to nitrocellulose and probed for 6-His using anti-6-His antibody and peroxidase-conjugated anti-mouse IgG. Samples were loaded as follows: EZ Run Marker (lane 1), extract containing plsC (lane 2), empty vector lysate (lane 3), extract containing 12-His CGI-58 (lane 4), 100 ng partially purified 12-His CGI-58 (lane 5).

dose-dependent response in PA formation. PlsC reaction kinetics have not been well defined in the published literature. It is possible that plsC is a highly active enzyme and, at the concentrations of substrate tested, the activity may have been limited by available substrate, yielding maximal PA formation at even the lowest amount of lysate tested. These results suggest that CGI-58 is not an LPAAT.

GST-tagged CGI-58 lacks LPAAT activity – PlsC binds avidly to metal affinity resin due to the positive charge. To avoid plsC contamination, the cDNA for mouse CGI-58 was subcloned into the pGEX-4T-1 plasmid for expression and purification of a Glutathione S-transferase (GST) N-terminally tagged CGI-58. GST-CGI-58 was expressed and purified from BL21(DE3) *E. coli*. Purified GST-CGI-58 was unstable; immunoblots using anti-GST antibodies or anti-CGI-58 antiserum revealed lower molecular weight degradation products that increased with time of storage (data not shown). Instead, the LPAAT activity of GST-CGI-58 was assessed in cell lysates. Bl21(DE3) cells express the membrane-bound LPAAT, plsC; therefore, centrifugation of cell lysates at 16,000 x *g* pellets membrane fractions containing plsC effectively removes detectable LPAAT activity from the cell lysate (data not shown). Immunoblots of GST-tagged CGI-58 reveal that expression levels are similar in either the whole cell lysate or in 16,000 x *g* supernatant (Figure 14). The LPAAT activity of BL21(DE3) whole cell lysates containing GST-tagged CGI-58 and the supernatants of similar lysates centrifuged at 16,000 x *g* were assessed (Figure 15). Duplicate reactions containing 2.5, 5, or 10 μg of each extract were incubated with

Figure 14

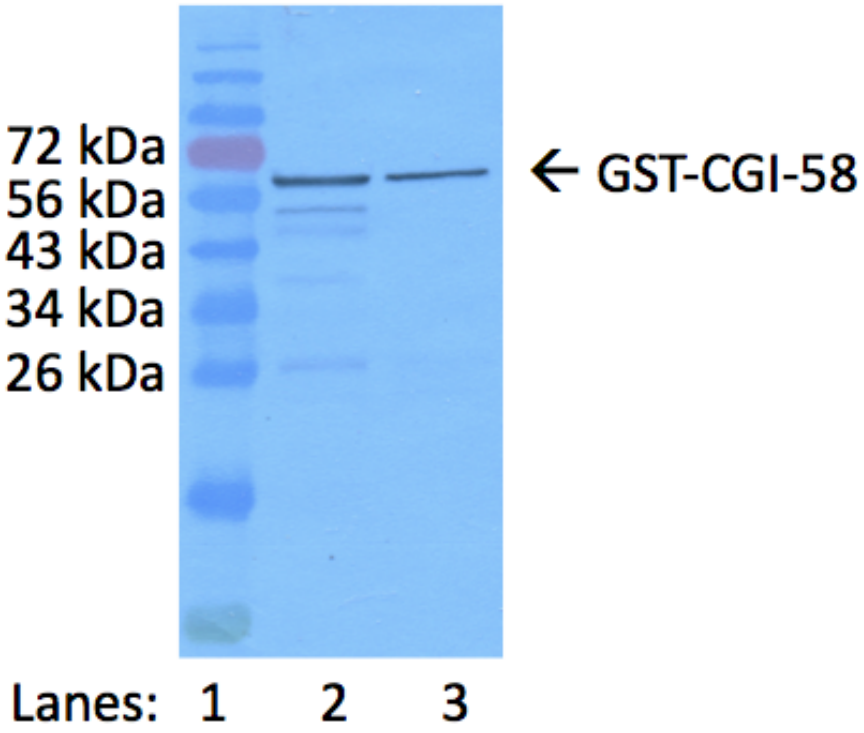

Figure 14. Immunoblot of GST-tagged CGI-58 in Bl21(DE3) cell lysates. 20 µg of cell lysates were eluted on a 12% SDS-PAGE gel. After electrophoresis, samples were transferred to nitrocellulose and probed for GST-CGI-58 using an anti-GST antibody and peroxidase conjugated anti-goat IgG. Lanes contain: EZ Run Molecular Weight marker (lane 1), 20 µg protein from whole cell lysate (lane 2), 20 µg protein from 16,000 x *g* extract (lane 3).

Figure 15

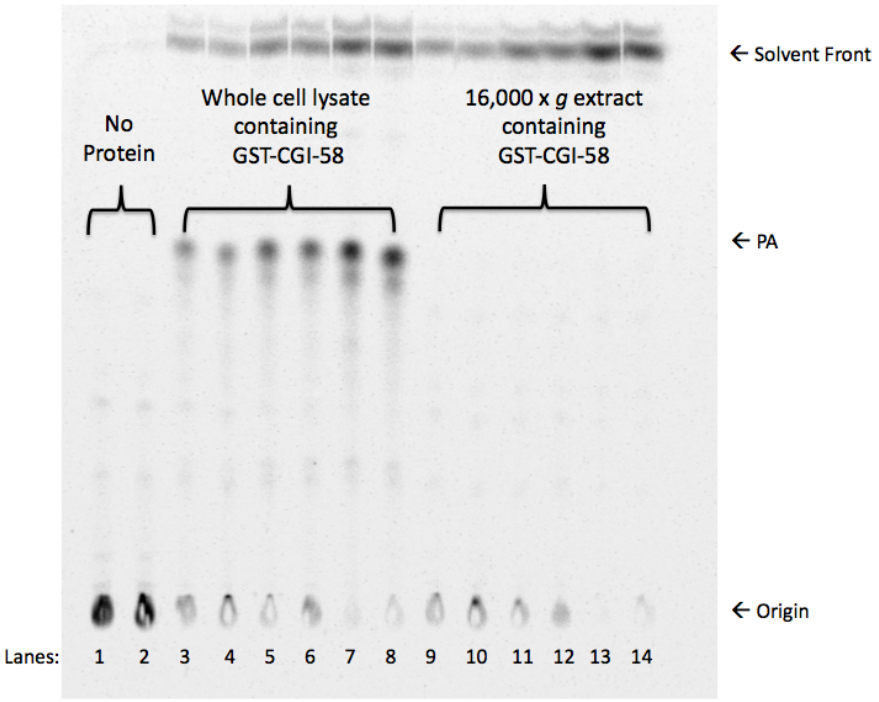

Figure 15. GST-tagged CGI-58 lacks LPAAT activity. Bl21(DE3) cells overexpressing GST-tagged CGI-58 were lysed in PBS with 0.5 mg/ml lysozyme in the presence of Sigma protease inhibitors. A fraction of the lysate was centrifuged at 16,000 x *g* to remove membranes. Both whole cell lysates and 16,000 x *g* extracts were subjected to a LPAAT activity assay. Extracted lipids were eluted on a TLC plate. Lanes contain: no lysate blanks (lanes 1,2), 2.5 µg protein from whole cell lysate (lanes 3,4), 5 µg protein from whole cell lysate (lanes 5,6), 10 µg protein from whole cell lysate (lanes 7,8), 2.5 µg protein from 16,000 x *g* supernatant (lanes 9,10), 5 µg protein from 16,000 x *g* supernatant (lanes 11,12), 10 µg protein from 16,000 x *g* supernatant (lanes 13,14). Elution of radiolabeled PA was identified by comparison to a cold PA standard spotted on the same plate.

LPA and radiolabeled oleoyl-CoA for 10 min at 37°C. Whole cell lysates containing endogenous plsC and recombinant GST-tagged CGI-58 showed a dose-dependent increase in LPAAT activity, as expected. The 16,000 x *g* supernatants containing recombinant GST-tagged CGI-58 lacked PA. These results suggest that GST-tagged CGI-58 does not contribute to the LPAAT activity of Bl21(DE3) lysates.

LPAAT activity in purified preparations of CGI-58 corresponds to levels of contaminant proteins – Previous experiments have shown that LPAAT activity correlated to levels of contaminant proteins (Figures 8 and 9). Therefore, it is essential to reduce contaminant protein levels in preparations of partially purified CGI-58. The initial purification protocol utilized a single buffer for lysis of cells and column wash steps, including 50 mM Tris pH 7.5, 20 mM imidazole, and 300 mM NaCl. Following examination of the literature [57] and discussions with Rutgers colleagues (members of the Storch group), the protocol was altered. There are now different buffers for lysis and column wash steps; 1 mM DTT was added to all buffers and 20 and 100 mM imidazole were added to the lysis and wash buffers, respectively. The addition of DTT prevented inappropriate disulfide bond formation reducing cross-linking of contaminant proteins to CGI-58. The imidazole concentration of the wash buffer was increased to elute greater levels of contaminant proteins during wash steps, while minimizing early elution of CGI-58. These changes increased the purity of 12-His-tagged CGI-58 preparations. As visualized on a Coomassie stained SDS-PAGE gel (Figure 16), CGI-58 expressed in

Figure 16

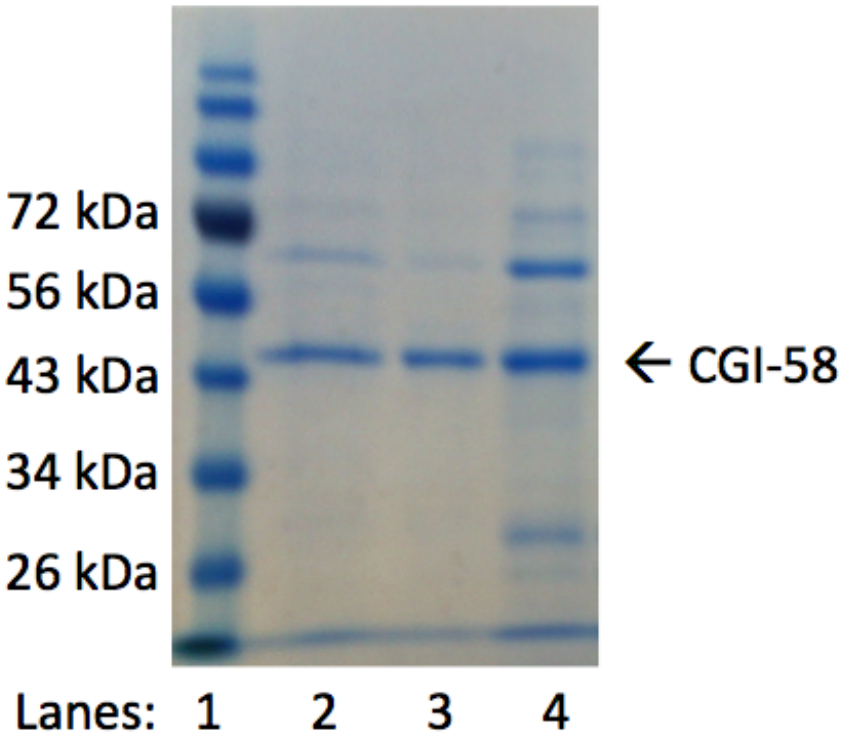

Figure 16. A stringent wash buffer reduced contaminant protein concentrations in preparations of purified 12-His CGI-58. A 12% SDS-PAGE gel was loaded with 1 µg of partially purified CGI-58 and proteins were visualized using Coomassie stain. Samples were loaded as follows: EZ Run Marker (lane 1), 1 µg CGI-58 from SM2-1(DE3) (lane 2), 1 µg CGI-58 from BL21 using the updated purification protocol, and 1 µg CGI-58 from Bl21(DE3) using the older purification protocol (lane 3).

either SM2-1(DE3) or Bl21(DE3) *E. coli* strains and purified using this updated protocol lacks detectable protein contaminants of 27 kDa.

The LPAAT activity of recombinant CGI-58 purified from Bl21(DE3) cells using the original protocol was assessed in comparison to the activity of recombinant CGI-58 purified from BL21(DE3) or SM2-1(DE3) cells using the new protocol. Duplicate reactions containing 0.25, 0.5, or 1 μg of protein from each of the three purified CGI-58 preparations were tested for LPAAT activity. Recombinant CGI-58 purified using the new protocol lacks LPAAT activity (Figure 17). However, recombinant CGI-58 purified using the original protocol shows a dose-dependent increase in PA formation. When CGI-58 preparations that contained LPAAT activity were preincubated with DTT (1 mM), there was no inhibitory effect when compared to preparations without DTT (data not shown). In summary, these experiments suggest that the previously observed LPAAT activity is due to the contaminant protein plsC.

CGI-58 purified using the improved protocol activates ATGL – To verify that the updated purification protocol yields functional CGI-58, the ability of partially purified recombinant CGI-58 from both SM2-1(DE3) and BL21(DE3) cells to co-activation of ATGL was assessed relative to recombinant CGI-58 purified using the original protocol. Post-nuclear Sf9 extracts (50 μg protein) containing recombinant 6-His tagged murine ATGL were mixed with 0.25, 0.5, or 1 μg of purified recombinant 12-His tagged CGI-58 (Figure 18). Reaction mixtures were incubated with radiolabeled TAG substrate emulsified with PC:PI (3:1) for 1 hour at 37°C. All

Figure 17

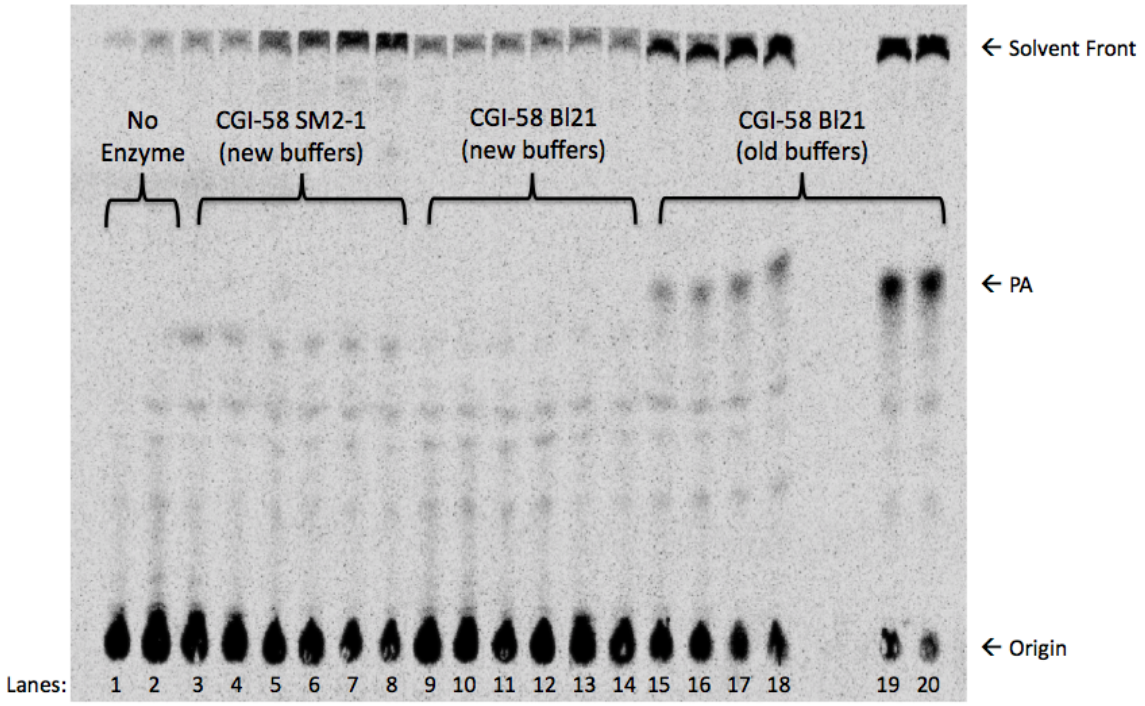

Figure 17. Preparations of CGI-58 lacking detectable contaminant proteins at 27 kDa lack LPAAT activity. Recombinant12-His tagged CGI-58 partially purified from either SM2-1(DE3) or BL21(DE3) *E. coli* strains were subjected to an LPAAT activity assay. Resulting PA from duplicate reactions was extracted and spotted on a TLC as follows: no protein blanks (lanes 1,2), 0.25 – 1 µg CGI-58 purified from SM2-1 using the updated protocol (lanes 3-8), 0.25 – 1 µg CGI-58 purified from BL21(DE3) using the updated purification protocol (lanes 9-14), and 0.25 – 1 µg CGI-58 purified from BL21(DE3) using the older purification protocol (lanes 15-20).

Figure 18

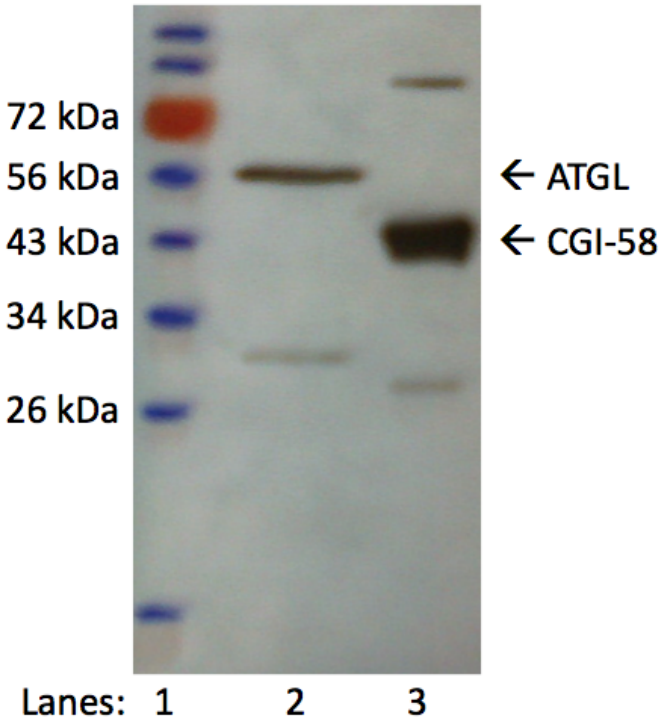

Figure 18. Immunoblot of Sf9 extract containing ATGL and partially purified 12-His CGI-58. After electrophoresis, samples were transferred to nitrocellulose and probed for 6-His using anti-6-His antibody and peroxidase conjugated anti-mouse IgG. Lanes contain: EZ Run Molecular Weight marker (lane 1), 40 µg Sf9 extract containing ATGL (lane 2), 300 ng partially purified recombinant CGI-58 (lane 3).

preparations of CGI-58 increased ATGL-mediated TAG hydrolase activity (Figure 19); there were no significant differences between either preparations of CGI-58 or experimental repetitions. These data demonstrate that recombinant CGI-58 purified from either SM2-1(DE3) or BL21(DE3) using the improved purification protocol functions similarly to recombinant CGI-58 purified using the original protocol. Therefore, the loss of LPAAT activity from preparations of CGI-58 from either BL21(DE3) or SM2-1(DE3) cells was likely not due to structural changes in CGI-58 during handling of samples. Importantly, LPAAT activity is not required for the activity of CGI-58 in promoting TAG hydrolase activity of ATGL.

CGI-58 binds PIPs and not LPA – A previous study used tryptophan quenching assays to show that CGI-58 binds fatty acyl-CoA and LPA substrates for LPAAT activity [106]. Given the recent discoveries of significant contamination of these previous preparations of CGI-58 with a bacterial LPAAT, the lipid binding activity of CGI-58 was re-examined.

To assess the binding of lipids to CGI-58, lipid overlay assays were performed using a wide variety of lipids substrates. Membranes containing 100 pmol/spot of various lipids were incubated with partially purified CGI-58 (12.8 nM) and then probed with either anti-6-His antibodies or anti-CGI-58 antiserum. Strong signals for CGI-58 binding were observed on spots corresponding to PI(3)P and PI(5)P. Weaker signals were observed on spots corresponding to PI(4)P, PI(3,5)P_2, and PA (Figure 20). There was no detectable signal on spots corresponding to the LPAAT substrate, LPA, suggesting that CGI-58 does not bind LPA.

Figure 19

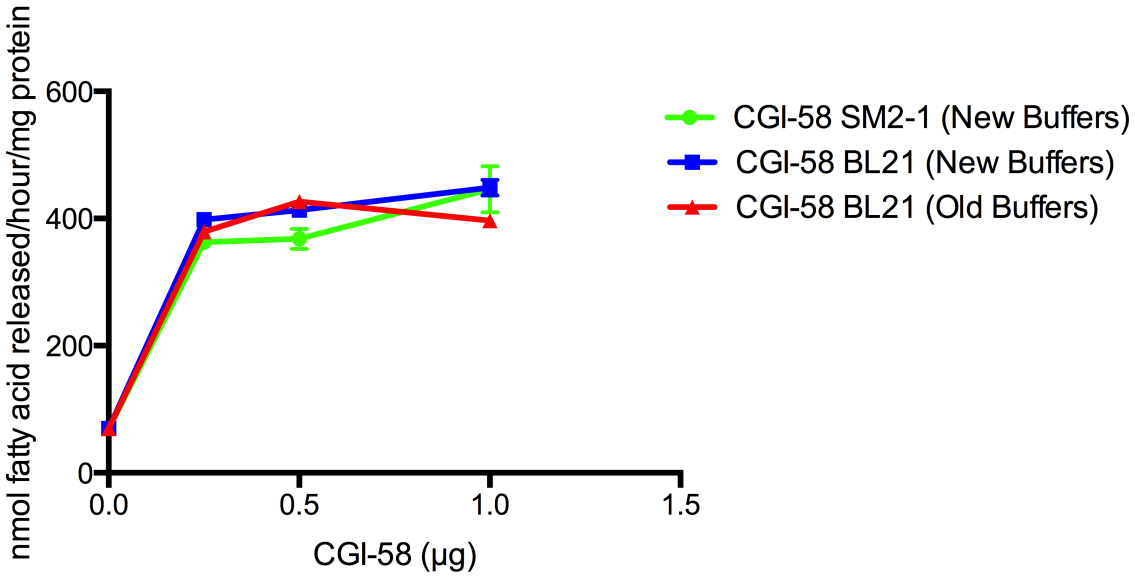

Figure 19. CGI-58 purified using either protocol comparably increases ATGL TAG lipase activity – Post-nuclear Sf9 cell extracts containing recombinant 6 His-tagged ATGL (50 µg protein) were mixed with up to 1 µg of 12-His tagged CGI-58 partially purified from either Bl21(DE3) or SM2-1(DE3) cell lines. Reactions were mixed with an emulsion of [9,10-^{3}H] triolein with PC:PI (3:1). Data are the mean ± standard deviation of duplicate reactions. Data for CGI-58 purified using the new buffers was compared to CGI-58 purified using the old buffers using a two-way ANOVA. Samples containing CGI-58 were not significantly different from each other regardless of purification buffer or CGI-58 protein concentration. All samples containing CGI-58 were significantly different from samples containing ATGL-only ($p < 0.001$). Where error bars are not visible, they are contained within the symbol.

Figure 20

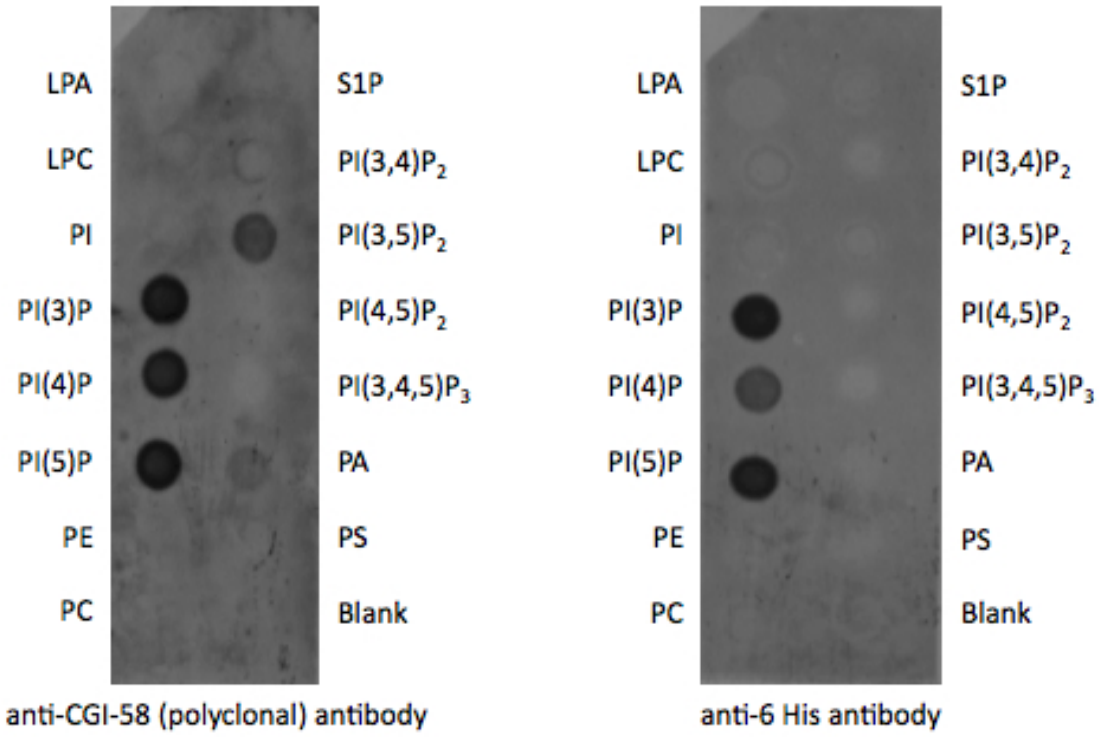

Figure 20. CGI-58 binds PI(3)P, PI(4)P, and PI(5)P. 12.8 nM of partially purified 12-His tagged CGI-58 was incubated with strips containing 100 pmol/spot of various lipids. CGI-58 was detected using anti-CGI-58 antiserum and peroxidase conjugated anti-rabbit IgG or anti-6-His antibody and peroxidase conjugated anti-mouse IgG.

To evaluate relative affinities of PIP binding, partially purified recombinant 12-His CGI-58 (12.8 nM) was incubated with a PIP array containing 1.56 – 100 pmol of various PIPs per spot (Figure 21). Following immunoblotting with a 6-His antibody, brief exposure times revealed signals representing dose-dependent binding of CGI-58 to both PI(3)P and PI(5)P. With longer exposures, the signals for CGI-58 binding to PI(3)P and PI(5)P intensified, while signals for CGI-58 binding to PI(4)P and PI(3,5)P_2 became faintly detectable. These data suggest that CGI-58 binds to PI(3)P and PI(5)P with high affinity, and PI(4)P and PI(3,5)P_2 with reduced affinity. To confirm that CGI-58 was binding these lipids, spots of CGI-58 bound to PI(3)P and PI(5)P from similar assays were cut from the membrane and boiled in 2x LSB then eluted across a 12% SDS-PAGE gel. After being transferred to nitrocellulose, the membrane was probed for CGI-58, revealing a signal at 42 kDa, the molecular weight of CGI-58 (data not shown). These results confirmed that CGI-58, not a contaminant protein, was bound to PI(3)P and PI(5)P.

PIP binding to CGI-58 does not alter CGI-58 stimulation of ATGL TAG hydrolase activity – We sought to determine if PIP binding to CGI-58 alters ATGL activity. First, lipids were incubated with CGI-58 to promote binding; water-soluble (C:8) PI(3)P, PI(5)P, or PI(4,5)P_2 were added in a 100:1 molar ratio to CGI-58, and incubated at room temperature for 20 minutes. CGI-58 pre-incubated with the various lipids was then mixed with Sf9 post-nuclear supernatants containing recombinant ATGL. ATGL lipase activity was increased equally by CGI-58 in the

Figure 21

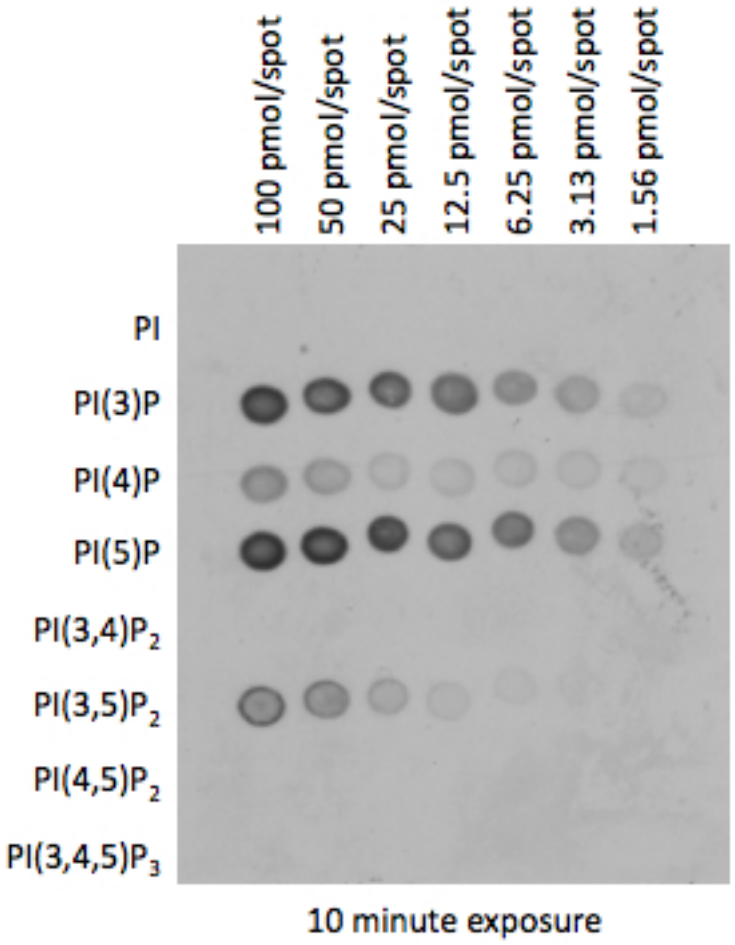

Figure 21. CGI-58 binds PI(3)P and PI(5)P with high affinity. 12.8 nM of partially purified 12-His tagged CGI-58 was incubated with strips containing 1.56 – 100 pmol/spot of various lipids. CGI-58 was detected using anti-6-His antibody and peroxidase conjugated anti-mouse IgG.

presence or absence of PIPs (Figure 22). These data suggest that PIP binding does not impact CGI-58 interaction with ATGL. Hence, PIPs may bind to a site of CGI-58 distinct from the ATGL binding site, or the PIPs may be displaced when CGI-58 binds to ATGL.

In the PIP overlay assays (Figures 20 and 21), the lipids used contained C16:0 fatty acids; however, in the enzyme assay for ATGL interaction, water-soluble C8:0 forms of PIPs were used (Figure 22). In this assay, it was assumed that the water-soluble PIPs bind to CGI-58 with comparable efficiency as the longer acyl chain versions. To quantify the affinity of CGI-58 to these ligands, tryptophan quenching was performed to assess any changes in protein structure following binding of these lipids. These experiments showed variable results, likely due to varying levels of the co-purification of bacterial lipids bound to partially purified CGI-58 from different preparations. Therefore, two methods of delipidation of recombinant CGI-58 were tested.

The first method used was acetone precipitation [165], which effectively denatures and precipitates proteins while solubilizing lipids. Preparations of partially purified CGI-58 were incubated overnight at 4°C in 2 volumes of 1 mM HCL in acetone. The following day, samples were centrifuged at 16,000 x *g* to pellet the precipitated protein. After drying the protein pellet under a stream of nitrogen gas, sodium phosphate buffer at pH 7.5 with 0, 150, or 300 mM of sodium chloride was added in equal volume to the starting material to solubilize the protein pellets. Unfortunately, this method was not useful due to difficulties in solubilizing CGI-58 after precipitation. As an alternative approach, hydroxylalkoxypropyl-dextran

Figure 22

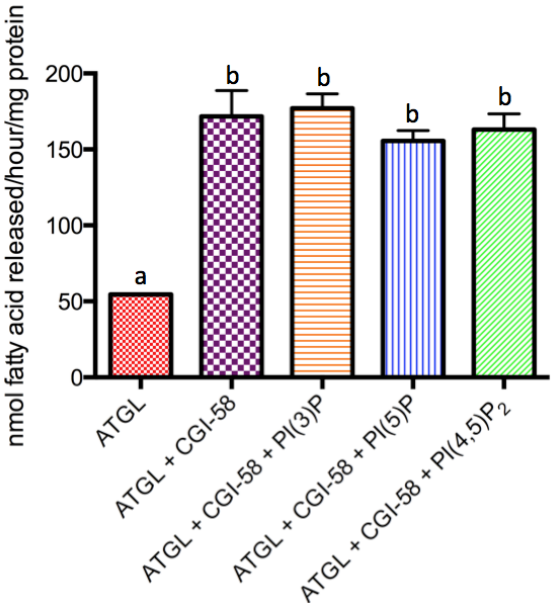

Figure 22. Preincubation of CGI-58 with PI(3)P or PI(5)P does not alter CGI-58's function in co-activation of ATGL - CGI-58 was preincubated with a 100-fold molar excess of indicated C8 PIP molecules for 20 minutes at room temperature. Post-nuclear Sf9 cell extracts containing recombinant 6 His-tagged ATGL (50 µg of protein) were mixed with 1 µg of 12-His tagged CGI-58 partially purified from Bl21(DE3) *E coli*, pre-bound with lipids. Enzyme reactions were mixed with [9,10-^{3}H] triolein emulsified with PC:PI (3:1) and incubated for 1 hour at 37°C. There were no significant differences between reactions containing CGI-58 and various PIPs. Reactions containing CGI-58 were significantly greater ($p < 0.001$) than ATGL-only reactions. Data are the mean ± standard deviation of duplicate reactions and were analyzed using a one-way ANOVA. Where error bars are not visible, they are contained within the symbol. This figure is from one representative experiment of three.

(Sigma), a lipid binding resin, was used to attempt to remove lipids from the preparations of CGI-58. Several passes of partially purified CGI-58 through a column containing hydroxylalkoxypropyl-dextran resin at 37°C did not remove the lipids from the protein. Subsequent solvent extracts of CGI-58 revealed a variety of lipids by TLC (Figure 23). Due to the difficulty in removing bound lipids from recombinant CGI-58, the relative binding efficiency of C8 acyl chain PIPs to CGI-58 has yet to be determined.

Measurement of TAG content of NLSDi fibroblasts expressing WT CGI-58 or mutated variants of CGI-58 – In a search for amino acid residues critical to CGI-58 function, several conserved acidic or basic residues were mutated; in some cases, the mutations mimicked known human mutations found in NLSDi patients. Cultured NLSDi fibroblasts store high levels of TAG due, at least in part, to a defect in the incorporation of lipid intermediates from TAG hydrolysis into phospholipids [130]. Overexpression of CGI-58 in these cells causes a decrease in TAG levels and an increase in fatty acid movement from TAG to phospholipids [106]. The major lipase of human skin fibroblasts is uncharacterized, so it is currently unknown whether expression of CGI-58 decreases levels of TAG through co-activation of ATGL, or another mechanism. Variants of CGI-58 were overexpressed in NLSDi fibroblasts to assess their ability to reduce TAG levels of the cells.

The effect of CGI-58, containing mutations to key amino acids, on TAG levels in NLSDi fibroblasts was measured. Residues H329 and D334 were selected for

Figure 23

Figure 23. Hydroxylalkoxypropyl-dextran does not delipidate preparations of CGI-58 - Lipids were solvent extracted from partially purified preparations of recombinant 12-His-tagged CGI-58 before (lane 1) and after (lane 2) treatment with hydroxylalkoxypropyl-dextran and were eluted on a TLC plate. Lipids were visualized using iodine staining.

mutation since they are putative acyltransferase residues. CGI-58 harboring the point mutations H84R [166] and E262K [49], which are mutations found in NLSDi patients, were also tested. In mammalian CGI-58, the serine residue located in the lipase consensus motif, GXSXG, is mutated to asparagine [49]; however homology studies reveal that this residue is serine in *C. elegans* CGI-58 (Figure 4). Therefore, N155 was mutated to either serine or alanine. The highly conserved acidic residue D303, a residue predicted to be potentially catalytic by molecular modeling experiments, was also mutated to asparagine or alanine. Each of these mutated variants of CGI-58 was expressed in NLSDi cells. TAG content of cells was measured 48 hours after the addition of adenoviral expression vectors. If these residues contribute to the activity or structure of CGI-58, then the TAG levels of NLSDi cells should remain elevated following expression of CGI-58; however, if CGI-58 harboring any of these mutations functions correctly, then TAG levels should be reduced comparably to WS1 cells, normal human skin fibroblasts that express endogenous CGI-58. Due to the number of variants tested, CGI-58 with mutations to the acidic residues were tested in one set of experiments, whereas cells expressing CGI-58 with mutations to basic residues or to N155 were tested in another set of experiments.

CGI-58 variants harboring these various point mutations were expressed at relatively similar levels (Figures 24 and 25) in cultured NLSDi fibroblasts via an adenoviral expression system. When CGI-58 was expressed in NLSDi cells, TAG levels were comparable to those of normal human skin fibroblasts (Figures 26 and 27) affirming that elevated TAG in NLSDi cells is due to the absence of functional

Figure 24

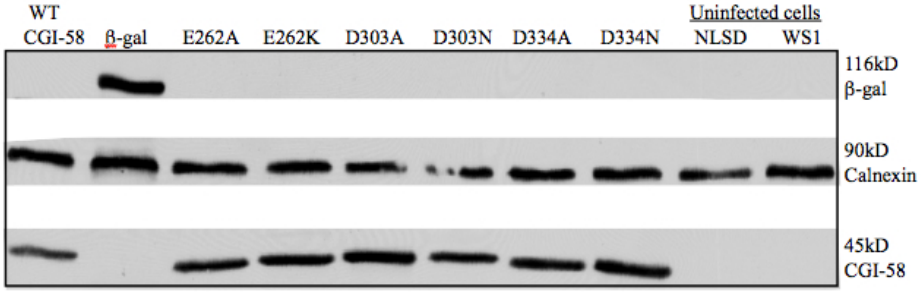

Figure 24. Immunoblot of NLSDi cells expressing variants of CGI-58 with mutations to acidic residues. NLSDi cells lysates (40 µg) were eluted on a 10% SDS-PAGE gel, transferred to nitrocellulose, and probed with antiserum raised against mouse CGI-58 or anti-β-galactosidase antibodies. Calnexin was probed for as a loading. WS1 cells did not show detectable levels of endogenous CGI-58 after probing with antibodies raised against mouse CGI-58.

Figure 25

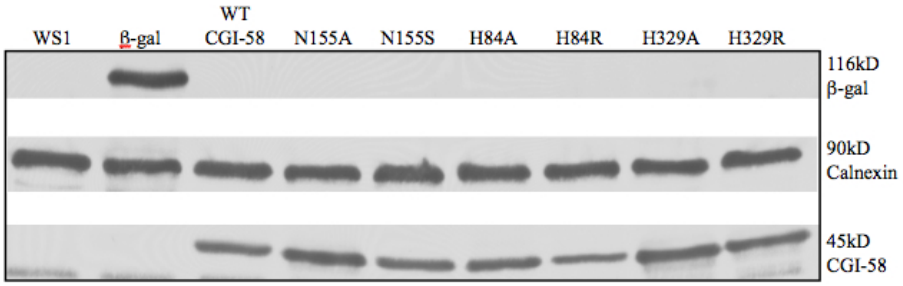

Figure 25. Immunoblot of NLSDi cells expressing variants of CGI-58 with mutations to basic residues. NLSDi cells lysates (40 μg) were eluted on a 10% SDS-PAGE gel, transferred to nitrocellulose, and probed with antiserum raised against mouse CGI-58 or anti-β-galactosidase antibodies. Calnexin was probed for as a loading control. WS1 cells did not show detectable levels of endogenous CGI-58 after probing with antibodies raised against mouse CGI-58.

CGI-58. TAG levels remained elevated in NLSDi fibroblasts transduced with adenovirus to drive expression of β-galactosidase.

TAG levels of NLSDi cells expressing mutated variants of CGI-58 were compared to TAG levels of WS1 cells, NLSDi cells expressing WT CGI-58, and NLSDi cells expressing β -galactosidase. When CGI-58 variants E262A, E262K, D303A, D303N, D334A, or D334N were expressed in NLSDi cells, TAG levels were reduced comparably to NLSDi cells expressing WT CGI-58 (Table 2, Figure 26). Hence, these conserved acidic residues are not required for CGI-58 function in the maintenance of TAG homeostasis. Interestingly, CGI-58 variant E262K, a known human mutation causing NLSDi, reduced accumulated TAG effectively. This unexpected result may be due to overexpression of a partially functional protein.

The second set of the experiments examined TAG levels of NLSDi cells in which CGI-58 with mutations to the conserved basic residues as well as the lipase catalytic motif residue N155 (Table 2, Figure 27). Expression of CGI-58 with mutations N155A or N155S reduced cellular TAG levels comparably to expression of WT CGI-58 in NLSDi cells. Thus, the asparagine residue within the conserved lipase motif is not critical residue for CGI-58 function. Similarly, NLSDi cells expressing H329A, H329R (Figure 27), D334A, and D334N (Figure 26) reduced TAG levels comparably to WT CGI-58 expression, revealing that the putative acyltransferase sites are not necessary for CGI-58 function in TAG homeostasis. In contrast, NLSDi cells expressing CGI-58 with the known NLSDi mutation H84R, retained high levels of TAG, indicating that the H84R CGI-58 variant has reduced function. Expression of the H84A CGI-58 variant reduced TAG levels comparably to expression of

Figure 26

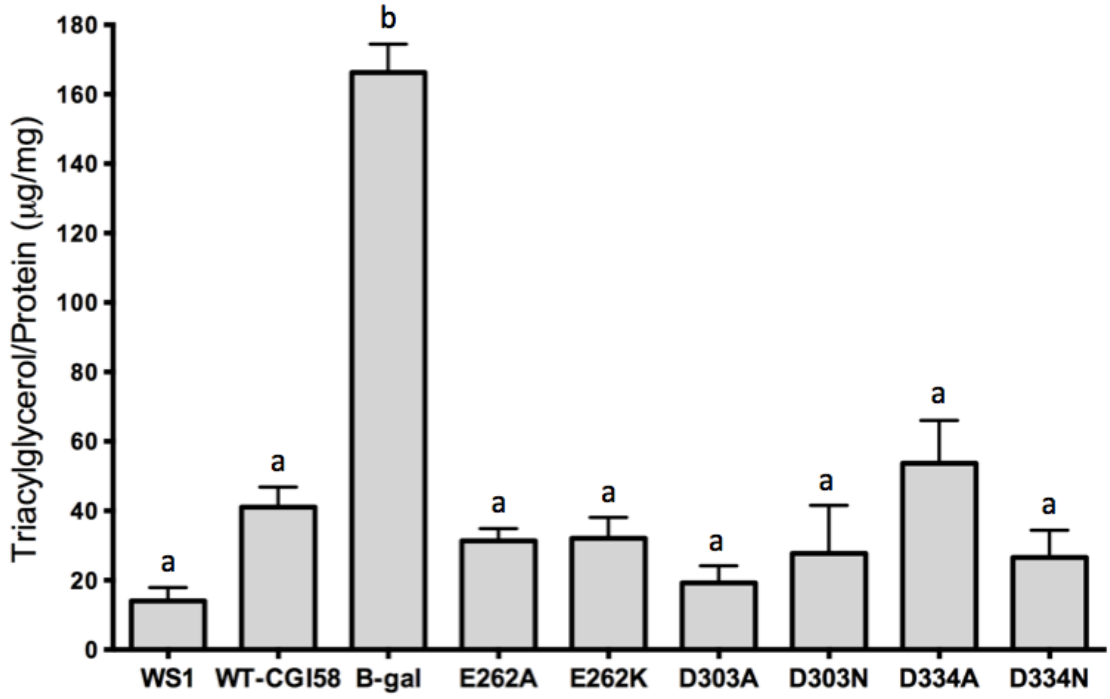

Figure 26. TAG levels of NLSDi cells expressing ectopic CGI-58 containing various mutations to acidic residues. TAG content of cells was determined 48 hours after treatment with adenoviral vectors. TAG levels of NLSDi cells expressing CGI-58 variants were not significantly different from those expressing WT CGI-58 or WS1 cells. Cells expressing β-galactosidase had significantly higher ($p < 0.001$) TAG content than all other samples. Data are the mean ± standard deviation of triplicate reactions and were compared using one-way ANOVA. These data are the combined results of three experiments.

Figure 27

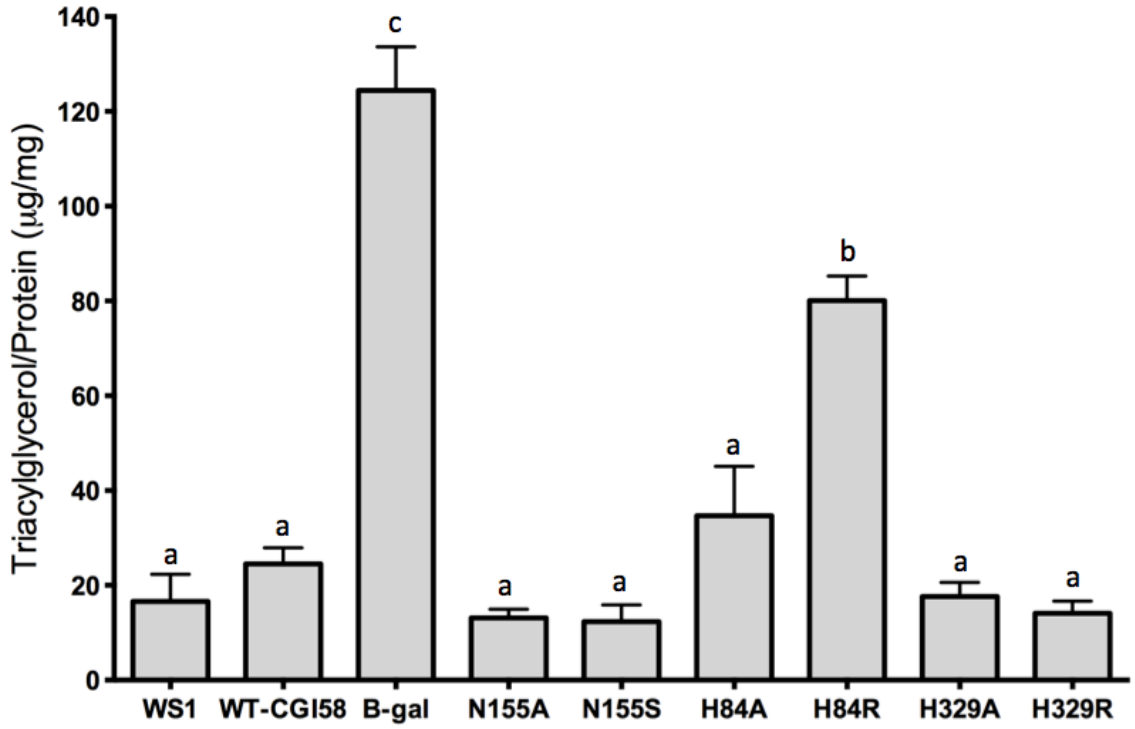

Figure 27. TAG levels of NLSDi cells expressing ectopic CGI-58 containing various mutations to basic residues or N155. TAG content of cells was determined 48 hours after treatment with adenoviral vectors. Samples containing H84R were significantly different ($p < 0.01$) than all other samples. Data are the mean ± standard deviation of triplicate reactions and were compared using one-way ANOVA. These data are the combined results of three experiments.

WT CGI-58. Together, these results suggest that H84 is not critical for function, but a substitution with arginine reduces CGI-58's function to regulate TAG homeostasis. It is possible that the substitution of histidine with arginine causes a conformational change in CGI-58 leading to a misfolded and partially functional protein.

***In vitro* studies of H84 mutated CGI-58 –** To further examine CGI-58 variants H84A and H84R, CGI-58 harboring these mutations was tested for the ability to co-activate ATGL *in vitro*. Post-nuclear Sf9 extracts containing recombinant 6-His tagged ATGL were incubated with 1 μg of partially purified recombinant CGI-58 at 37°C for 1 hour with radiolabeled TAG substrate emulsified with PC:PI (3:1). While WT CGI-58 increased ATGL TAG hydrolase activity, neither H84 variant increased TAG hydrolase activity relative to samples containing only ATGL (Figure 28). These data reveal that neither H84A nor H84R functions as a co-activator of ATGL in an *in vitro* assay.

Figure 28

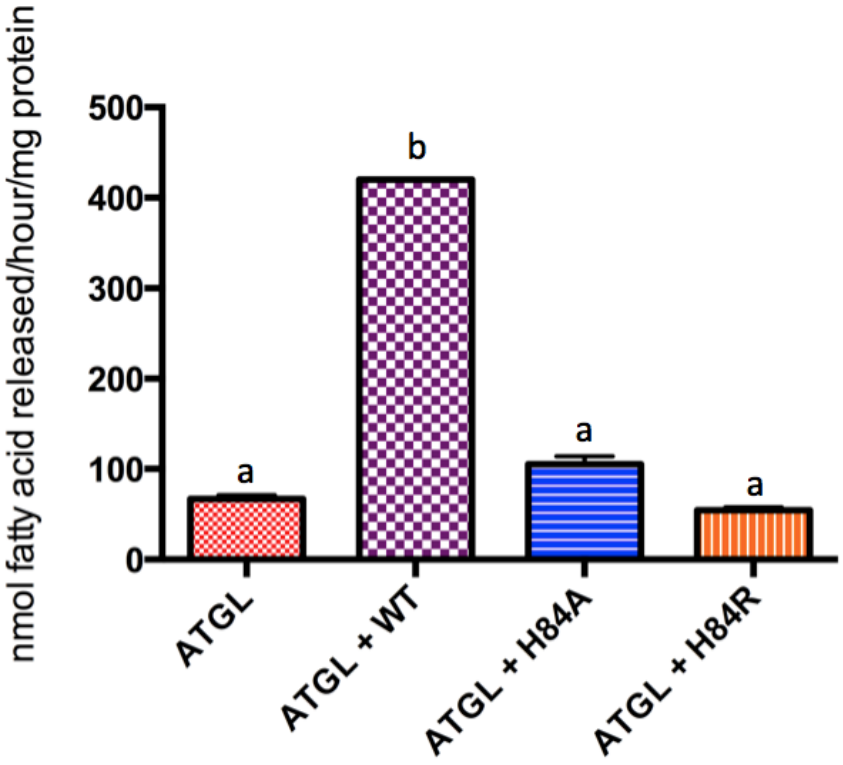

Figure 28. CGI-58 with mutations H84A or H84R does not activate ATGL TAG hydrolase activity *in vitro* - Post-nuclear Sf9 cell extracts containing recombinant 6 His-tagged ATGL (50 µg protein) were mixed with 1 µg of 12-His tagged CGI-58 partially purified from Bl21(DE3) *E coli*. Enzyme reactions were mixed with [9,10-^{3}H] triolein TAG emulsified with PC:PI (3:1) and incubated for 1 hour at 37°C. Reactions containing ATGL with WT CGI-58 were significantly different than all other reactions ($p < 0.001$). Data are the mean ± standard deviation of duplicate reactions and were analyzed by one-way ANOVA. Where error bars are not visible, they are contained within the symbol. This figure is from one representative experiment of three.

Discussion

Overall aims

The central aim of this dissertation project was to determine if CGI-58 LPAAT activity is necessary for the co-activation of ATGL TAG hydrolase activity. Our original approach was to mutate the conserved putative acyltransferase active site residues, H329 and D334, of murine CGI-58 to eliminate LPAAT activity. We would then test these mutated variants of CGI-58 to determine if they could increase ATGL TAG hydrolase activity *in vitro* comparably to WT CGI-58. Also, by expressing these variants in NLSDi fibroblasts (cells lacking functional CGI-58), we could determine if mutated CGI-58 lacking LPAAT activity is able to rescue the phenotype of excessive accumulation of TAG.

Major findings

Recombinant CGI-58 variants containing mutations to the putative LPAAT catalytic active site residues, H329 or D334, were purified from BL21(DE3) *E. coli* and used for LPAAT activity assays. Unexpectedly, partially purified H329A and D334A variants showed increased LPAAT activity relative to WT CGI-58. Moreover, mutations of additional conserved acidic and histidine residues in potential catalytic clefts also failed to reduce LPAAT activity. Preparations of H329A and D334A displayed greater levels of contaminant proteins relative to WT CGI-58, therefore we hypothesized that a contaminant protein was responsible for LPAAT activity. Importantly, purification of BL21(DE3) *E. coli* extracts lacking CGI-58 over cobalt or

nickel affinity resins revealed LPAAT activity in eluants, indicating co-purification of a bacterial LPAAT with CGI-58. *E. coli* express a single LPAAT, plsC.

PlsC purification over metal affinity resins

E. coli plsC is a 27 kDa, positively charged protein that has a calculated isoelectric point of 9.61 and an estimated charge of 12.0 at pH 7.5 (the pH of the lysis buffers employed) [167]. The estimated charge of plsC suggests a strong affinity for metal-affinity resins that are used to purify 6-histidine-fusion proteins. The observed 27 kDa contaminant protein in partially purified CGI-58 preparations and the corresponding LPAAT activity of *E. coli* extracts lacking CGI-58 eluted over a cobalt affinity resin suggests that plsC contamination is responsible for the previously reported LPAAT activity of CGI-58 [105,106]. At this time, there are no commercial antibodies available to detect plsC. Therefore, it is difficult to directly assess plsC contamination in purified protein preparations. Instead, the SM2-1 *E. coli* strain, which contains an inactivating mutation in plsC [164] can be used to study putative LPAATs. These cells show temperature sensitive growth at 30°C, but not 42°C.

Other researchers have been misled by the identification of LPAAT activity in preparations of proteins isolated by metal affinity purification. Endophilins [168,169] and CtBP/BARS (carboxy-terminal binding protein/brefeldin A-ribosylated substrate) [170] have been identified as LPAATs. Endophilin A is enriched in synaptic vesicles and is required for their formation [171,172]. CtBP/BARS has been implicated in membrane fission of vesicles involved in

transport from Golgi to the plasma membrane [173,174]. LPA causes positive curvature in membranes while PA causes negative curvature [175], therefore these proteins were thought to function in vesicle formation by converting LPA to PA [168,170,176]. In 2005, Harvey McMahon and colleagues used the plsC-deficient cell line SM2-1 to determine that endophilins and CtBP/BARS, are not LPAATs [177]. PlsC-deficient cells expressing endophilin A or CTBP/BARS were unable to grow at 42°C, while the same cell line expressing functional plsC was able to grow. These results suggest that endophilin and CtBP/BARS lack the required LPAAT activity to overcome the strain's temperature-sensitive phenotype. We also attempted this type of growth study using the SM2-1(DE3) cell line, but were unsuccessful. The pET-28a vector requires IPTG induction for transcription of CGI-58. We have found that IPTG reduces the growth rate of SM2-1(DE3) cells, adding a confounding factor to measurements of cell growth. To pursue an alternative approach, CGI-58 was purified from the SM2-1(DE3) line and used in *in vitro* LPAAT activity assays; the experiment revealed that, in the absence of plsC contamination, CGI-58 is not a LPAAT.

CGI-58 binds PI(3)P and PI(5)P

Given the findings that CGI-58 lacks LPAAT activity, we decided to revisit lipid-binding activity of CGI-58. Consistent with the lack of LPAAT activity of more highly purified CGI-58, binding of CGI-58 to LPA, an LPAAT substrate, was not detected. Interestingly, CGI-58 was observed to bind both PI(3)P and PI(5)P. Using preliminary densitometry data obtained from the PIP array, CGI-58 binds to PI(3)P

and PI(5)P with an estimated apparent dissociation constant of 6.36 and 5.88 μM, respectively; these values are within the range of previously published apparent dissociation constants of PIP-binding proteins [178-181]. This unexpected result opens up a new focus of study for CGI-58. Although PI(3)P and PI(5)P have not yet been detected on lipid droplets, there is evidence that proteins associated with these lipids interact with and reside on lipid droplets. PI3-kinase (PI3K), an enzyme capable of converting PI to PI(3)P, has been identified as a lipid droplet-associated protein in human leukocytes [182], cells that are affected by NLSDi [51,53]. Chapman and colleagues found PI, the substrate of PI3K, in lipid droplet fractions [2]; however the mass spectrometry method employed does not distinguish between PIPs and PI. Therefore, further analysis of lipid droplet phospholipids with a focus on detecting PIPs would clarify whether they are present in the surface monolayers of lipid droplets. If PI(3)P or PI(5)P are components of lipid droplets, this may explain how CGI-58, when bound to ATGL, interacts with the surfaces of lipid droplets in a PLIN1-independent manner.

PI(3)P is found in various cellular compartments, allowing proteins containing a PI(3)P binding domain to interact with the surface of membranes. In mammalian cells, PI(3)P is produced by three classes of PI3ks [183,184]. Class I and II PI3Ks can phosphorylate PI to form PI(3)P *in vitro*, but also have reactivity towards other PIP substrates [184]. In mammals, there is only one class III PI3K, vacuolar protein sorting homologue (hVps), which produces only PI(3)P [185]. PI(3)P is also produced by the dephosphorylation of PI(3,4)P_2 or PI(3,5)P_2 by eight members of the myotubularin family of proteins [186]. These kinases and

phosphatases have been identified as components of early and late endosomes, the nucleus, clathrin-coated vesicles of the trans-Golgi network, and the plasma membrane. Thus, PI(3)P is produced in many compartments of the cell, where it binds to a wide variety of proteins. An example of how PI(3)P alters protein function has been revealed by studies of the protein sorting nexin 1 which interacts with PI(3)P on early endosomes and acts to drive membrane tubulation [187]. Through this interaction, sorting nexin 1 assists the transport of cation-independent mannose 6-phosphate receptor from the endosome to the trans Golgi network [187]. Thus, PI(3)P provides proteins with an interaction site on the surface of the membrane, promoting protein localization to the correct subcellular compartment. Similarly, binding of CGI-58 to PI(3)P may direct CGI-58 localization to lipid droplets.

PI(5)P is the least characterized of the seven PIPs. PI(5)P is constitutively present in various cell types, with increasing concentrations during insulin stimulation [188,189]. PI(5)P is localized to nuclear membranes [190,191], ER [188], and Golgi. A PI 5-kinase has not been identified yet in mammals, however PI(5)P can be generated through dephosphorylation of PI(4,5)P_2 by the enzymes PI(4,5)P_2 4-phosphatase I and II [192,193]. PI(5)P in nuclear membranes binds to the ING2 protein, a putative tumor suppressor protein [194]. ING2 stimulates acetylation of the tumor suppressor gene product p53 [195], leading to its activation and induction of cell-cycle arrest [196]. ING2 binds both PI(3)P and PI(5)P *in vitro* [194]; however, ING2 interaction with PI(5)P in cultured cells determines its

localization and activity. This example provides insight into PI(5)P function; PI(5)P, like PI(3)P, functions to localize proteins to specific membranes.

Protein interaction with PIPs occurs through conserved binding sites. Proteins interact with PI(3)P through three of five known PIP binding modules: the PH (pleckstrin homology), FYVE (Fab1p, YOTB, Vac1p, EEA1), or PX (phox, phagocyte oxidase) domains [197]. The PH domain consists of 100-120 amino acids that form a seven-stranded antiparallel β-sheet forming a fold that envelopes PI(3)P [184]. There are 251 proteins identified as having PH domains in the human proteome; these proteins include GTPases, motor proteins, and lipid-modifying proteins. The FYVE domain consists of 60-70 amino acids that form two β-hairpins with a C-terminal α-helix held together by two Zn^{2+} binding structures, forming a positively charged pocket [197]. There are more than 27 human proteins known to have the FYVE domain. These proteins are involved in endocytosis, growth factor signaling, and actin cytoskeleton remodeling. The PX domain consists of 120 amino acids which binds a PIP molecule between a 3-stranded β-sheet and an α-helix [197]. This domain is found in NADPH-oxidase, class II PI3K-C2γ, and sorting nexins [184]. Sorting nexins bind to PI(3)P rich membranes, such as an endosomal membranes, and also mediate binding of other proteins to these membranes [198]. Not all proteins that interact with PIPs have these domains; some PIP-binding proteins contain sequences of basic and hydrophobic residues that interact with the negatively charged PIP [184]. At this time, it is unclear if any of these motifs are used to bind PI(5)P.

A high-resolution crystal structure of CGI-58 would provide insight into identifying a PIP binding site. Currently, there is no crystal structure for CGI-58; however, from the computer-generated model developed in this thesis, CGI-58 may interact with PI(3)P or PI(5)P via a hydrophobic pocket containing the basic residues H84, H154, and H329. Based on the model, CGI-58 also contains patches of lysine and arginine residues on the external surface of the protein, such as R58, R64, and R145 or K53, K54, and R116. These positively charged external sites may provide interaction sites with negatively charged PIPs, while the internal hydrophobic pocket might serve another function. In either case, CGI-58 with substitutions of these positively charged residues would be interesting to assay for PIP binding. Such a variant could then be expressed in NLSDi cells or used in *in vitro* assays with ATGL to characterize how PIP binding affects CGI-58 localization or function.

Preliminary work during this project investigated the effect of PIP binding on CGI-58's function in co-activation of ATGL. Pre-binding of partially purified CGI-58 to C8:0 versions of these PIPs did not alter the ability of CGI-58 to activate ATGL *in vitro*. These results suggest that PIP binding might not affect the mechanism by which CGI-58 increases ATGL TAG hydrolase activity. One limitation of these experiments is that the binding affinity of these water soluble PIPs to CGI-58 was not measured. In *in vitro* TAG hydrolase assays, TAG is emulsified using PC and PI. An alternate method of studying the effects of PIPs on the interaction of CGI-58 with ATGL would be to replace the PI in this emulsion with either PI(3)P or PI(5)P and then measure the rate of TAG hydrolase activity of ATGL in the presence of CGI-58.

This method would allow the use of the same C16:0 PI(3)P or PI(5)P that binds to CGI-58 in the lipid-overlay assays shown in this thesis. Furthermore, in this method, the PIPs would be in the surface phospholipid monolayer of the lipid emulsion, which may more accurately mimic the physiological location of these lipids.

CGI-58 co-activates ATGL through an unknown mechanism

The mechanism by which CGI-58 activates ATGL has not been identified. The early assays demonstrating CGI-58 co-activation of ATGL included proteins added in undefined cell extracts from COS-7 cells [41]. Uncharacterized components of these extracts may have contributed to the observed activity. Since the initial discovery, other researchers have reported similar observations [57,60], but never using two purified recombinant proteins; one of the proteins has always been added to the assay in a cell extract. Oberer and colleagues demonstrated CGI-58 activation of ATGL using extracts of recombinant proteins in either COS-7 lysates or *E. coli* lysates [57]. This dissertation work demonstrates that ATGL co-activation by CGI-58 can also by observed when using insect cell extract. Therefore, if an additional factor is needed to activate TAG hydrolase activity, then mammalian, bacterial, and insect cells can each provide this component. A series of experiments would be useful to identify if a component of a cell extract is necessary for synergy. If both recombinant CGI-58 and ATGL are purified, lipase activity could then be measured with or without a cell extract or a boiled cell extract. By boiling the extract, proteins will be denatured, leaving lipids and small molecules intact. These extracts could be further defined by using protein or lipid extracts from various subcellular fractions. This

type of experiment would help to identify other proteins or small molecules necessary for synergy.

CGI-58 binds to ATGL [41,57,60]; however, it is unclear how this binding functions to increase ATGL TAG hydrolase activity. Increasing the levels of substrates or decreasing the levels of end products can drive enzymatic reactions forward. When bound to ATGL, CGI-58 could present substrate to ATGL or remove end products to increase ATGL hydrolase activity. Although CGI-58 increases TAG hydrolase activity of ATGL it does not serve the same function for HSL [41] or adiponutrin [199], a close relative of ATGL. Moreover, as shown in this dissertation, recombinant CGI-58 does not bind TAG, DAG, or FA in lipid overlay assays. However, binding of CGI-58 to ATGL may cause a conformational change in CGI-58, allowing the binding of the substrate or end products of TAG hydrolysis. Therefore, the lipid overlay experiments could be repeated with or without CGI-58 pre-bound to catalytically inactive ATGL to determine if CGI-58 increases the binding efficiency of ATGL for TAG or if the complex can bind DAG or FA.

Alternatively, CGI-58 could function to recruit ATGL to the surface of the lipid droplet. To test this, recombinant purified ATGL or CGI-58, alone or in combination, could be incubated with TAG emulsified in PC and PI. Centrifugation of these mixtures in a sucrose gradient would separate the lipid fractions from unbound protein, thus providing insight as to whether CGI-58 is necessary for ATGL to interact with the emulsions. Moreover, the PI(3)P or PI(5)P could be added to the emulsified substrate to investigate whether the presence of PIPs influences CGI-58's interaction with the emulsion. Additionally, partially purified recombinant variants

of CGI-58, known to cause NLSD in humans, could be used in these experiments to evaluate any loss of function. Together, these experiments would provide clues to the mechanism by which CGI-58 co-activates ATGL.

CGI-58 may be more than a co-activator of ATGL

There are several observations that suggest that CGI-58 has a function in addition to the activation of ATGL TAG hydrolase activity. Humans lacking functional CGI-58 (NLSDi) have some similarities, but some differences from humans lacking functional ATGL (NLSDm); NLSDm patients suffer from cardiomyopathy, but not ichthyosis (reviewed in [59]). The hearts of NLSDm patients cannot efficiently utilize stored TAG as an energy source and excessive storage of TAG causes arrhythmia. Cardiomyopathy is not present in NLSDi patients, suggesting that CGI-58 is not absolutely required for TAG hydrolase activity in hearts, even though ATGL is required. In contrast, NLSDi patients suffer from ichthyosis, and *CGI-58*$^{-/-}$ mice have a skin barrier defect, that is not found in *ATGL*$^{-/-}$ mice, derived from a decrease in ω-OH-ceramides bound to structural proteins of corneocytes [61]. These findings suggest a unique ATGL-independent role for CGI-58.

In a separate study, Brown and colleagues used ASO's to decrease CGI-58 protein expression in the adipose tissues and livers of mice. Interestingly, ASO-treated mice had smaller adipose fat pads relative to WT mice, even when challenged on a HFD. This contrasts with increased fat pad mass when ATGL is ablated [47]. Much like in NLSDi patients, who are not obese, TAG lipolysis in

adipocytes proceeds with reduced or absent CGI-58 activity. These results suggest that CGI-58 has a role separate from the co-activation of ATGL.

Due to these inconsistencies between human phenotypes and mouse models, the idea that CGI-58 acts solely to increase ATGL activity has been revised. Zechner and colleagues hypothesize that CGI-58 may additionally activate an unknown TAG lipase in skin that releases fatty acids for acylceramide synthesis [200]. This may be possible, since there are three putative lipases, LIPK, LIPM, and LIPN, that are exclusively expressed in the epidermis; each contains an α/β hydrolase fold [201]. In particular, LIPN, when mutated, causes late-onset ichthyosis [202]. Similarly, PNPLA1, a close relative in the same protein family as ATGL, is also expressed in skin [201] and, when mutated, causes autosomal recessive congenital ichthyosis in humans [203]. Since mutations in either LIPN or PNPLA1 cause ichthyosis, an *in vitro* characterization of their respective enzymatic activities, and possible interaction with CGI-58, may help to further understand the development of ichthyosis and the roles that all of these proteins play in lipid homeostasis in skin.

CGI-58 has been proposed to have a role in the generation of lipid signaling molecules

Recently, Brown and colleagues published findings suggesting that CGI-58 plays a role in the generation of signaling lipids in liver [204], putatively through the previously described LPAAT activity [105,106]. LPAAT activity generates PA and removes LPA, two potent signaling molecules [205-207]. Increases in LPA levels in cells have been linked to increased PA formation [208], which has, in turn, been

implicated in multiple pathways, including the phosphorylation of mammalian target of rapamycin (mTOR) [209,210], a signaling protein, modulation of membrane curvature [175,211], and production of an inflammatory response [208] through increased levels of TNF-α, IL-1β, and IL-6 [212]. Brown and colleagues propose the following model for CGI-58 function in liver: when TNFα, IL-1β, and IL-6 are increased in response to inflammatory stimuli such as a HFD, CGI-58 generates signaling lipids through either LPAAT activity or activation of ATGL TAG hydrolysis [204]. Signaling lipids activate downstream cytokine-induced stress kinases, such as IKK-β, S6K1, and mTOR, which, in turn, phosphorylate insulin receptor substrate-1 (IRS-1), decreasing hepatic insulin signaling. These effects were observed only in liver and not in adipose tissue. Follow knock down of CGI-58 protein levels, hepatic TAG increases due to reduced activation of ATGL, and the response of hepatocytes to insulin is improved, presumably due to the inactivation of IKK-β, S6K1, and mTOR. These researchers examined liver lipid levels of CGI-58 ASO-treated mice compared to WT mice by LC/MS; there were no significant changes in total hepatic PA levels, however there were changes in PA species [63]. Our current results indicate that CGI-58 is not an LPAAT. However, the DAG produced by CGI-58's interaction with ATGL may be converted to PA through DAG kinase activity, producing a local, transient increase in PA levels. Therefore, signaling pathways activated by PA may indeed be responsible for the observed phenotype in CGI-58 ASO-treated mice.

Development of insulin resistance has been correlated to elevated tissue ceramide content [213]. Brown and colleagues have shown that livers of mice

treated with CGI-58 ASO and fed either chow or a HFD show increases in all measured ceramide species (C16:0, C18:0, C20:0, C22:0, C24:1, C24:0) relative to control ASO-treated mice on a similar diet [63]. Total ceramide concentrations of the livers of ASO-treated mice were doubled compared to those of control mice. Ceramides have been implicated in activating protein phosphatase 2A and protein kinase Cζ, which inhibit Akt/PKB, thereby attenuating insulin signaling [214-216]. However, the CGI-58 ASO-treated mice showed an increase in hepatic insulin sensitivity, demonstrating a metabolic paradox of hepatic steatosis accompanied by increased ceramide levels, yet improved hepatic insulin sensitivity. These data suggest that total ceramide content is not the sole determinant of insulin resistance, and that CGI-58 plays a role in the development of insulin resistance in liver. Inhibition of CGI-58 activity in liver has therapeutic potential in the treatment of insulin resistance.

Analysis of the liver content of other lipids in CGI-58 ASO-treated mice is potentially informative. There was a 10-fold increase in hepatic PG levels of CGI-58 ASO-treated mice accompanied by a slight decrease in cardiolipin levels [63]. PG is a precursor for cardiolipin, which is an important component of mitochondrial membranes, serving as a proton trap during oxidative phosphorylation [217]. Interestingly, knockdown of CGI-58 protein expression in cultured hepatocytes revealed a reduction in β-oxidation of FA [218]. Suggesting that either fatty acid supply to mitochondria or mitochondrial function is impaired. Together, these two studies may provide clues to a potential mechanism of how CGI-58 plays a role in the fate of FA; CGI-58, through its interaction with ATGL produces FA, and through

alteration of levels of PG and cardiolipin, may also control the rate of β-oxidation in cells through altering mitochondrial activity. Overall, these results suggest that CGI-58 may play a role in regulating lipid metabolism through altering the levels of ceramide and PG rather than through the generation of PA or depletion of LPA.

Characterization of the H84R mutation of CGI-58

NLSDi is caused by a variety of mutations in CGI-58. In this dissertation, we have begun *in vitro* characterization of the previously described H84R variant of CGI-58 that causes NLSDi [166]. H84A and H84R mutated variants of CGI-58 were expressed in NLSDi fibroblasts that store excessive levels of TAG; expression of H84A, but not H84R, was accompanied by the reduction of accumulated TAG levels similarly to unmodified CGI-58, revealing that H84A is functionally similar to WT CGI-58. These results suggest that the histidine residue is not critical to CGI-58 function, but arginine substitution reduces protein function. It is possible that an arginine substitution causes an alteration in secondary or tertiary structure. Changes in the conformation of partially purified recombinant H84 variants relative to unmodified CGI-58 could be assessed utilizing either nuclear magnetic resonance spectroscopy or circular dichroism.

The TAG content of the NLSDi cells was determined 48 hours after addition of adenoviral vectors. This single time point limited the experiment. The experimental design did not allow assessment of the rate of TAG hydrolysis. To further understand the effect of CGI-58 mutations on the rate of TAG clearance, an experiment that determines TAG content of cells at multiple time points after

initiation of CGI-58 expression is necessary. Another potential complication is a high level of adenoviral-mediated overexpression of CGI-58 in fibroblasts that normally express very low levels of endogenous CGI-58. Massive overexpression of these variants may mask partially functional protein activity.

To gain understanding of the importance of H84, partially purified preparations of CGI-58 variants H84A and H84R were tested for their ability to activate ATGL TAG hydrolase activity *in vitro*. Both H84A and H84R variants were unable to increase lipase activity above ATGL-only reactions. However, throughout experimental repetition, reactions containing H84A CGI-58 always displayed slightly higher lipase activity than ATGL-only reactions. These results, suggest that the H84A variant may be partially functional, but that the H84R variant is nonfunctional. Thus, it is important to carefully measure the rate of TAG hydrolysis when these variants are expressed in cultured NLSDi cells. Further experiments are also required to reveal if H84A or H84R variants of CGI-58 bind to ATGL as efficiently as WT CGI-58, which will provide a better understanding for how the arginine substitution alters CGI-58 function.

Conclusions

The central aim of this thesis was to determine if CGI-58 LPAAT activity is necessary for the co-activation of ATGL TAG hydrolase activity. Throughout the course of answering this question, I have shown that CGI-58 is not a LPAAT through multiple experiments. Instead, the observed LPAAT activity was due to a contaminant protein, plsC, removal of which eliminated LPAAT activity from preparations of CGI-58. Although partial purifications from *E. coli* are a frequently utilized technique to produce proteins for functional characterization, caution must be exercised when using metal affinity resins for one-step purifications, since contaminant proteins are co-purified and may interfere with downstream experiments.

Unexpectedly, CGI-58 was observed to bind to PI(3)P and PI(5)P. Preliminary experiments in this dissertation suggest that PIP binding to CGI-58 does not alter co-activation of ATGL. More in-depth studies utilizing a CGI-58 variant, unable to bind PIPs, would provide more detailed information on how PIP binding influences CGI-58 function or localization. Therefore, an important step for future research is to identify the PIP binding site of CGI-58. The computer generated model of CGI-58 may provide clues on which residues to target for mutagenesis.

Finally, the H84R mutation of CGI-58, found in some individuals with NLSDi, was shown to have reduced function both in *in vitro* assays and in cells. As this mutation is further characterized, the information gained may be valuable in identifying the mechanism by which CGI-58 activates ATGL TAG hydrolase activity.

References

1. Ogden CL, Carroll ME, Kit BK, Flegal KM: Prevalence of obesity in the United States, 2009-2010. NCHS Data Brief 2012:1-8.
2. Bartz R, Li WH, Venables B, Zehmer JK, Roth MR, Welti R, Anderson RG, Liu P, Chapman KD: Lipidomics reveals that adiposomes store ether lipids and mediate phospholipid traffic. J Lipid Res 2007;48:837-847.
3. Tauchi-Sato K, Ozeki S, Houjou T, Taguchi R, Fujimoto T: The surface of lipid droplets is a phospholipid monolayer with a unique Fatty Acid composition. J Biol Chem 2002;277:44507-44512.
4. Blanchette-Mackie EJ, Dwyer NK, Barber T, Coxey RA, Takeda T, Rondinone CM, Theodorakis JL, Greenberg AS, Londos C: Perilipin is located on the surface layer of intracellular lipid droplets in adipocytes. J Lipid Res 1995;36:1211-1226.
5. Lafontan M, Langin D: Lipolysis and lipid mobilization in human adipose tissue. Prog Lipid Res 2009;48:275-297.
6. Carel JC, Le Stunff C, Condamine L, Mallet E, Chaussain JL, Adnot P, Garabedian M, Bougneres P: Resistance to the lipolytic action of epinephrine: a new feature of protein Gs deficiency. J Clin Endocrinol Metab 1999;84:4127-4131.
7. Horowitz JF, Klein S: Whole body and abdominal lipolytic sensitivity to epinephrine is suppressed in upper body obese women. Am J Physiol Endocrinol Metab 2000;278:E1144-1152.
8. Mairal A, Langin D, Arner P, Hoffstedt J: Human adipose triglyceride lipase (PNPLA2) is not regulated by obesity and exhibits low in vitro triglyceride hydrolase activity. Diabetologia 2006;49:1629-1636.
9. Berndt J, Kralisch S, Kloting N, Ruschke K, Kern M, Fasshauer M, Schon MR, Stumvoll M, Bluher M: Adipose triglyceride lipase gene expression in human visceral obesity. Exp Clin Endocrinol Diabetes 2008;116:203-210.
10. Large V, Reynisdottir S, Langin D, Fredby K, Klannemark M, Holm C, Arner P: Decreased expression and function of adipocyte hormone-sensitive lipase in subcutaneous fat cells of obese subjects. J Lipid Res 1999;40:2059-2066.
11. Jocken JW, Langin D, Smit E, Saris WH, Valle C, Hul GB, Holm C, Arner P, Blaak EE: Adipose triglyceride lipase and hormone-sensitive lipase protein expression is decreased in the obese insulin-resistant state. J Clin Endocrinol Metab 2007;92:2292-2299.
12. Watt MJ, Carey AL, Wolsk-Petersen E, Kraemer FB, Pedersen BK, Febbraio MA: Hormone-sensitive lipase is reduced in the adipose tissue of patients with type 2 diabetes mellitus: influence of IL-6 infusion. Diabetologia 2005;48:105-112.
13. Wang Y, Sullivan S, Trujillo M, Lee MJ, Schneider SH, Brolin RE, Kang YH, Werber Y, Greenberg AS, Fried SK: Perilipin expression in human adipose tissues: effects of severe obesity, gender, and depot. Obes Res 2003;11:930-936.
14. Eckel RH, Grundy SM, Zimmet PZ: The metabolic syndrome. Lancet 2005;365:1415-1428.

15. Yang X, Lu X, Lombes M, Rha GB, Chi YI, Guerin TM, Smart EJ, Liu J: The G(0)/G(1) switch gene 2 regulates adipose lipolysis through association with adipose triglyceride lipase. Cell Metab 2010;11:194-205.
16. Lu X, Yang X, Liu J: Differential control of ATGL-mediated lipid droplet degradation by CGI-58 and G0S2. Cell Cycle 2010;9:2719-2725.
17. Subramanian V, Rothenberg A, Gomez C, Cohen AW, Garcia A, Bhattacharyya S, Shapiro L, Dolios G, Wang R, Lisanti MP, Brasaemle DL: Perilipin A mediates the reversible binding of CGI-58 to lipid droplets in 3T3-L1 adipocytes. J Biol Chem 2004;279:42062-42071.
18. Sztalryd C, Xu G, Dorward H, Tansey JT, Contreras JA, Kimmel AR, Londos C: Perilipin A is essential for the translocation of hormone-sensitive lipase during lipolytic activation. J Cell Biol 2003;161:1093-1103.
19. Brasaemle DL, Levin DM, Adler-Wailes DC, Londos C: The lipolytic stimulation of 3T3-L1 adipocytes promotes the translocation of hormone-sensitive lipase to the surfaces of lipid storage droplets. Biochim Biophys Acta 2000;1483:251-262.
20. Honnor RC, Dhillon GS, Londos C: cAMP-dependent protein kinase and lipolysis in rat adipocytes. II. Definition of steady-state relationship with lipolytic and antilipolytic modulators. J Biol Chem 1985;260:15130-15138.
21. Taylor SS, Yang J, Wu J, Haste NM, Radzio-Andzelm E, Anand G: PKA: a portrait of protein kinase dynamics. Biochim Biophys Acta 2004;1697:259-269.
22. Lampidonis AD, Rogdakis E, Voutsinas GE, Stravopodis DJ: The resurgence of Hormone-Sensitive Lipase (HSL) in mammalian lipolysis. Gene 2011;477:1-11.
23. Greenberg AS, Egan JJ, Wek SA, Garty NB, Blanchette-Mackie EJ, Londos C: Perilipin, a major hormonally regulated adipocyte-specific phosphoprotein associated with the periphery of lipid storage droplets. J Biol Chem 1991;266:11341-11346.
24. Anthonsen MW, Ronnstrand L, Wernstedt C, Degerman E, Holm C: Identification of novel phosphorylation sites in hormone-sensitive lipase that are phosphorylated in response to isoproterenol and govern activation properties in vitro. J Biol Chem 1998;273:215-221.
25. Wang H, Hu L, Dalen K, Dorward H, Marcinkiewicz A, Russell D, Gong D, Londos C, Yamaguchi T, Holm C, Rizzo MA, Brasaemle D, Sztalryd C: Activation of hormone-sensitive lipase requires two steps, protein phosphorylation and binding to the PAT-1 domain of lipid droplet coat proteins. J Biol Chem 2009;284:32116-32125.
26. Granneman JG, Moore HP, Krishnamoorthy R, Rathod M: Perilipin controls lipolysis by regulating the interactions of AB-hydrolase containing 5 (Abhd5) and adipose triglyceride lipase (Atgl). J Biol Chem 2009;284:34538-34544.
27. Soni KG, Mardones GA, Sougrat R, Smirnova E, Jackson CL, Bonifacino JS: Coatomer-dependent protein delivery to lipid droplets. J Cell Sci 2009;122:1834-1841.

28. Tornqvist H, Belfrage P: Purification and some properties of a monoacylglycerol-hydrolyzing enzyme of rat adipose tissue. J Biol Chem 1976;251:813-819.
29. Khoo JC, Reue K, Steinberg D, Schotz MC: Expression of hormone-sensitive lipase mRNA in macrophages. J Lipid Res 1993;34:1969-1974.
30. Kraemer FB, Patel S, Saedi MS, Sztalryd C: Detection of hormone-sensitive lipase in various tissues. I. Expression of an HSL/bacterial fusion protein and generation of anti-HSL antibodies. J Lipid Res 1993;34:663-671.
31. Garton AJ, Campbell DG, Carling D, Hardie DG, Colbran RJ, Yeaman SJ: Phosphorylation of bovine hormone-sensitive lipase by the AMP-activated protein kinase. A possible antilipolytic mechanism. Eur J Biochem 1989;179:249-254.
32. Daval M, Diot-Dupuy F, Bazin R, Hainault I, Viollet B, Vaulont S, Hajduch E, Ferre P, Foufelle F: Anti-lipolytic action of AMP-activated protein kinase in rodent adipocytes. J Biol Chem 2005;280:25250-25257.
33. Su CL, Sztalryd C, Contreras JA, Holm C, Kimmel AR, Londos C: Mutational analysis of the hormone-sensitive lipase translocation reaction in adipocytes. J Biol Chem 2003;278:43615-43619.
34. Osuga J, Ishibashi S, Oka T, Yagyu H, Tozawa R, Fujimoto A, Shionoiri F, Yahagi N, Kraemer FB, Tsutsumi O, Yamada N: Targeted disruption of hormone-sensitive lipase results in male sterility and adipocyte hypertrophy, but not in obesity. Proc Natl Acad Sci U S A 2000;97:787-792.
35. Wang SP, Laurin N, Himms-Hagen J, Rudnicki MA, Levy E, Robert MF, Pan L, Oligny L, Mitchell GA: The adipose tissue phenotype of hormone-sensitive lipase deficiency in mice. Obes Res 2001;9:119-128.
36. Haemmerle G, Zimmermann R, Hayn M, Theussl C, Waeg G, Wagner E, Sattler W, Magin TM, Wagner EF, Zechner R: Hormone-sensitive lipase deficiency in mice causes diglyceride accumulation in adipose tissue, muscle, and testis. J Biol Chem 2002;277:4806-4815.
37. Harada K, Shen WJ, Patel S, Natu V, Wang J, Osuga J, Ishibashi S, Kraemer FB: Resistance to high-fat diet-induced obesity and altered expression of adipose-specific genes in HSL-deficient mice. Am J Physiol Endocrinol Metab 2003;285:E1182-1195.
38. Zimmermann R, Strauss JG, Haemmerle G, Schoiswohl G, Birner-Gruenberger R, Riederer M, Lass A, Neuberger G, Eisenhaber F, Hermetter A, Zechner R: Fat mobilization in adipose tissue is promoted by adipose triglyceride lipase. Science 2004;306:1383-1386.
39. Villena JA, Roy S, Sarkadi-Nagy E, Kim KH, Sul HS: Desnutrin, an adipocyte gene encoding a novel patatin domain-containing protein, is induced by fasting and glucocorticoids: ectopic expression of desnutrin increases triglyceride hydrolysis. J Biol Chem 2004;279:47066-47075.
40. Jenkins CM, Mancuso DJ, Yan W, Sims HF, Gibson B, Gross RW: Identification, cloning, expression, and purification of three novel human calcium-independent phospholipase A2 family members possessing triacylglycerol lipase and acylglycerol transacylase activities. J Biol Chem 2004;279:48968-48975.

41. Lass A, Zimmermann R, Haemmerle G, Riederer M, Schoiswohl G, Schweiger M, Kienesberger P, Strauss JG, Gorkiewicz G, Zechner R: Adipose triglyceride lipase-mediated lipolysis of cellular fat stores is activated by CGI-58 and defective in Chanarin-Dorfman Syndrome. Cell Metab 2006;3:309-319.
42. Lake AC, Sun Y, Li JL, Kim JE, Johnson JW, Li D, Revett T, Shih HH, Liu W, Paulsen JE, Gimeno RE: Expression, regulation, and triglyceride hydrolase activity of Adiponutrin family members. J Lipid Res 2005;46:2477-2487.
43. Zandbergen F, Mandard S, Escher P, Tan NS, Patsouris D, Jatkoe T, Rojas-Caro S, Madore S, Wahli W, Tafuri S, Muller M, Kersten S: The G0/G1 switch gene 2 is a novel PPAR target gene. Biochem J 2005;392:313-324.
44. Ahmadian M, Abbott MJ, Tang T, Hudak CS, Kim Y, Bruss M, Hellerstein MK, Lee HY, Samuel VT, Shulman GI, Wang Y, Duncan RE, Kang C, Sul HS: Desnutrin/ATGL is regulated by AMPK and is required for a brown adipose phenotype. Cell Metab 2011;13:739-748.
45. Mason RR, Meex RC, Lee-Young RS, Canny BJ, Watt MJ: Phosphorylation of Adipose Triglyceride Lipase (ATGL) Ser404 is not related to 5'AMP kinase activation during moderate intensity exercise in humans. Am J Physiol Endocrinol Metab 2012.
46. Pagnon J, Matzaris M, Stark R, Meex RC, Lance Macaulay S, Brown W, O'Brien PE, Tiganis T, Watt MJ: Identification and Functional Characterization of Protein Kinase A Phosphorylation Sites in the Major Lipolytic Protein, Adipose Triglyceride Lipase. Endocrinology 2012.
47. Haemmerle G, Lass A, Zimmermann R, Gorkiewicz G, Meyer C, Rozman J, Heldmaier G, Maier R, Theussl C, Eder S, Kratky D, Wagner EF, Klingenspor M, Hoefler G, Zechner R: Defective lipolysis and altered energy metabolism in mice lacking adipose triglyceride lipase. Science 2006;312:734-737.
48. Lai CH, Chou CY, Ch'ang LY, Liu CS, Lin W: Identification of novel human genes evolutionarily conserved in Caenorhabditis elegans by comparative proteomics. Genome Res 2000;10:703-713.
49. Lefevre C, Jobard F, Caux F, Bouadjar B, Karaduman A, Heilig R, Lakhdar H, Wollenberg A, Verret JL, Weissenbach J, Ozguc M, Lathrop M, Prud'homme JF, Fischer J: Mutations in CGI-58, the gene encoding a new protein of the esterase/lipase/thioesterase subfamily, in Chanarin-Dorfman syndrome. Am J Hum Genet 2001;69:1002-1012.
50. Bruno C, Bertini E, Di Rocco M, Cassandrini D, Ruffa G, De Toni T, Seri M, Spada M, Li Volti G, D'Amico A, Trucco F, Arca M, Casali C, Angelini C, Dimauro S, Minetti C: Clinical and genetic characterization of Chanarin-Dorfman syndrome. Biochem Biophys Res Commun 2008;369:1125-1128.
51. Chanarin I, Patel A, Slavin G, Wills EJ, Andrews TM, Stewart G: Neutral-lipid storage disease: a new disorder of lipid metabolism. Br Med J 1975;1:553-555.
52. Slavin G, Wills EJ, Richmond JE, Chanarin I, Andrews T, Stewart G: Morphological features in a neutral lipid storage disease. J Clin Pathol 1975;28:701-710.
53. Dorfman ML, Hershko C, Eisenberg S, Sagher F: Ichthyosiform dermatosis with systemic lipidosis. Arch Dermatol 1974;110:261-266.

54. Igal RA, Rhoads JM, Coleman RA: Neutral lipid storage disease with fatty liver and cholestasis. J Pediatr Gastroenterol Nutr 1997;25:541-547.
55. Campagna F, Nanni L, Quagliarini F, Pennisi E, Michailidis C, Pierelli F, Bruno C, Casali C, DiMauro S, Arca M: Novel mutations in the adipose triglyceride lipase gene causing neutral lipid storage disease with myopathy. Biochem Biophys Res Commun 2008;377:843-846.
56. Fischer J, Lefevre C, Morava E, Mussini JM, Laforet P, Negre-Salvayre A, Lathrop M, Salvayre R: The gene encoding adipose triglyceride lipase (PNPLA2) is mutated in neutral lipid storage disease with myopathy. Nat Genet 2007;39:28-30.
57. Gruber A, Cornaciu I, Lass A, Schweiger M, Poeschl M, Eder C, Kumari M, Schoiswohl G, Wolinski H, Kohlwein SD, Zechner R, Zimmermann R, Oberer M: The N-terminal region of comparative gene identification-58 (CGI-58) is important for lipid droplet binding and activation of adipose triglyceride lipase. J Biol Chem 2010;285:12289-12298.
58. Kienesberger PC, Oberer M, Lass A, Zechner R: Mammalian patatin domain containing proteins: a family with diverse lipolytic activities involved in multiple biological functions. J Lipid Res 2009;50 Suppl:S63-68.
59. Schweiger M, Lass A, Zimmermann R, Eichmann TO, Zechner R: Neutral lipid storage disease: genetic disorders caused by mutations in adipose triglyceride lipase/PNPLA2 or CGI-58/ABHD5. Am J Physiol Endocrinol Metab 2009;297:E289-296.
60. Cornaciu I, Boeszoermenyi A, Lindermuth H, Nagy HM, Cerk IK, Ebner C, Salzburger B, Gruber A, Schweiger M, Zechner R, Lass A, Zimmermann R, Oberer M: The minimal domain of adipose triglyceride lipase (ATGL) ranges until leucine 254 and can be activated and inhibited by CGI-58 and G0S2, respectively. PLoS One 2011;6:e26349.
61. Radner FP, Streith IE, Schoiswohl G, Schweiger M, Kumari M, Eichmann TO, Rechberger G, Koefeler HC, Eder S, Schauer S, Theussl HC, Preiss-Landl K, Lass A, Zimmermann R, Hoefler G, Zechner R, Haemmerle G: Growth retardation, impaired triacylglycerol catabolism, hepatic steatosis, and lethal skin barrier defect in mice lacking comparative gene identification-58 (CGI-58). J Biol Chem 2010;285:7300-7311.
62. Hirano K, Ikeda Y, Zaima N, Sakata Y, Matsumiya G: Triglyceride deposit cardiomyovasculopathy. N Engl J Med 2008;359:2396-2398.
63. Brown JM, Betters JL, Lord C, Ma Y, Han X, Yang K, Alger HM, Melchior J, Sawyer J, Shah R, Wilson MD, Liu X, Graham MJ, Lee R, Crooke R, Shulman GI, Xue B, Shi H, Yu L: CGI-58 knockdown in mice causes hepatic steatosis but prevents diet-induced obesity and glucose intolerance. J Lipid Res 2010;51:3306-3315.
64. Yamaguchi T, Omatsu N, Matsushita S, Osumi T: CGI-58 interacts with perilipin and is localized to lipid droplets. Possible involvement of CGI-58 mislocalization in Chanarin-Dorfman syndrome. J Biol Chem 2004;279:30490-30497.
65. Wang H, Bell M, Sreenevasan U, Hu H, Liu J, Dalen K, Londos C, Yamaguchi T, Rizzo MA, Coleman R, Gong D, Brasaemle D, Sztalryd C: Unique regulation of

adipose triglyceride lipase (ATGL) by perilipin 5, a lipid droplet-associated protein. J Biol Chem 2011;286:15707-15715.
66. Karlsson M, Contreras JA, Hellman U, Tornqvist H, Holm C: cDNA cloning, tissue distribution, and identification of the catalytic triad of monoglyceride lipase. Evolutionary relationship to esterases, lysophospholipases, and haloperoxidases. J Biol Chem 1997;272:27218-27223.
67. Taschler U, Radner FP, Heier C, Schreiber R, Schweiger M, Schoiswohl G, Preiss-Landl K, Jaeger D, Reiter B, Koefeler HC, Wojciechowski J, Theussl C, Penninger JM, Lass A, Haemmerle G, Zechner R, Zimmermann R: Monoglyceride lipase deficiency in mice impairs lipolysis and attenuates diet-induced insulin resistance. J Biol Chem 2011;286:17467-17477.
68. Kirkham TC, Williams CM, Fezza F, Di Marzo V: Endocannabinoid levels in rat limbic forebrain and hypothalamus in relation to fasting, feeding and satiation: stimulation of eating by 2-arachidonoyl glycerol. Br J Pharmacol 2002;136:550-557.
69. Londos C, Brasaemle DL, Gruia-Gray J, Servetnick DA, Schultz CJ, Levin DM, Kimmel AR: Perilipin: unique proteins associated with intracellular neutral lipid droplets in adipocytes and steroidogenic cells. Biochem Soc Trans 1995;23:611-615.
70. Servetnick DA, Brasaemle DL, Gruia-Gray J, Kimmel AR, Wolff J, Londos C: Perilipins are associated with cholesteryl ester droplets in steroidogenic adrenal cortical and Leydig cells. J Biol Chem 1995;270:16970-16973.
71. Lu X, Gruia-Gray J, Copeland NG, Gilbert DJ, Jenkins NA, Londos C, Kimmel AR: The murine perilipin gene: the lipid droplet-associated perilipins derive from tissue-specific, mRNA splice variants and define a gene family of ancient origin. Mamm Genome 2001;12:741-749.
72. Brasaemle DL, Rubin B, Harten IA, Gruia-Gray J, Kimmel AR, Londos C: Perilipin A increases triacylglycerol storage by decreasing the rate of triacylglycerol hydrolysis. J Biol Chem 2000;275:38486-38493.
73. Clifford GM, McCormick DK, Londos C, Vernon RG, Yeaman SJ: Dephosphorylation of perilipin by protein phosphatases present in rat adipocytes. FEBS Lett 1998;435:125-129.
74. Zhang HH, Souza SC, Muliro KV, Kraemer FB, Obin MS, Greenberg AS: Lipase-selective functional domains of perilipin A differentially regulate constitutive and protein kinase A-stimulated lipolysis. J Biol Chem 2003;278:51535-51542.
75. Miyoshi H, Perfield JW, 2nd, Souza SC, Shen WJ, Zhang HH, Stancheva ZS, Kraemer FB, Obin MS, Greenberg AS: Control of adipose triglyceride lipase action by serine 517 of perilipin A globally regulates protein kinase A-stimulated lipolysis in adipocytes. J Biol Chem 2007;282:996-1002.
76. Hickenbottom SJ, Kimmel AR, Londos C, Hurley JH: Structure of a lipid droplet protein; the PAT family member TIP47. Structure 2004;12:1199-1207.
77. Brasaemle DL: Thematic review series: adipocyte biology. The perilipin family of structural lipid droplet proteins: stabilization of lipid droplets and control of lipolysis. J Lipid Res 2007;48:2547-2559.

78. Martinez-Botas J, Anderson JB, Tessier D, Lapillonne A, Chang BH, Quast MJ, Gorenstein D, Chen KH, Chan L: Absence of perilipin results in leanness and reverses obesity in Lepr(db/db) mice. Nat Genet 2000;26:474-479.
79. Tansey JT, Sztalryd C, Gruia-Gray J, Roush DL, Zee JV, Gavrilova O, Reitman ML, Deng CX, Li C, Kimmel AR, Londos C: Perilipin ablation results in a lean mouse with aberrant adipocyte lipolysis, enhanced leptin production, and resistance to diet-induced obesity. Proc Natl Acad Sci U S A 2001;98:6494-6499.
80. Gandotra S, Le Dour C, Bottomley W, Cervera P, Giral P, Reznik Y, Charpentier G, Auclair M, Delepine M, Barroso I, Semple RK, Lathrop M, Lascols O, Capeau J, O'Rahilly S, Magre J, Savage DB, Vigouroux C: Perilipin deficiency and autosomal dominant partial lipodystrophy. N Engl J Med 2011;364:740-748.
81. Gandotra S, Lim K, Girousse A, Saudek V, O'Rahilly S, Savage DB: Human frame shift mutations affecting the carboxyl terminus of perilipin increase lipolysis by failing to sequester the adipose triglyceride lipase (ATGL) coactivator AB-hydrolase-containing 5 (ABHD5). J Biol Chem 2011;286:34998-35006.
82. Jiang HP, Serrero G: Isolation and characterization of a full-length cDNA coding for an adipose differentiation-related protein. Proc Natl Acad Sci U S A 1992;89:7856-7860.
83. Brasaemle DL, Barber T, Wolins NE, Serrero G, Blanchette-Mackie EJ, Londos C: Adipose differentiation-related protein is an ubiquitously expressed lipid storage droplet-associated protein. J Lipid Res 1997;38:2249-2263.
84. Wolins NE, Quaynor BK, Skinner JR, Schoenfish MJ, Tzekov A, Bickel PE: S3-12, Adipophilin, and TIP47 package lipid in adipocytes. J Biol Chem 2005;280:19146-19155.
85. Imamura M, Inoguchi T, Ikuyama S, Taniguchi S, Kobayashi K, Nakashima N, Nawata H: ADRP stimulates lipid accumulation and lipid droplet formation in murine fibroblasts. Am J Physiol Endocrinol Metab 2002;283:E775-783.
86. Listenberger LL, Ostermeyer-Fay AG, Goldberg EB, Brown WJ, Brown DA: Adipocyte differentiation-related protein reduces the lipid droplet association of adipose triglyceride lipase and slows triacylglycerol turnover. J Lipid Res 2007;48:2751-2761.
87. Chang BH, Li L, Paul A, Taniguchi S, Nannegari V, Heird WC, Chan L: Protection against fatty liver but normal adipogenesis in mice lacking adipose differentiation-related protein. Mol Cell Biol 2006;26:1063-1076.
88. Wolins NE, Rubin B, Brasaemle DL: TIP47 associates with lipid droplets. J Biol Chem 2001;276:5101-5108.
89. Yamaguchi T, Matsushita S, Motojima K, Hirose F, Osumi T: MLDP, a novel PAT family protein localized to lipid droplets and enriched in the heart, is regulated by peroxisome proliferator-activated receptor alpha. J Biol Chem 2006;281:14232-14240.
90. Wolins NE, Quaynor BK, Skinner JR, Tzekov A, Croce MA, Gropler MC, Varma V, Yao-Borengasser A, Rasouli N, Kern PA, Finck BN, Bickel PE: OXPAT/PAT-1 is a PPAR-induced lipid droplet protein that promotes fatty acid utilization. Diabetes 2006;55:3418-3428.

91. Diaz E, Pfeffer SR: TIP47: a cargo selection device for mannose 6-phosphate receptor trafficking. Cell 1998;93:433-443.
92. Wilson C, Wardell MR, Weisgraber KH, Mahley RW, Agard DA: Three-dimensional structure of the LDL receptor-binding domain of human apolipoprotein E. Science 1991;252:1817-1822.
93. Saito H, Dhanasekaran P, Baldwin F, Weisgraber KH, Lund-Katz S, Phillips MC: Lipid binding-induced conformational change in human apolipoprotein E. Evidence for two lipid-bound states on spherical particles. J Biol Chem 2001;276:40949-40954.
94. Xu G, Sztalryd C, Londos C: Degradation of perilipin is mediated through ubiquitination-proteasome pathway. Biochim Biophys Acta 2006;1761:83-90.
95. Brasaemle DL, Barber T, Kimmel AR, Londos C: Post-translational regulation of perilipin expression. Stabilization by stored intracellular neutral lipids. J Biol Chem 1997;272:9378-9387.
96. Miura S, Gan JW, Brzostowski J, Parisi MJ, Schultz CJ, Londos C, Oliver B, Kimmel AR: Functional conservation for lipid storage droplet association among Perilipin, ADRP, and TIP47 (PAT)-related proteins in mammals, Drosophila, and Dictyostelium. J Biol Chem 2002;277:32253-32257.
97. Bell M, Wang H, Chen H, McLenithan JC, Gong DW, Yang RZ, Yu D, Fried SK, Quon MJ, Londos C, Sztalryd C: Consequences of lipid droplet coat protein downregulation in liver cells: abnormal lipid droplet metabolism and induction of insulin resistance. Diabetes 2008;57:2037-2045.
98. Bulankina AV, Deggerich A, Wenzel D, Mutenda K, Wittmann JG, Rudolph MG, Burger KN, Honing S: TIP47 functions in the biogenesis of lipid droplets. J Cell Biol 2009;185:641-655.
99. Scherer PE, Bickel PE, Kotler M, Lodish HF: Cloning of cell-specific secreted and surface proteins by subtractive antibody screening. Nat Biotechnol 1998;16:581-586.
100. Wolins NE, Skinner JR, Schoenfish MJ, Tzekov A, Bensch KG, Bickel PE: Adipocyte protein S3-12 coats nascent lipid droplets. J Biol Chem 2003;278:37713-37721.
101. Dalen KT, Dahl T, Holter E, Arntsen B, Londos C, Sztalryd C, Nebb HI: LSDP5 is a PAT protein specifically expressed in fatty acid oxidizing tissues. Biochim Biophys Acta 2007;1771:210-227.
102. Granneman JG, Moore HP, Mottillo EP, Zhu Z, Zhou L: Interactions of perilipin-5 (Plin5) with adipose triglyceride lipase. J Biol Chem 2011;286:5126-5135.
103. Wang H, Sreenevasan U, Hu H, Saladino A, Polster BM, Lund LM, Gong DW, Stanley WC, Sztalryd C: Perilipin 5, a lipid droplet-associated protein, provides physical and metabolic linkage to mitochondria. J Lipid Res 2011;52:2159-2168.
104. Bosma M, Minnaard R, Sparks LM, Schaart G, Losen M, de Baets MH, Duimel H, Kersten S, Bickel PE, Schrauwen P, Hesselink MK: The lipid droplet coat protein perilipin 5 also localizes to muscle mitochondria. Histochem Cell Biol 2012;137:205-216.

105. Ghosh AK, Ramakrishnan G, Chandramohan C, Rajasekharan R: CGI-58, the causative gene for Chanarin-Dorfman syndrome, mediates acylation of lysophosphatidic acid. J Biol Chem 2008;283:24525-24533.
106. Montero-Moran G, Caviglia JM, McMahon D, Rothenberg A, Subramanian V, Xu Z, Lara-Gonzalez S, Storch J, Carman GM, Brasaemle DL: CGI-58/ABHD5 is a coenzyme A-dependent lysophosphatidic acid acyltransferase. J Lipid Res 2010;51:709-719.
107. Kume K, Shimizu T: cDNA cloning and expression of murine 1-acyl-sn-glycerol-3-phosphate acyltransferase. Biochem Biophys Res Commun 1997;237:663-666.
108. Stamps AC, Elmore MA, Hill ME, Kelly K, Makda AA, Finnen MJ: A human cDNA sequence with homology to non-mammalian lysophosphatidic acid acyltransferases. Biochem J 1997;326 (Pt 2):455-461.
109. West J, Tompkins CK, Balantac N, Nudelman E, Meengs B, White T, Bursten S, Coleman J, Kumar A, Singer JW, Leung DW: Cloning and expression of two human lysophosphatidic acid acyltransferase cDNAs that enhance cytokine-induced signaling responses in cells. DNA Cell Biol 1997;16:691-701.
110. Hollenback D, Bonham L, Law L, Rossnagle E, Romero L, Carew H, Tompkins CK, Leung DW, Singer JW, White T: Substrate specificity of lysophosphatidic acid acyltransferase beta -- evidence from membrane and whole cell assays. J Lipid Res 2006;47:593-604.
111. Eberhardt C, Gray PW, Tjoelker LW: Human lysophosphatidic acid acyltransferase. cDNA cloning, expression, and localization to chromosome 9q34.3. J Biol Chem 1997;272:20299-20305.
112. Ye GM, Chen C, Huang S, Han DD, Guo JH, Wan B, Yu L: Cloning and characterization a novel human 1-acyl-sn-glycerol-3-phosphate acyltransferase gene AGPAT7. DNA Seq 2005;16:386-390.
113. Agarwal AK, Barnes RI, Garg A: Functional characterization of human 1-acylglycerol-3-phosphate acyltransferase isoform 8: cloning, tissue distribution, gene structure, and enzymatic activity. Arch Biochem Biophys 2006;449:64-76.
114. Yamashita A, Nakanishi H, Suzuki H, Kamata R, Tanaka K, Waku K, Sugiura T: Topology of acyltransferase motifs and substrate specificity and accessibility in 1-acyl-sn-glycero-3-phosphate acyltransferase 1. Biochim Biophys Acta 2007;1771:1202-1215.
115. Lu B, Jiang YJ, Zhou Y, Xu FY, Hatch GM, Choy PC: Cloning and characterization of murine 1-acyl-sn-glycerol 3-phosphate acyltransferases and their regulation by PPARalpha in murine heart. Biochem J 2005;385:469-477.
116. Takeuchi K, Reue K: Biochemistry, physiology, and genetics of GPAT, AGPAT, and lipin enzymes in triglyceride synthesis. Am J Physiol Endocrinol Metab 2009;296:E1195-1209.
117. Chen X, Hyatt BA, Mucenski ML, Mason RJ, Shannon JM: Identification and characterization of a lysophosphatidylcholine acyltransferase in alveolar type II cells. Proc Natl Acad Sci U S A 2006;103:11724-11729.

118. Nakanishi H, Shindou H, Hishikawa D, Harayama T, Ogasawara R, Suwabe A, Taguchi R, Shimizu T: Cloning and characterization of mouse lung-type acyl-CoA:lysophosphatidylcholine acyltransferase 1 (LPCAT1). Expression in alveolar type II cells and possible involvement in surfactant production. J Biol Chem 2006;281:20140-20147.
119. Soupene E, Fyrst H, Kuypers FA: Mammalian acyl-CoA:lysophosphatidylcholine acyltransferase enzymes. Proc Natl Acad Sci U S A 2008;105:88-93.
120. Eberhardt C, Gray PW, Tjoelker LW: cDNA cloning, expression and chromosomal localization of two human lysophosphatidic acid acyltransferases. Adv Exp Med Biol 1999;469:351-356.
121. Leung DW: The structure and functions of human lysophosphatidic acid acyltransferases. Front Biosci 2001;6:D944-953.
122. Aguado B, Campbell RD: Characterization of a human lysophosphatidic acid acyltransferase that is encoded by a gene located in the class III region of the human major histocompatibility complex. J Biol Chem 1998;273:4096-4105.
123. Gale SE, Frolov A, Han X, Bickel PE, Cao L, Bowcock A, Schaffer JE, Ory DS: A regulatory role for 1-acylglycerol-3-phosphate-O-acyltransferase 2 in adipocyte differentiation. J Biol Chem 2006;281:11082-11089.
124. Agarwal AK, Arioglu E, De Almeida S, Akkoc N, Taylor SI, Bowcock AM, Barnes RI, Garg A: AGPAT2 is mutated in congenital generalized lipodystrophy linked to chromosome 9q34. Nat Genet 2002;31:21-23.
125. Seip M, Trygstad O: Generalized lipodystrophy, congenital and acquired (lipoatrophy). Acta Paediatr Suppl 1996;413:2-28.
126. Garg A, Fleckenstein JL, Peshock RM, Grundy SM: Peculiar distribution of adipose tissue in patients with congenital generalized lipodystrophy. J Clin Endocrinol Metab 1992;75:358-361.
127. Chandalia M, Garg A, Vuitch F, Nizzi F: Postmortem findings in congenital generalized lipodystrophy. J Clin Endocrinol Metab 1995;80:3077-3081.
128. Cortes VA, Curtis DE, Sukumaran S, Shao X, Parameswara V, Rashid S, Smith AR, Ren J, Esser V, Hammer RE, Agarwal AK, Horton JD, Garg A: Molecular mechanisms of hepatic steatosis and insulin resistance in the AGPAT2-deficient mouse model of congenital generalized lipodystrophy. Cell Metab 2009;9:165-176.
129. Agarwal AK, Sukumaran S, Cortes VA, Tunison K, Mizrachi D, Sankella S, Gerard RD, Horton JD, Garg A: Human 1-acylglycerol-3-phosphate O-acyltransferase isoforms 1 and 2: biochemical characterization and inability to rescue hepatic steatosis in Agpat2(-/-) gene lipodystrophic mice. J Biol Chem 2011;286:37676-37691.
130. Igal RA, Coleman RA: Acylglycerol recycling from triacylglycerol to phospholipid, not lipase activity, is defective in neutral lipid storage disease fibroblasts. J Biol Chem 1996;271:16644-16651.
131. Igal RA, Coleman RA: Neutral lipid storage disease: a genetic disorder with abnormalities in the regulation of phospholipid metabolism. J Lipid Res 1998;39:31-43.

132. Kelley LA, Sternberg MJ: Protein structure prediction on the Web: a case study using the Phyre server. Nat Protoc 2009;4:363-371.
133. Laskowski RA, Moss DS, Thornton JM: Main-chain bond lengths and bond angles in protein structures. J Mol Biol 1993;231:1049-1067.
134. Hooft RW, Vriend G, Sander C, Abola EE: Errors in protein structures. Nature 1996;381:272.
135. Colovos C, Yeates TO: Verification of protein structures: patterns of nonbonded atomic interactions. Protein Sci 1993;2:1511-1519.
136. Luthy R, Bowie JU, Eisenberg D: Assessment of protein models with three-dimensional profiles. Nature 1992;356:83-85.
137. Pontius J, Richelle J, Wodak SJ: Deviations from standard atomic volumes as a quality measure for protein crystal structures. J Mol Biol 1996;264:121-136.
138. Stratagene QuikChange® XL Site-Directed Mutagenesis Manual 240010 Revision #066004j.
139. Stratagene Adeasy Adenoviral System Instruction Manual 240009 Revision #066004j.
140. Laemmli UK: Cleavage of structural proteins during the assembly of the head of bacteriophage T4. Nature 1970;227:680-685.
141. Schwartz DM, Wolins NE: A simple and rapid method to assay triacylglycerol in cells and tissues. J Lipid Res 2007;48:2514-2520.
142. Holm C, Osterlund T: Hormone-sensitive lipase and neutral cholesteryl ester lipase. Methods Mol Biol 1999;109:109-121.
143. Heath RJ, Rock CO: A conserved histidine is essential for glycerolipid acyltransferase catalysis. J Bacteriol 1998;180:1425-1430.
144. Vallat BK, Pillardy J, Majek P, Meller J, Blom T, Cao B, Elber R: Building and assessing atomic models of proteins from structural templates: learning and benchmarks. Proteins 2009;76:930-945.
145. Vallat BK, Pillardy J, Elber R: A template-finding algorithm and a comprehensive benchmark for homology modeling of proteins. Proteins 2008;72:910-928.
146. Teodorescu O, Galor T, Pillardy J, Elber R: Enriching the sequence substitution matrix by structural information. Proteins 2004;54:41-48.
147. Meller J, Elber R: Linear programming optimization and a double statistical filter for protein threading protocols. Proteins 2001;45:241-261.
148. Tobi D, Elber R: Distance-dependent, pair potential for protein folding: results from linear optimization. Proteins 2000;41:40-46.
149. Zhang Y: I-TASSER server for protein 3D structure prediction. BMC Bioinformatics 2008;9:40.
150. Roy A, Kucukural A, Zhang Y: I-TASSER: a unified platform for automated protein structure and function prediction. Nat Protoc 2010;5:725-738.
151. Roy A, Yang J, Zhang Y: COFACTOR: an accurate comparative algorithm for structure-based protein function annotation. Nucleic Acids Res 2012;40:W471-477.
152. Torda AE, Procter JB, Huber T: Wurst: a protein threading server with a structural scoring function, sequence profiles and optimized substitution matrices. Nucleic Acids Res 2004;32:W532-535.

153. Karplus K, Barrett C, Hughey R: Hidden Markov models for detecting remote protein homologies. Bioinformatics 1998;14:846-856.
154. Karplus K, Karchin R, Barrett C, Tu S, Cline M, Diekhans M, Grate L, Casper J, Hughey R: What is the value added by human intervention in protein structure prediction? Proteins 2001;Suppl 5:86-91.
155. Karplus K, Karchin R, Draper J, Casper J, Mandel-Gutfreund Y, Diekhans M, Hughey R: Combining local-structure, fold-recognition, and new fold methods for protein structure prediction. Proteins 2003;53 Suppl 6:491-496.
156. Karplus K, Katzman S, Shackleford G, Koeva M, Draper J, Barnes B, Soriano M, Hughey R: SAM-T04: what is new in protein-structure prediction for CASP6. Proteins 2005;61 Suppl 7:135-142.
157. Shackelford G, Karplus K: Contact prediction using mutual information and neural nets. Proteins 2007;69 Suppl 8:159-164.
158. Katzman S, Barrett C, Thiltgen G, Karchin R, Karplus K: PREDICT-2ND: a tool for generalized protein local structure prediction. Bioinformatics 2008;24:2453-2459.
159. Chivian D, Kim DE, Malmstrom L, Bradley P, Robertson T, Murphy P, Strauss CE, Bonneau R, Rohl CA, Baker D: Automated prediction of CASP-5 structures using the Robetta server. Proteins 2003;53 Suppl 6:524-533.
160. Raman S, Vernon R, Thompson J, Tyka M, Sadreyev R, Pei J, Kim D, Kellogg E, DiMaio F, Lange O, Kinch L, Sheffler W, Kim BH, Das R, Grishin NV, Baker D: Structure prediction for CASP8 with all-atom refinement using Rosetta. Proteins 2009;77 Suppl 9:89-99.
161. Thompson J, Baker D: Incorporation of evolutionary information into Rosetta comparative modeling. Proteins 2011;79:2380-2388.
162. Golczak M, Kiser PD, Sears AE, Lodowski DT, Blaner WS, Palczewski K: Structural Basis for the Acyltransferase Activity of Lecithin:Retinol Acyltransferase-like Proteins. J Biol Chem 2012;287:23790-23807.
163. Coleman J: Characterization of the Escherichia coli gene for 1-acyl-sn-glycerol-3-phosphate acyltransferase (plsC). Mol Gen Genet 1992;232:295-303.
164. Coleman J: Characterization of Escherichia coli cells deficient in 1-acyl-sn-glycerol-3- phosphate acyltransferase activity. J Biol Chem 1990;265:17215-17221.
165. Liou HL, Dixit SS, Xu S, Tint GS, Stock AM, Lobel P: NPC2, the protein deficient in Niemann-Pick C2 disease, consists of multiple glycoforms that bind a variety of sterols. J Biol Chem 2006;281:36710-36723.
166. Schleinitz N, Fischer J, Sanchez A, Veit V, Harle JR, Pelissier JF: Two new mutations of the ABHD5 gene in a new adult case of Chanarin Dorfman syndrome: an uncommon lipid storage disease. Arch Dermatol 2005;141:798-800.
167. Putnam C: Protein Calculator v3.3. In, 2006.
168. Schmidt A, Wolde M, Thiele C, Fest W, Kratzin H, Podtelejnikov AV, Witke W, Huttner WB, Soling HD: Endophilin I mediates synaptic vesicle formation by transfer of arachidonate to lysophosphatidic acid. Nature 1999;401:133-141.

169. Modregger J, Schmidt AA, Ritter B, Huttner WB, Plomann M: Characterization of Endophilin B1b, a brain-specific membrane-associated lysophosphatidic acid acyl transferase with properties distinct from endophilin A1. J Biol Chem 2003;278:4160-4167.
170. Weigert R, Silletta MG, Spano S, Turacchio G, Cericola C, Colanzi A, Senatore S, Mancini R, Polishchuk EV, Salmona M, Facchiano F, Burger KN, Mironov A, Luini A, Corda D: CtBP/BARS induces fission of Golgi membranes by acylating lysophosphatidic acid. Nature 1999;402:429-433.
171. Schuske KR, Richmond JE, Matthies DS, Davis WS, Runz S, Rube DA, van der Bliek AM, Jorgensen EM: Endophilin is required for synaptic vesicle endocytosis by localizing synaptojanin. Neuron 2003;40:749-762.
172. Guichet A, Wucherpfennig T, Dudu V, Etter S, Wilsch-Brauniger M, Hellwig A, Gonzalez-Gaitan M, Huttner WB, Schmidt AA: Essential role of endophilin A in synaptic vesicle budding at the Drosophila neuromuscular junction. EMBO J 2002;21:1661-1672.
173. Hidalgo Carcedo C, Bonazzi M, Spano S, Turacchio G, Colanzi A, Luini A, Corda D: Mitotic Golgi partitioning is driven by the membrane-fissioning protein CtBP3/BARS. Science 2004;305:93-96.
174. Bonazzi M, Spano S, Turacchio G, Cericola C, Valente C, Colanzi A, Kweon HS, Hsu VW, Polishchuck EV, Polishchuck RS, Sallese M, Pulvirenti T, Corda D, Luini A: CtBP3/BARS drives membrane fission in dynamin-independent transport pathways. Nat Cell Biol 2005;7:570-580.
175. Kooijman EE, Chupin V, Fuller NL, Kozlov MM, de Kruijff B, Burger KN, Rand PR: Spontaneous curvature of phosphatidic acid and lysophosphatidic acid. Biochemistry 2005;44:2097-2102.
176. Shemesh T, Luini A, Malhotra V, Burger KN, Kozlov MM: Prefission constriction of Golgi tubular carriers driven by local lipid metabolism: a theoretical model. Biophys J 2003;85:3813-3827.
177. Gallop JL, Butler PJ, McMahon HT: Endophilin and CtBP/BARS are not acyl transferases in endocytosis or Golgi fission. Nature 2005;438:675-678.
178. Ankem G, Mitra S, Sun F, Moreno AC, Chutvirasakul B, Azurmendi HF, Li L, Capelluto DG: The C2 domain of Tollip, a Toll-like receptor signalling regulator, exhibits broad preference for phosphoinositides. Biochem J 2011;435:597-608.
179. Kumar N, Zhao P, Tomar A, Galea CA, Khurana S: Association of villin with phosphatidylinositol 4,5-bisphosphate regulates the actin cytoskeleton. J Biol Chem 2004;279:3096-3110.
180. Kachel N, Erdmann KS, Kremer W, Wolff P, Gronwald W, Heumann R, Kalbitzer HR: Structure determination and ligand interactions of the PDZ2b domain of PTP-Bas (hPTP1E): splicing-induced modulation of ligand specificity. J Mol Biol 2003;334:143-155.
181. van den Bogaart G, Meyenberg K, Diederichsen U, Jahn R: Phosphatidylinositol 4,5-bisphosphate increases Ca2+ affinity of synaptotagmin-1 by 40-fold. J Biol Chem 2012;287:16447-16453.

182. Yu W, Cassara J, Weller PF: Phosphatidylinositide 3-kinase localizes to cytoplasmic lipid bodies in human polymorphonuclear leukocytes and other myeloid-derived cells. Blood 2000;95:1078-1085.
183. De Matteis MA, Di Campli A, Godi A: The role of the phosphoinositides at the Golgi complex. Biochim Biophys Acta 2005;1744:396-405.
184. Roth MG: Phosphoinositides in constitutive membrane traffic. Physiol Rev 2004;84:699-730.
185. Backer JM: The regulation and function of Class III PI3Ks: novel roles for Vps34. Biochem J 2008;410:1-17.
186. Falasca M, Maffucci T: Rethinking phosphatidylinositol 3-monophosphate. Biochim Biophys Acta 2009;1793:1795-1803.
187. Carlton J, Bujny M, Peter BJ, Oorschot VM, Rutherford A, Mellor H, Klumperman J, McMahon HT, Cullen PJ: Sorting nexin-1 mediates tubular endosome-to-TGN transport through coincidence sensing of high- curvature membranes and 3-phosphoinositides. Curr Biol 2004;14:1791-1800.
188. Sarkes D, Rameh LE: A novel HPLC-based approach makes possible the spatial characterization of cellular PtdIns5P and other phosphoinositides. Biochem J 2010;428:375-384.
189. Sbrissa D, Ikonomov OC, Strakova J, Shisheva A: Role for a novel signaling intermediate, phosphatidylinositol 5-phosphate, in insulin-regulated F-actin stress fiber breakdown and GLUT4 translocation. Endocrinology 2004;145:4853-4865.
190. Jones DR, Bultsma Y, Keune WJ, Halstead JR, Elouarrat D, Mohammed S, Heck AJ, D'Santos CS, Divecha N: Nuclear PtdIns5P as a transducer of stress signaling: an in vivo role for PIP4Kbeta. Mol Cell 2006;23:685-695.
191. Clarke JH, Letcher AJ, D'Santos C S, Halstead JR, Irvine RF, Divecha N: Inositol lipids are regulated during cell cycle progression in the nuclei of murine erythroleukaemia cells. Biochem J 2001;357:905-910.
192. Zou J, Marjanovic J, Kisseleva MV, Wilson M, Majerus PW: Type I phosphatidylinositol-4,5-bisphosphate 4-phosphatase regulates stress-induced apoptosis. Proc Natl Acad Sci U S A 2007;104:16834-16839.
193. Ungewickell A, Hugge C, Kisseleva M, Chang SC, Zou J, Feng Y, Galyov EE, Wilson M, Majerus PW: The identification and characterization of two phosphatidylinositol-4,5-bisphosphate 4-phosphatases. Proc Natl Acad Sci U S A 2005;102:18854-18859.
194. Gozani O, Karuman P, Jones DR, Ivanov D, Cha J, Lugovskoy AA, Baird CL, Zhu H, Field SJ, Lessnick SL, Villasenor J, Mehrotra B, Chen J, Rao VR, Brugge JS, Ferguson CG, Payrastre B, Myszka DG, Cantley LC, Wagner G, Divecha N, Prestwich GD, Yuan J: The PHD finger of the chromatin-associated protein ING2 functions as a nuclear phosphoinositide receptor. Cell 2003;114:99-111.
195. Nagashima M, Shiseki M, Miura K, Hagiwara K, Linke SP, Pedeux R, Wang XW, Yokota J, Riabowol K, Harris CC: DNA damage-inducible gene p33ING2 negatively regulates cell proliferation through acetylation of p53. Proc Natl Acad Sci U S A 2001;98:9671-9676.

196. Tang Y, Zhao W, Chen Y, Zhao Y, Gu W: Acetylation is indispensable for p53 activation. Cell 2008;133:612-626.
197. Lemmon MA: Phosphoinositide recognition domains. Traffic 2003;4:201-213.
198. Carlton J, Bujny M, Rutherford A, Cullen P: Sorting nexins--unifying trends and new perspectives. Traffic 2005;6:75-82.
199. Kumari M, Schoiswohl G, Chitraju C, Paar M, Cornaciu I, Rangrez AY, Wongsiriroj N, Nagy HM, Ivanova PT, Scott SA, Knittelfelder O, Rechberger GN, Birner-Gruenberger R, Eder S, Brown HA, Haemmerle G, Oberer M, Lass A, Kershaw EE, Zimmermann R, Zechner R: Adiponutrin functions as a nutritionally regulated lysophosphatidic acid acyltransferase. Cell Metab 2012;15:691-702.
200. Radner FP, Grond S, Haemmerle G, Lass A, Zechner R: Fat in the skin: Triacylglycerol metabolism in keratinocytes and its role in the development of neutral lipid storage disease. Dermatoendocrinol 2011;3:77-83.
201. Toulza E, Mattiuzzo NR, Galliano MF, Jonca N, Dossat C, Jacob D, de Daruvar A, Wincker P, Serre G, Guerrin M: Large-scale identification of human genes implicated in epidermal barrier function. Genome Biol 2007;8:R107.
202. Israeli S, Khamaysi Z, Fuchs-Telem D, Nousbeck J, Bergman R, Sarig O, Sprecher E: A mutation in LIPN, encoding epidermal lipase N, causes a late-onset form of autosomal-recessive congenital ichthyosis. Am J Hum Genet 2011;88:482-487.
203. Grall A, Guaguere E, Planchais S, Grond S, Bourrat E, Hausser I, Hitte C, Le Gallo M, Derbois C, Kim GJ, Lagoutte L, Degorce-Rubiales F, Radner FP, Thomas A, Kury S, Bensignor E, Fontaine J, Pin D, Zimmermann R, Zechner R, Lathrop M, Galibert F, Andre C, Fischer J: PNPLA1 mutations cause autosomal recessive congenital ichthyosis in golden retriever dogs and humans. Nat Genet 2012;44:140-147.
204. Lord CC, Betters JL, Ivanova PT, Milne SB, Myers DS, Madenspacher J, Thomas G, Chung S, Liu M, Davis MA, Lee RG, Crooke RM, Graham MJ, Parks JS, Brasaemle DL, Fessler MB, Brown HA, Brown JM: CGI-58/ABHD5-derived signaling lipids regulate systemic inflammation and insulin action. Diabetes 2012;61:355-363.
205. Fang Y, Vilella-Bach M, Bachmann R, Flanigan A, Chen J: Phosphatidic acid-mediated mitogenic activation of mTOR signaling. Science 2001;294:1942-1945.
206. Hla T, Lee MJ, Ancellin N, Paik JH, Kluk MJ: Lysophospholipids--receptor revelations. Science 2001;294:1875-1878.
207. Wymann MP, Schneiter R: Lipid signalling in disease. Nat Rev Mol Cell Biol 2008;9:162-176.
208. Tou JS, Gill JS: Lysophosphatidic acid increases phosphatidic acid formation, phospholipase D activity and degranulation by human neutrophils. Cell Signal 2005;17:77-82.
209. Chen Y, Zheng Y, Foster DA: Phospholipase D confers rapamycin resistance in human breast cancer cells. Oncogene 2003;22:3937-3942.

210. Avila-Flores A, Santos T, Rincon E, Merida I: Modulation of the mammalian target of rapamycin pathway by diacylglycerol kinase-produced phosphatidic acid. J Biol Chem 2005;280:10091-10099.
211. Kooijman EE, Chupin V, de Kruijff B, Burger KN: Modulation of membrane curvature by phosphatidic acid and lysophosphatidic acid. Traffic 2003;4:162-174.
212. Lim HK, Choi YA, Park W, Lee T, Ryu SH, Kim SY, Kim JR, Kim JH, Baek SH: Phosphatidic acid regulates systemic inflammatory responses by modulating the Akt-mammalian target of rapamycin-p70 S6 kinase 1 pathway. J Biol Chem 2003;278:45117-45127.
213. Samuel VT, Shulman GI: Mechanisms for insulin resistance: common threads and missing links. Cell 2012;148:852-871.
214. Straczkowski M, Kowalska I, Nikolajuk A, Dzienis-Straczkowska S, Kinalska I, Baranowski M, Zendzian-Piotrowska M, Brzezinska Z, Gorski J: Relationship between insulin sensitivity and sphingomyelin signaling pathway in human skeletal muscle. Diabetes 2004;53:1215-1221.
215. Summers SA: Ceramides in insulin resistance and lipotoxicity. Prog Lipid Res 2006;45:42-72.
216. Planavila A, Alegret M, Sanchez RM, Rodriguez-Calvo R, Laguna JC, Vazquez-Carrera M: Increased Akt protein expression is associated with decreased ceramide content in skeletal muscle of troglitazone-treated mice. Biochem Pharmacol 2005;69:1195-1204.
217. Haines TH, Dencher NA: Cardiolipin: a proton trap for oxidative phosphorylation. FEBS Lett 2002;528:35-39.
218. Brown JM, Chung S, Das A, Shelness GS, Rudel LL, Yu L: CGI-58 facilitates the mobilization of cytoplasmic triglyceride for lipoprotein secretion in hepatoma cells. J Lipid Res 2007;48:2295-2305.